

AD-A102 367

CALIFORNIA INST OF TECH PASADENA GRADUATE AERONAUTIC--ETC F/G 11/4
A STUDY OF THE TIME DEPENDENCE IN FRACTURE PROCESSES RELATING T--ETC(U)
APR 81 W G KNAUSS F49620-77-C-0051

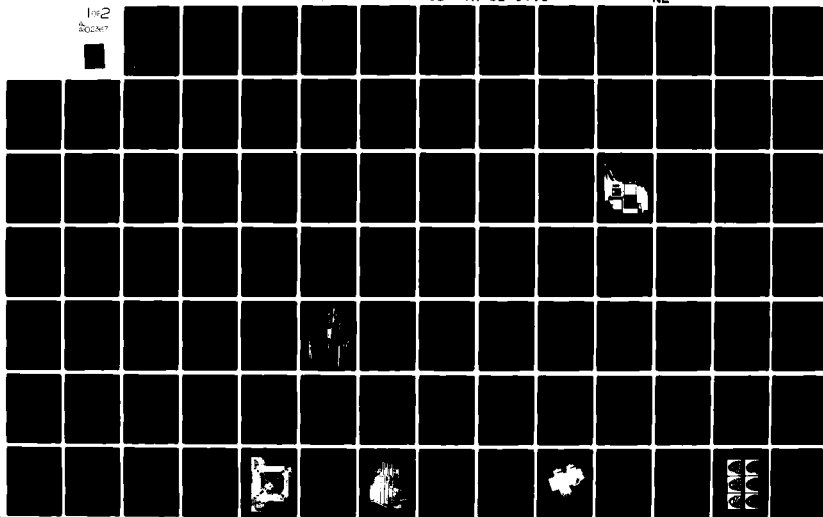
UNCLASSIFIED

GALCIT-SM-81-3

AFOSR-TR-81-0590

NL

1 of 2
inocket



AD A102367

AFOSR TR-81-0590

LEVEL

12

SM 81-3

Technical
Final Report on

A STUDY OF THE TIME DEPENDENCE IN FRACTURE PROCESSES
RELATING TO SERVICE LIFE PREDICTION
OF ADHESIVE JOINTS AND ADVANCED COMPOSITES

F49620-77-C-0051

DTIC
SELECTED
AUG 3 1981

Approved for public release;
distribution unlimited.

To the

Airforce Office of Scientific Research

30 April 1981

W.G. Knauss

California Institute of Technology
Pasadena, California

DTIC FILE COPY

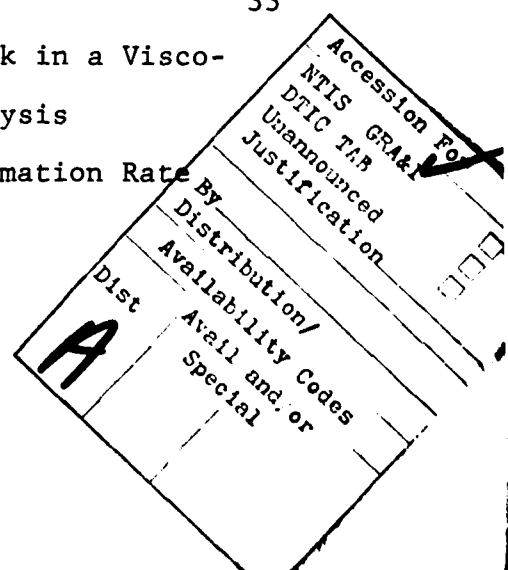
81 8 9 2 006

REPORT DOCUMENTATION PAGE		READ INSTRUCTIONS BEFORE COMPLETING FORM
1. REPORT NUMBER AFOSR-TR- 81 -0590	2. GOVT ACCESSION NO. AD-A102 367	3. RECIPIENT'S CATALOG NUMBER
4. TITLE (and Subtitle) A STUDY OF THE TIME DEPENDENCE IN FRACTURE PROCESSES RELATING TO SERVICE LIFE PREDICTION OF ADHESIVE JOINTS AND ADVANCED COMPOSITES	5. TYPE OF REPORT & PERIOD COVERED FINAL 1 Feb 1977-28 Feb 1981	6. PERFORMING ORG. REPORT NUMBER
7. AUTHOR(s) W G KNAUSS	8. CONTRACT OR GRANT NUMBER(s) F49620-77-C-0051	
9. PERFORMING ORGANIZATION NAME AND ADDRESS CALIFORNIA INSTITUTE OF TECHNOLOGY GRADUATE AERONAUTICAL LABORATORIES 105-50 PASADENA, CA 91125	10. PROGRAM ELEMENT, PROJECT, TASK AREA & WORK UNIT NUMBERS 2307/B1 61102F	
11. CONTROLLING OFFICE NAME AND ADDRESS AIR FORCE OFFICE OF SCIENTIFIC RESEARCH/NA BOLLING AFB, DC 20332	12. REPORT DATE 30 APRIL 1981	13. NUMBER OF PAGES 156
14. MONITORING AGENCY NAME & ADDRESS (if different from Controlling Office)	15. SECURITY CLASS. (of this report) UNCLASSIFIED	15a. DECLASSIFICATION/DOWNGRADING SCHEDULE
16. DISTRIBUTION STATEMENT (of this Report) Approved for public release; distribution unlimited.		
17. DISTRIBUTION STATEMENT (of the abstract entered in Block 20, if different from Report)		
18. SUPPLEMENTARY NOTES		
19. KEY WORDS (Continue on reverse side if necessary and identify by block number) BONDING STRUCTURAL JOINT FRACTURE		
20. ABSTRACT (Continue on reverse side if necessary and identify by block number) This report deals with developments in understanding adhesive fracture as related to structural bonds and composite materials. Both fracture mechanics based considerations as well as material related aspects are considered experimentally. One thrust of the program with the detailed measurements of the crack opening profile of a crack at a polymer-rigid (glass) interface. Very high resolution optical interferometry allowed a careful examination of the linearity response of the displacements in		

the fracture-critical area. The surprising results was that even at average strains across the bond line (in shear and in bond-normal deformation) on the order of 0.2% significant deviation from linear response is readily apparent. Crack propagation at the adherend-adhesive interface under combined shear and normal loading of the bond follows a criterion which states that crack growth proceeds at a given rate as long as the displacement components tangential (t) and normal (n) to the bond line combine (vectorially) to an absolute displacement s ($s = \sqrt{t^2 + n^2}$). For the case of infinitesimal deformations this criterion reduces to the energy release rate argument of linear fracture mechanics. In view of the need to better understand the effect of moisture and temperature on the time dependence of adhesion and matrix materials hygro-thermoviscoelastic behavior of two materials was studied. Resolution of apparently complex material behavior was accomplished through a "free volume" argument for the material behavior. Based on this result the idea was close at hand that mechanical dilatation at relatively high stresses could lead to non-linear viscoelastic behavior, a concept that was born out with surprising accuracy in an analytical and experimental study. Description of pertinent (non-trivial) equipment developments round out this report.

UNCLASSIFIED

ABSTRACT	4
I INTRODUCTION	6
II SUMMARY OF RESULTS	11
1 Equipment Construction	11
a) Creep torsiometer	11
b) Thermomechanical loading device	12
c) Hydraulic loading device for fatigue studies	13
2 Material Characterization	16
a) Properties of Polyvinylacetate (PVAc)	16
b) Non-linear viscoelastic response resulting from free volume charge	18
c) Thermomechanical properties of FM-73	19
3 Studies in the Mechanics of Adhesive-Failure	21
a) Bond separation profiles	22
b) Rate effects in disbonding	24
III Coupling Activities	26
IV Educational Contribution and Technology Transfer	28
V Publications	30
VI References	33
1 On the Steady Propagation of a Crack in a Visco- elastic Sheet: Experiments and Analysis	
2 Fracture of Solids Possessing Deformation Rate Sensitive Material Properties	



VII FIGURES	34
VIII APPENDICES	39
A A Simple Creep Torsiometer and Its Use in the Thermorheological Characterization of a Structural Adhesive	
B Crack Propagation at Material Interfaces:	
I. Experimental Technique to Determine Crack Profiles	
C On the Hygrothermomechanical Characterization of Polyvinyl Acetate	
D Non-Linear Viscoelasticity Based on Free Volume Consideration	
E Crack Propagation at Material Interfaces:	
II. Experiments on Mode Interaction	

AIR FORCE OFFICE OF SCIENTIFIC RESEARCH (AFSC)
NOTICE OF TRANSMITTAL TO DDC
This technical report has been reviewed and is
approved for public release IAW AFR 190-12 (7b).
Distribution is unlimited.
A. D. BLOSE
Technical Information Officer

ABSTRACT

This report deals with developments in understanding adhesive fracture as related to structural bonds and composite materials. Both fracture mechanics based considerations as well as material related aspects are considered experimentally.

One thrust of the program dealt with the detailed measurements of the crack opening profile of a crack at a polymer-rigid (glass) interface. Very high resolution optical interferometry allowed a careful examination of the linearity response of the displacements in the fracture-critical area. The surprising result was that even at average strains across the bond line (in shear and in bond-normal deformation) on the order of 0.2% significant deviation from linear response is readily apparent.

Crack propagation at the adherend-adhesive interface under combined shear and normal loading of the bond follows a criterion which states that crack growth proceeds at a given rate as long as the displacement components tangential (t) and normal (n) to the bond line combine (vectorially) to an absolute displacement s ($s = \sqrt{t^2+n^2}$). For the case of infinitesimal deformations this criterion reduces to the energy release rate argument of linear fracture mechanics.

In view of the need to better understand the effect of moisture and temperature on the time dependence of adhesions and

matrix materials hygrothermoviscoelastic behavior of two materials was studied. Resolution of apparently complex material behavior was accomplished through a "free volume" argument for the material behavior. Based on this result the idea was close at hand that mechanical dilatation at relatively high stresses could lead to non-linear viscoelastic behavior, a concept that was born out with surprising accuracy in an analytical and experimental study. Description of pertinent (non-trivial) equipment developments round out this report.

I INTRODUCTION

The past two decades have seen a large increase in the use of polymers in aerospace structures. Today the, perhaps, most visible application of structural polymers is in fiber composites. Problems which root strictly in the polymeric nature of the matrix material and (Kevlar) fibers have been fully recognized only rather recently, namely creep as affected by temperature and/or moisture ingressions. The application of elastomeric polymers to particulate composites (solid propellant rocket fuels) somewhat precedes the fiber composite materials, but basic problems in understanding their deformation and fracture response as needed in the integrity analysis of rocket motors is even less adequate than that for fiber reinforced (rigid) polymers.

Use of (rigid) polymers in structural bonding is much older than their application in the just mentioned examples. Although adhesively bonded aerospace structures offer decided advantages over those fabricated with conventional fastening methods (fatigue resistance, weight and potential cost savings in fabrication their reliability has been somewhat less than acceptable. However, adhesive bonds are not inherently un-

reliable. Rather, analysis methods of the past have not been geared to deal with the special (viscoelastic) properties of the adhesive and their influence on the failure process. Because of this lack of understanding the failure behavior has appeared erratic. One purpose of our investigations was, therefore, to better elucidate the influence of the various material properties involved in forming the bond, regardless of whether this bond relates to a structural bond, to adhesion between fiber and matrix in fiber reinforced epoxies, or to adhesion between aluminum and ammoniumperchlorate particles in solid propellants.

Beyond these more generic interests in bond failure several more specific questions motivated this work:

The first question relates to how the viscoelasticity in the adhesive effects the time dependence of the unbonding process. The second one concerns the effect of loading (bond normal and shear) on this time dependent failure process. Specifically, as a result of observing that bonds tend to be disproportionately stronger in shear than in tension, one wonders whether it is primarily the local bond-normal stresses at the crack tip that are responsible for failure propagation. Moreover if second order or non-linear effects were present in the crack tip displacement field they might be important contributors to

discrepancies between (simple) analyses and experience.

These questions are especially pertinent in view of the fact that it is - with few exceptions - common practice to restrict analyses to the limitations of the linear theory of elasticity. Because of this limitation and the lack of a careful scrutiny of this application it was deemed necessary to carefully examine this question experimentally.

As a guide in that examination of time dependent bond separation we draw on the failure behavior of monolithic viscoelastic solids. The theory for viscoelastic fracture [1,2] was developed prior to inception of this program and establishes the interrelation of geometric, material and loading parameters in their effect on the rate of crack propagation. The major difference between in interfacial and monolithic crack growth consists in involving two material properties, one of which is normally considered to be elastic (that of the adherend). The source and significance of viscoelastic behavior remains unaltered and the inherent strength of the bond is characterized by a rate and time independent fracture energy.

Because the viscoelastic failure theory involves a primary dependence of crackgrowth on the creep behavior of the adhesive, this program payed close attention to material characterization under different thermal and moisture conditions. This material characterization effort was developed partially in

conjunction with a DOE program, and evolved then into a careful initial characterization of an adhesive extensively used in Airforce structures, namely FM73. Extension of that work produced advances in the description of non-linear viscoelastic behavior which work was accomplished in conjunction with an ONR funded effort.

The total work under this present contract dealt thus with several interrelated areas:

- 1) Adhesion studies with distinct attention focused on
 - a) non-linear effects in interface separation
 - b) Viscoelastic or time dependent effects in the rate of interface crack growth.
- 2) Hygrothermoviscoelastic characterization of polyvinyl-acetate (PVAc) and structural adhesive, FM73 under
 - a) small deformations and
 - b) into the non linear range;
- 3) Preparations for work on fatigue crack behavior in structural adhesives and composites.

In support of these investigations major pieces of equipment were developed or redesigned, namely a

- 1) Bond line straining apparatus which could control displacements on the order of $1/4 \mu\text{m}$.
- 2) Precision creep torsionmeter (second design) and interfaced with microprocessor for semi automatic data reduction.
- 3) Servohydraulic testing facility for fatigue studies;

for cost-reasons this system was designed and assembled in house.

Most of these areas of endeavor have been previously summarized in reports or papers published or submitted for publication. It appears somewhat superfluous to repeat these developments here in detail. Instead, we shall summarize the pertinent developments in this final report and attach the earlier reports as appendices for detail reference. We hope that the presentation of the important accomplishments will thus gain in clarity.

All through this work we were very conscious of the need to interact with the user, either within Airforce personnel or with industrial researchers. We have therefore made a concerted effort of promulgating our results to technology users. These coupling activities are reported here also.

Finally we list the educational benefits derived from this program at the end of this report, as well as the reports documenting work done partially or totally under this contract.

II SUMMARY OF RESULTS

We delineate here the results or accomplishments in the three major areas indicated in the introduction. Because these studies required a considerable amount of specialized equipment for time dependent studies of material behavior we report these special developments here. The use of that equipment in the two areas of a) material characterization and b) adhesion studies is then reported in a summary manner. Because all this work has been documented in previous reports it shall suffice for the present purposes to highlight these developments here and to relegate details to those documents which are appended as parts of this report.

1) EQUIPMENT CONSTRUCTION

a) Creep-torsiometer. In order to characterize the visco-elastic behavior of polymers, and of adhesives in particular, it is necessary to determine relaxation or creep response. This may be accomplished in either a shear or elongational deformation mode. After years of experimentation with various arrangements we constructed an experimental torisometer which measures shear creep in torsional deformation. This experimental device was perfected and reduced to a tool for standard operation with automatic data reduction via a microprocessor. Its salient features are described in Appendix A without the microprocessor addition.

The most important aspect of its successful operation is the use of air bearings to support all moving parts in addition to close temperature and moisture control capability during prolonged test periods (in excess of 48 hrs).

This apparatus became the basis of several refined creep measurements at different temperatures and under different humidity conditions which ultimately led us to the development of the non-linear viscoelastic theory as described under Subsection 2) later on. Moreover, measurements on the Airforce adhesive FM73 were carefully carried out to support the AFML program at GD/Fort Worth.

b) Thermomechanical loading device. A major design challenge arose with regard to prescribing and controlling displacements on a bonded joint at the micrometer level. The objective here was to

1) measure the separation of the flanks of an interfacial crack between one adherend and the adhesive to an accuracy of at least one micron;

2) prescribe the relative displacements across a butt joint having a 20 mil bond line thickness, also to within at least one micron.

Only two means were found adequate to those requirements, namely optical interferometry and displacement generation through thermally controlled expansion and contraction of steel actuators. Control of these small, thermally induced displacements

needed to be accomplished through a Michelson interferometer pick-up, the output of which was fed to a microprocessor which in turn would compare the signal with a pre-specified one and adjust the temperature of the actuators. The operational principle is much like that of a servo-hydraulic testing machine, except that instead of a fluid heat is used as the displacement controller to achieve accurate prescription of the extremely small displacements.

This apparatus which worked very well is described in Appendix B documentation of its use is summarized under sub-heading 3 below.

c) Hydraulic loading device for fatigue studies. In order to study the fatigue failure of adhesively bonded joints and of the adhesive itself it was necessary to purchase or develop a displacement or load controlled straining device which permitted prescription of displacements far in excess of those allowed by the thermal device described under b) above. There existed the choice of developing a motor driven device for a special (limited) test geometries and for limited deformation history, or to develop a more versatile apparatus which could more readily be adapted to different test geometries and different strain or load histories. In view of the importance of time or rate dependence in the fatigue process of structural polymers it seemed exceedingly important to allow for a device that is very flexible with respect to the prescription of load or deformation histories.

That flexibility is provided most suitably by servo-hydraulic test machines. For this reason it was decided to construct a servo-hydraulic loading device (SLD) patterned after the MTS system. The purchase of such complete system was impossible because of limited funds. However, since the biggest portion of the expense covers the electronic controls the use of the already available microprocessor for that purpose scaled down the estimated cost considerable. The hardware for the system was therefore purchased piecemeal from suppliers to MTS at considerable savings.

This loading system, shown in figure 1 is now operational. A simplified hydraulic and electrical schematic of this device is presented in fig. 2. The mechanical portions of the SLD are contained in three basic modules:

- 1) the hydraulic power supply,
- 2) a flow control module containing valving, accumulators and filters, and
- 3) the load frame, to which the servovalve, actuator, load cell and LDVT are attached.

The hydraulic power supply (Miller Fluid Power Corp., Model 66) incorporates a 20 HP electric motor, a positive displacement pump rated 11.6 GPM at 2670 psi and a 40 gal. reservoir. In anticipation of the heat dissipation requirements associated with performing fatigue tests over protracted periods of time, this power unit was ordered modified to include a four pass heat exchanger. Cooling water flow is controlled by a

thermally activated water control valve which is set to open when the hydraulic fluid temperature reaches 125°F. We have further modified the power supply by the addition of a thermal switch which will cause shut-down if the hydraulic fluid temperature should exceed 145°F.

The flow control module contains all the hydraulic circuit elements necessary for both the pressure line to and return line from the servovalve. In the pressure line a 3/4 gallon nitrogen charged bladder type accumulator will act both as a shock absorber and as a source of reserve volume flow, necessary for applying large displacement "step" loading. A solenoid-operated directional control valve permits either direct flow at rated power supply output to the servovalve, or flow at pressures as low as 75 psi (due to the pressure reducing valve); the latter option will provide a "smooth start-up" feature for the SLD. A 1-quart accumulator, placed in the return line to protect the return line filter from hydraulic transient overpressures, is located in the flow control module, as are the high and low pressure filters.

The load frame (MTS Systems Corp., Model 312.21A-01) which is rated at 22,000 lbs., has been fitted with a double rod end hydraulic cylinder (Miller Fluid Power Corp., Model 53R) which was modified to attach an LVDT probe and accommodate the LVDT case (G.L. Vollins Corp., Model LMT 711P32) in a 6-inch deep hole provided in the lower end of the rod. The LVDT case is supported

by a housing which is rigidly attached to the actuator body. A servovalve (Moog, Inc., Model A076-233) which is rated for 10 GPM at 3000 psi is mounted on the loading frame. The close proximity of the servovalve to the actuator is desirable for maximum high frequency system response. Anticipating fatigue studies on polymeric specimens at relatively low load levels we purchased a load cell (Strainstert Co., Model FFL [1.8/1.2] which is fatigue rated at 1200 lbs. This facility has been checked out and is now fully operational for future fatigue studies.

2) MATERIAL CHARACTERIZATION

Several aspects of material behavior are important in this context: creep behavior under small and large strains as well as the influence of temperature and moisture, when applied separately and combined. This section summarizes the most important results.

a) Properties of Polyvinylacetate (PVAc). This material has a glass transition temperature of about 30°C. For this reason it is an ideal material for investigating phenomena that occur in the vicinity of the glass transition. Initially the material was used in this program to check out the operation of the creep-torsiometer because we were familiar with the manufacture of flawless specimens. However, it turned out that in the course of subsequent measurements features developed that lead to investi-

gating its properties further as model investigations for structural polymers. Notable amongst these are the similar behavior of this model polymer under changes of temperature and water content. The following results emerged:

- i) PVAc is thermorheologically simple, and within all measurements made is so through the glass transition region. This is new information since most investigations of thermorheological behavior are limited to the temperature range above the glass transition. The shift factor for thermorheological behavior exhibits, however, a break in slope at the glass transition temperature when plotted as a function of temperature. The knowledge of this behavior is needed in order to cope with residual stresses resulting from the cure process.
- ii) PVAc is hygrorheologically simple at temperatures below transition (not measured above T_g , since that domain is not very interesting for structural purposes); a well defined shift factor for various moisture contents resulted.
- iii) The volume change resulting from different temperature changes and those resulting from different moisture contents were measured.
- iv) When the shift factors for thermal and for moisture variations were plotted against relative volume change associated with temperature and moisture change the same shift factors were obtained.

v) This last result indicated that a free volume concept could explain combined effects of moisture and temperature changes in structural polymers.

These results are presented in more detail in Appendix C.

b) Non-linear Viscoelastic Response Resulting from Free Volume Change

Recall that under a) above the viscoelastic or time dependent response depends on the (free) volume change regardless as to whether that change is caused by temperature or by moisture. That observation immediately precipitates the idea that viscoelastic behavior should be affected if stress-induced volume changes occur. Such an effect is tantamount to saying that non-linearly viscoelastic effects should result.

This idea was pursued analytically and experimentally, details being given in Appendix D. Briefly, the Doolittle equation relating the shift factor to the free volume is used to incorporate the (free) volume dependence on the isotropic component of the stress tensor (average positive or negative pressure). The resulting volume dilatation increases then with stress and, correspondingly the higher the stress level the more the relaxation or creep behavior is affected. Specifically, at higher stresses the creep rate is accelerated and thus strain accumulates faster than at lower stress levels.

The detailed exposition in Appendix D and comparison of computation with tests on PVAc are augmented by additional comparisons of computation with tests on loading-unloading cycles shown in graphs at the end of Appendix D. Clearly a very large amount of hysteresis is generated as a result of the non-linearly viscoelastic behavior when compared to the nearly negligible energy loss in the linearly viscoelastic solid.

These results are of importance in fatigue considerations, where the material at the crack tip experiences high stresses and consequently non-linear material response; under repetitive loading significant heating is expected at the crack tip.

c) Thermomechanical Properties of FM-73

Although many structural adhesives are in use in aircraft construction, FM-73 enjoys some advantages over most, in that it appears to possess a relatively large time scale of near constant properties, as well as relatively stable behavior under moisture ingress (slow diffusion of water). FM-73 was used in the PABST Program and is a mainstay of several Airforce (AFML) programs on bonding.

For this reason it appeared very desirable to participate in the material characterization effort through careful measurements. This characterization process is ongoing, especially with respect to moisture related behavior. Here we record only the characteristics obtained to date:

- i) The creep behavior of FM-73 in shear follows standard viscoelastic behavior; it cannot be represented by a power law as has been claimed (see fig. 4 in Appendix A).

ii) The coefficient of thermal expansion is well behaved with a fairly narrow transition range, both in the dry and in the wet state. Above 100°C water vaporization causes a rapid increase in volume (or linear) expansion. Since water in molecular form and quantities does not exhibit such both response we conclude that water enters the polymer in micropores large enough to allow water response as if it were in bulk (see figure 3).

iii) A 2x4x.040 inch sheet of FM-73 has been immersed in distilled water for nearly two months at a time. Figure 4 presents the weight gain data from this experiment. In addition, figure 4 also depicts the moisture take-up predicted by Fick's law for a final weight gain of 1.8%, 2.0%, 2.2%, and 2.4% with corresponding diffusion constants selected so that agreement with the initial (i.e. linear) portion of the experimental diffusion curve is obtained. The differences between our experimental results and the Fick's law predictions after times corresponding to 200 hour $\frac{1}{2}$ /in. are indicative of water absorbing process more complicated than classical diffusion. The results of moisture take-up tests on much thinner (less than .010-inch thick) sheets of FM-73 are also shown in figure . These tests were conducted in an environmental chamber at an average relative humidity of 68% and an average temperature of 32.5°C. Due to the small specimen

thickness, equilibrium is reached in several hours. The relative brevity of these tests evidently precludes the significant participation of mechanisms other than classical diffusion in the absorption process; this is indicated by the good agreement between the experimental data and Fick's law. Figure 4 also shows moisture take-up for FM-73 as determined at the Materials Research Laboratory of General Dynamics Corporation ; these data exhibit strongly non-Fickian behavior.

3) STUDIES IN THE MECHANICS OF ADHESION FAILURE

In this section we report on experiments designed to clarify the importance of

- a) non-linear deformation effects in the description of interfacial bond failure and
- b) the effect of bond-normal and bond-tangential loading on the rate of interfacial crack growth.

The basic apparatus used in these studies was already reviewed in section Ib and in Appendix B. Besides discussing here the results on measurements of the bond separation profiles, non-linear deformations at the crack front and rate effects in disbonding, we also emphasize here the need for extremely careful specimen preparation in order not to obscure

the interferometric measurements by aberrations due to poor specimen manufacture. Details on specimen preparation are also included in Appendix B.

a) Bond Separation Profiles

As stated earlier it was the purpose of this experimental effort to examine the bond fracture behavior as much as possible without reliance on analyses that depended on assumptions of constitutive behavior or/and infinitesimal deformations.

Correspondingly, the experiments relied to the greatest extent possible on measured displacements of the adherends and of the crack surfaces. This approach guarantees that

- i) the linear proportionality between crack surface displacements on the one hand and the applied displacements on the other are readily examined without recourse to (linear) elasticity analysis, and
- ii) The crack propagation behavior is related to a measured displacement (field) near or at the front of the crack rather than to a computed quantity such as a stress intensity factor.

The results of the examination of the non-linear response of crack tip displacements to displacements applied to the adherends are given in detail in Appendix E. Suffice it for now to summarize those findings here.

The measurement technique based on optical interferometry allowed only determination of the separation of the crack flanks.

Thus, whether adherend displacements were prescribed normal or tangential to the bond line, only the opening displacement across the crack are measured. When the adherend displacement is normal to the bond line the crack-opening displacement is in the same direction; however, if the adherend displacements are parallel to the bond line then the measured crack opening displacement is normal to the applied displacement and, correspondingly smaller than in the former case. However, we can infer from the relative magnitude of the two sets of measurements, what the relative magnitude of bond-parallel displacements is across the crack when the adherends are displaced normal to the bond line.

It was truly surprising how readily non-linear deformation effects became apparent. In bond testing it is not unusual to impose relative adherend displacements that correspond to several (tens) percent average strain across the bond thickness, and 50-100 percent near failure is not uncommon. We find that at 0.2 percent (!) average strain across the bond line one observes readily apparent non-linear behavior, and the non-linear behavior is then on the order of 10-20 percent, becoming a substantially larger portion with increasing average strain across the bond line (see Appendix E).

This finding casts significant doubt on the manyfold bond fracture investigations based on small deformation and linearized analyses. It is thus likely that many of the poorly explained discrepancies between theory and tests are ultimately tractable to an inadequate analysis of the true test situation.

b) Rate Effects in Disbonding

When viscoelastic (polymeric) bonding agents are employed, failure will, in general, be a time dependent process. The failure growth rate will then depend on both the time history of loading and on the time dependent properties of the bonding agent(s). It was with this idea in mind that the servo-controlled thermal straining device was constructed.

Apart from the time history of loading one needs to ask how type of loading, i.e. the combination of bond-normal and bond-tangential loading affects the rate of unbonding. Alternately, a criterion of unbonding must answer the question: What combination of tangential and normal loads will result in a given rate of unbonding.

We attempted to answer that criterion question in several ways. The first idea examined was whether the opening displacement at the crack front determines the rate of crack growth: it did not do so uniquely. The alternate question was raised as to whether the gradient of the crack opening displacement at the crack front would control crack growth: It did not. In both these cases considered, the attempted criteria undervalued the significance of the local shear deformation.

Finally, the description of the crack growth process was best accomplished in terms of the local crack tip displacements when they are combined vectorically. Specifically, if the size of the vector displacement, derived from the components parallel and normal to the bond line, attains a certain value the crack

will grow at a fixed rate. In the limit of small strains this criterion reduces to the energy release rate criterion of linear fracture mechanics.

Because the experimental study supplied only bond-normal displacements the evaluation of that criterion is subject to some clarification. The experimental study showed how well the linearized theory predicted the bond-normal displacements. If bond-parallel displacements were computed from the linearized theory one would expect differences from the true values with comparable accuracy. If one thus uses bond-parallel displacements computed from the linearized theory one should expect data compliance within the same accuracy underlying the linear estimate. That this observation is true is shown in more detail in Appendix E.

III COUPLING ACTIVITIES

Interaction with researchers at industrial and other academic institutions are important and informative. We were very conscious of the need for interaction, both to receive pertinent information and to disseminate information developed under this (and related) programs. Initially, while the program was concerned with equipment development such interaction was relatively small.

The present effort found its natural industrial counterpart in several AFML-funded programs on bonding mechanics at General Dynamics in the Fort Worth Division. Many crossfertilizing concepts and stimuli for detailed investigations resulted from that contact: so, for example the need for the careful mechanical, thermal and moisture characterization of FM-73 (see discussion under 2 above).

Partially because of the involvement in this program the P.I. participated as a team leader in the review of the Mechanics effort at the AF Material Laboratory at the Wright Aeronautical Laboratories in Dayton, Ohio (1977).

An additional coupling activity resulted from the visit of Dr. A.F. Grandt, then of the AFML, to our research group. While at Caltech Dr. Grandt did research on fatigue crack growth.

Beyond these in-depth activities with other Airforce sponsored programs our staff participated in numerous meetings and paper presentations:

- 1) Mechanics of Composites 1977, 1978, 1980
Bergamo Center Dayton
(presentations 1977, 1978)
- 2) Adhesion Society Meeting, Savannah Georgia 1978, 1980
paper presentations
- 3) Society of Civil Engineers, Engineering
Mechanics Division
(presentation of invited paper, Aug. 1979)
- 4) Ohio State University, Mechanical Engineering
(paper presentation, Feb. 1980)
- 5) American Physical Society, March Meeting
in New York City N.Y. 1980
- 6) Society of Experimental Stress Analysis
presentation of two papers, May 1980
- 7) Gordon Research Conference on Elastomers
invited paper, July 1980
- 8) Gordon Research Conference on Adhesion
invited paper August 1980
- 9) Virginia Polytechnic Institute and State Univ.
Mechanical Engineering Department, Nov. 1980
- 10) Corning Glass Works
Du Pont, Experimental Station
(research review on bonding) Nov. 1980
- 11) University of Houston
Mechanical Engineering, Feb. 1981

IV EDUCATIONAL CONTRIBUTIONS AND TECHNOLOGY TRANSFER

This research program has produced an excellent PhD graduate K.M. Liechti. After completing his studies Dr. Liechti joined the Fort Worth Division of General Dynamics where he is involved primarily in two Airforce programs on bonding. His contribution to those programs is significant. In particular, Dr. Liechti is examining under one of those AFML sponsored programs the applicability of the VCOD criterion under fatigue type loading. On the second AFML sponsored program Dr. Liechti is investigating the applicability of the non-linear constitutive model developed here (and documented in Appendix D) to FM-73 for incorporation into a finite element code for viscoelastic stress analyses of structural bonds.

Besides the P.I. a Senior Research fellow, Dr. V.H. Kenner, was associated with the program for two years. Dr. Kenner joined the faculty of Ohio State University last year. A further Senior Research fellow Dr. M.C. Gupta was instrumental in getting the work of FM-73 started. He is now employed at the Jet Propulsion Laboratory.

As students several individuals contributed to the program; in turn, some received their research experiences on this program which started them on the road towards their PhD studies (indicated by an asterix behind their name):

Samuel Chang(*)

Igor Emri(*)

Bernd von Bernstorff(*)

Peters Maarten

Michael Chen (instrumental in computer software-micro-
processor work)

PUBLICATIONS

SM-numbers refer to publications listing of the Graduate Aeronautical Laboratories, Solid Mechanics, California Institute of Technology, Pasadena, California

a) Published papers or those submitted for publication are

1) W.G. Knauss, V.H. Kenner On the Hygrothermomechanical Characterization of Polyvinyl Acetate SM 80-8	Appeared in J. Appl. Phys. 51(10), Oct. 1980 Appendix C
2) V.H. Kenner, W.G. Knauss A Simple Creep Torsionmeter and Its Use in the Thermorheological Characterization of a Structural Adhesive SM 80-13	going to press in Experimental Mechanics Appendix A
3) W.G. Knauss, I.J. Emri Non-Linear Viscoelasticity Based on Free Volume Consideration	Appeared in Computer & Struct. Vol. 13, pp. 123-128 Appendix D
4) K.M. Liechti, W.G. Knauss Crack Propagation at Material Interfaces: 1. Experimental Technique to Determine Crack Profiles SM 80-21	both submitted for publication to SESA Appendix B
5) K.M. Liechti, W.G. Knauss Crack Propagation at Material Interfaces: II. Experiments on Mode Interaction SM 80-21	to be published at SESA meeting June 1981 Appendix E

6) K.M. Liechti Thesis, Calif.
The Application of Optical Interferometry to Inst. of Tech.
Time Dependent Unbonding April 1980

b) Annual and Interim Reports

7) K.M. Liechti, W.G. Knauss: "Progress Report No 1 on Time-Dependent Fracture Processes Relating to Service Life Prediction of Adhesive Joints and Advanced Composites", SM 77-2, May 1977.

8) K.M. Liechti, W.G. Knauss: "Progress Report No.2 on Time-Dependent Fracture Processes Relating to Service Life Prediction of Adhesive Joints and Advanced Composites", SM 77-7, Oct. 1977.

9) K.M. Liechti, V.H. Kenner, W.G. Knauss: "Informal Progress Report No.3 on Time-Dependent Fracture Processes Relating to Service Life Prediction of Adhesive Joints and Advanced Composites" SM 78-6, June 1978.

10) K.M. Liechti, V.H. Kenner, W.G. Knauss: "Time Dependent Fracture Processes Relating to Service Life Prediction of Adhesive Joints and Advanced Composites", SM 79-10, Oct. 1979.

11) W.G. Knauss, K.M. Liechti: "First Annual Report on a Study of Time Dependence in Adhesive Joint Fracture", SM 78-4, Feb. 1978.

12) W.G. Knauss, V.H. Kenner, K.M. Liechti: "Annual Report on a Program on Time Dependent Fracture at Interfaces", SM 79-5, Feb. 1979.

13) W.G. Knauss, V.H. Kenner, K.M. Liechti: "Third Annual Report on a Study of Time Dependence in Adhesive Joint Fracture", March 1980.

14) K.M. Liechti: "Literature Review on Adhesive Bonding Behavior", SM 77-5, July 1977.

15) V.H. Kenner, W.G. Knauss: "Finite Element Analysis of Circular Torsion Specimens", SM 80-6

c) Papers and reports which benefitted from the planning or results of the research are

16) W.G. Knauss
Fracture of Solids Possessing Deformation
Rate Sensitive Material Properties
SM 76-11
Appeared in the
Mechanics of Fracture
ed. by F. Erdogan,
AMD-Vol.19, Amer.
Soc. of Mech. Eng.
N.Y., Dec. 1976.

17) W.G. Knauss, H.V. Mueller
Polymer Reinforcement from the Viewpoint of
Fracture Mechanics
SM 78-10
Appeared in Fracture
of Composite Materi-
als, G.S. Sih &
V.P. Tamuzs (eds.)
1079 Sijhoff &
Noordhoff

18) J.A. Ori, A.F. Grandt Jr.
An Experimental Evaluation of Single Edge
Cracked Coupons for Monitoring Service Loads
SM 78-1

19) H. Corten, D. Kaebel, R. Plunkett
External Review and Assessment of AFML Inhouse
Program Quality - Mechanics
SM 77-10

20) A precursor to paper #3 above, but as related to solid
propellant constitutive behavior was written in partial
support from a Navy program, but drew heavily on results
developed under an earlier Airforce program. It is now being
reworked for publication.

W.G. Knauss
Nonlinear Viscoelasticity as a Result of Stress-
Induced Micro-Fracturing
SM 78-2

VI REFERENCE

Ref. 1 W.G. Knauss, "On the Steady Propagation of a Crack in a Viscoelastic Sheet: Experiments and Analysis", Deformation and Fracture of High Polymers, edited by H. Henning Kausch, John A. Hassell and Robert I. Jaffe (Plenum Press, 1974).

Ref. 2 W.G. Knauss, "Fracture of Solids Possessing Deformation Rate Sensitive Material Properties", The Mechanics of Fracture, edited by F. Erdogan, AMD-Vol. 19, Amer. Soc. of Mech. Engineers, N.Y., 1976.

VII FIGURES

Fig. 1 Servo-hydraulic loading device

Fig. 2 Schematic of Servo-hydraulic loading device

Fig. 3 Thermal expansion of FM-73

Fig. 4 Moisture diffusion characteristics in FM-73

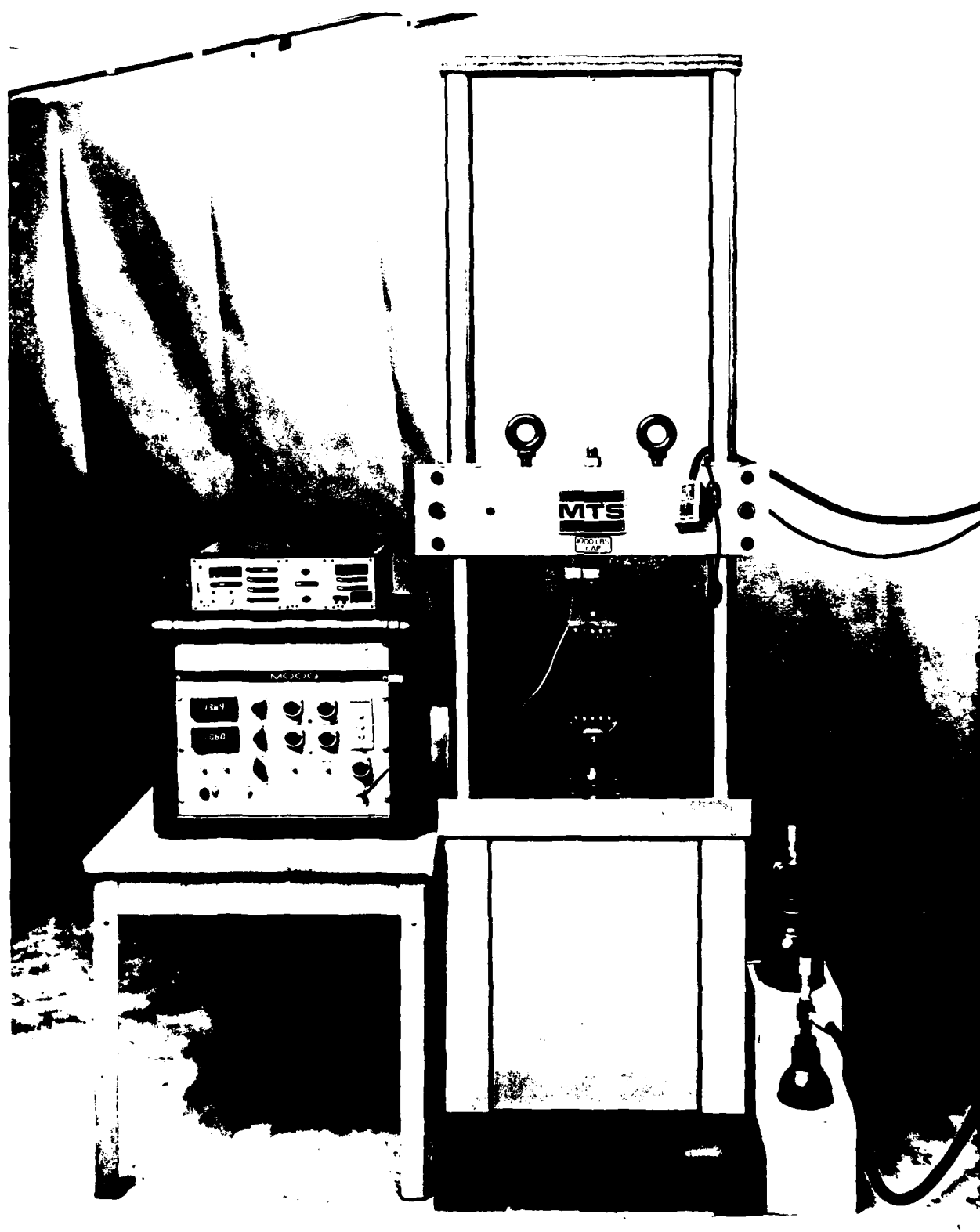


Fig. 1 Servo-Hydraulic Loading Device

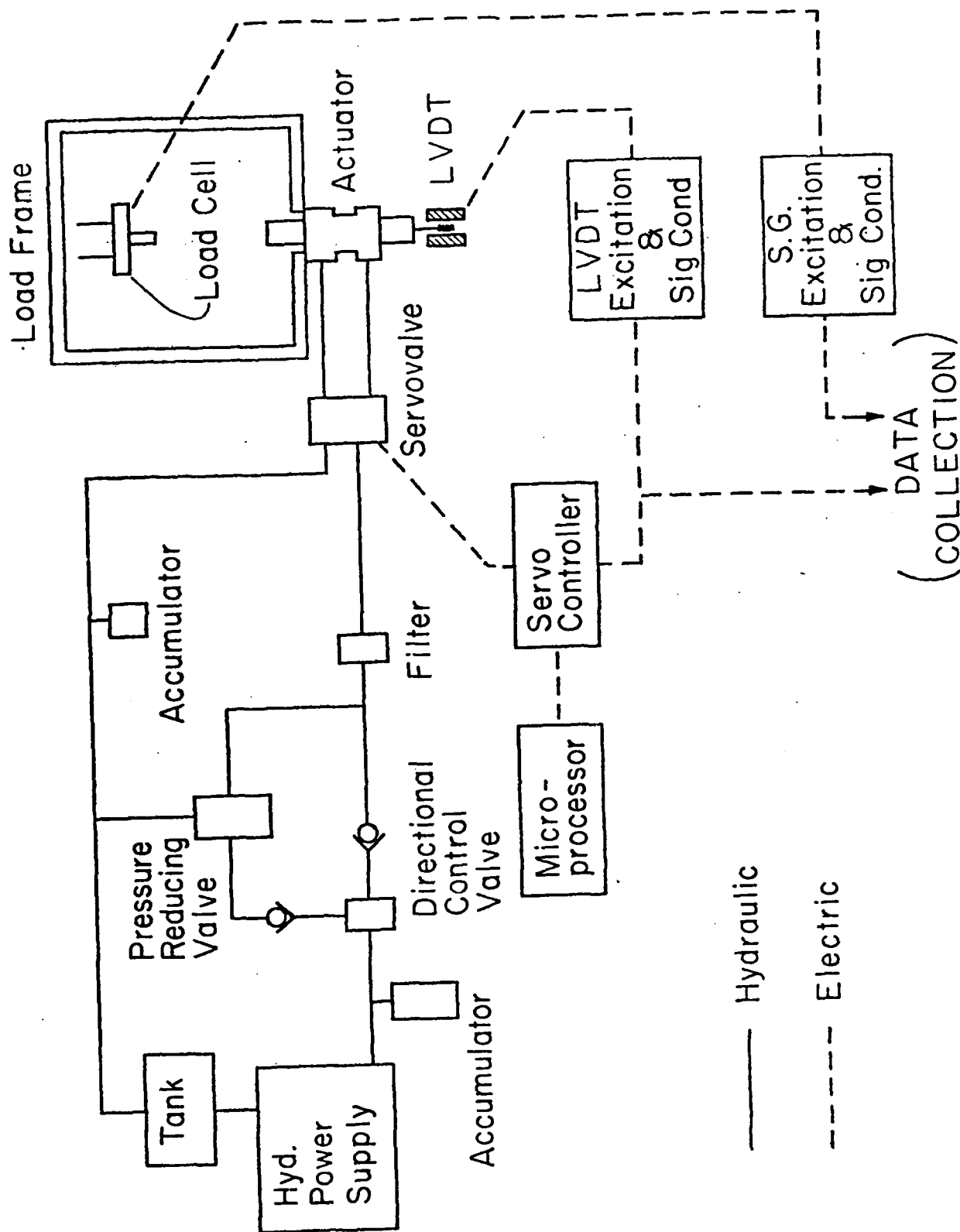
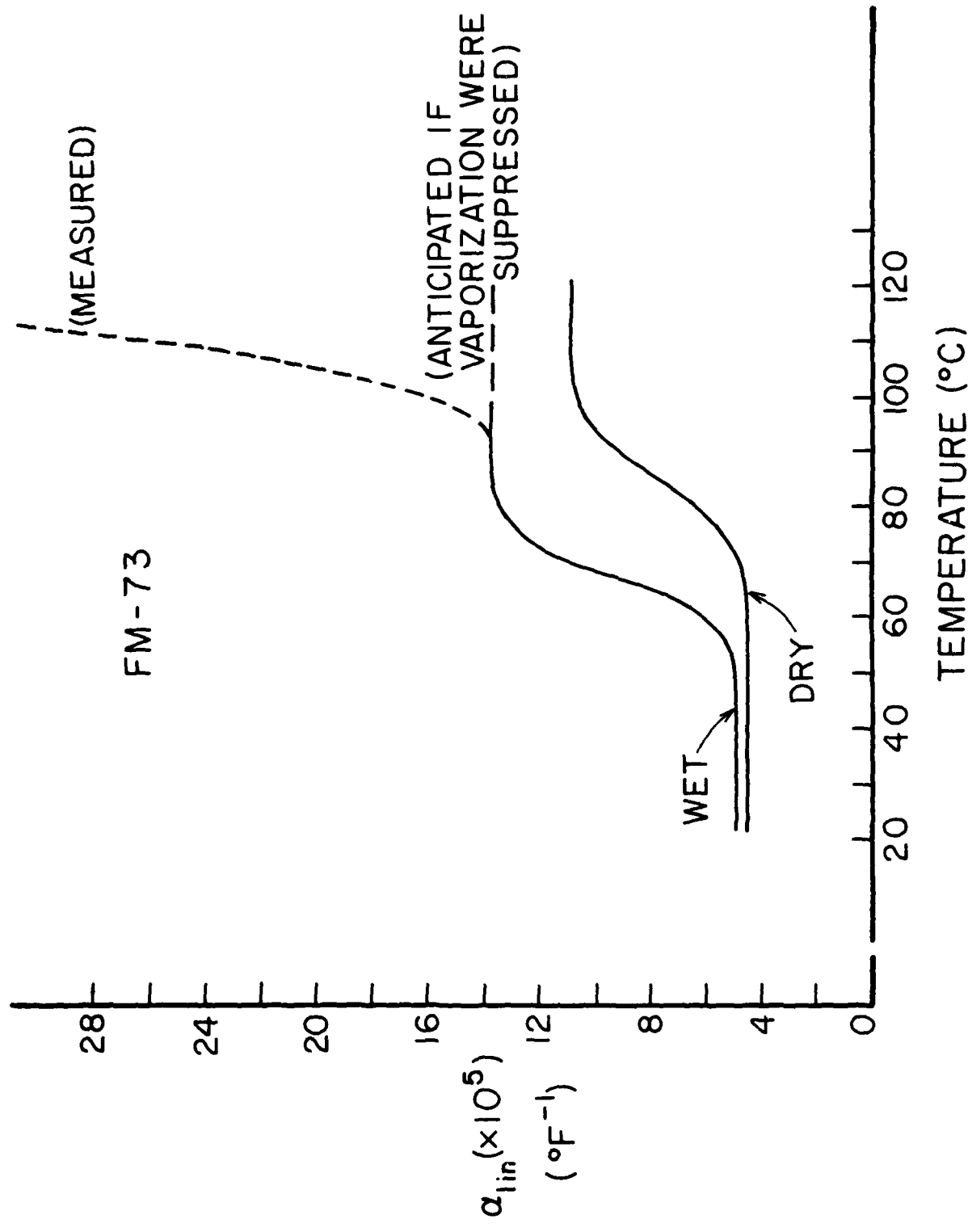


Fig. 2. Schematic Diagram for the Servo-hydraulic Loading Device.

Fig. 3. Thermal Expansion of FM-73.



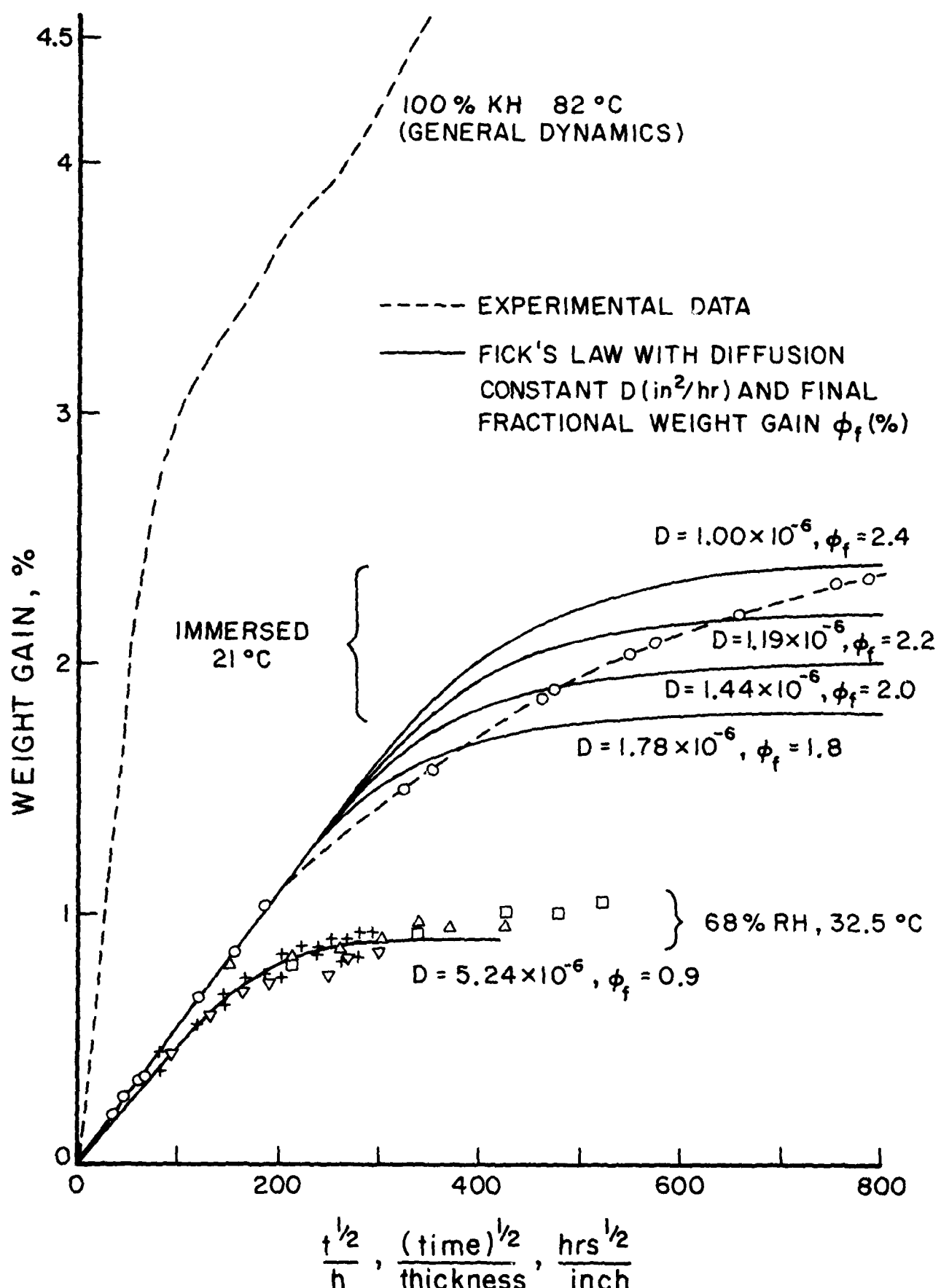


Fig. 4. Moisture Diffusion Characteristics in FM-73.

APPENDIX A

This paper is on the process of
printing for SESA. Original figures
are not available

A SIMPLE CREEP TORSIOMETER AND ITS USE IN THE
THERMORHEOLOGICAL CHARACTERIZATION OF A STRUCTURAL ADHESIVE

by

V. H. Kenner
W. G. Knauss

May 1980

Graduate Aeronautical Laboratories
California Institute of Technology
Pasadena, California

I Introduction

All structural work involving time dependent behavior of polymers requires careful viscoelastic material characterization. While in principle such characterization is straightforward, in practice considerable effort is required to produce reliable measurements. The only alternative to the expense of purchasing high quality equipment is the in-house construction of reliable instrumentation. In this paper we describe a relatively simple apparatus appropriate for material characterization in refined engineering analyses and present material properties measured with it on a structural polymer.

A strong reason for measuring viscoelastic properties in torsion is the direct need for shear properties in viscoelastic stress analyses where one requires, in general, two material functions, commonly the shear and the bulk, or volumetric behavior. Since the latter response typically varies much less over the glass-to-rubber transition than the former, one is often justified in approximating the bulk modulus as constant. In that event the shear behavior characterizes the viscoelasticity of the material completely. This is also true if one may assume that Poisson's ratio is constant as, for example, near either the rubbery or the glassy end of the time spectrum.

A second advantage of torsional creep testing involves specimen gripping. If material testing is to be accomplished under conditions that are unfavorable to the use of attached strain gages, e.g., soft materials or sizeable temperature or humidity variations, relative displacement of the specimen grips must serve to determine strains. The errors associated with grip slippage are more easily avoided for torsion than tension tests due to inherently lower gripping forces in the former case.

Accordingly, we describe here the mechanical aspects of a creep torsionmeter which is relatively easy to construct and use. We note here

that our instrument, designed with the objective of simplifying the testing of time-depend engineering materials, is at once both larger, by roughly two orders of magnitude, and less sensitive, by about the same amount, than torsimeters devised for investigations in polymer plastics where greater emphasis is given to the molecular (rather than the continuum) point of view.

Following the description of the torsimeter we provide an example of shear characterization for a commercial bonding agent, FM-73M. These data we then analyze in terms of time-temperature trade-off below and around the apparent glass transition temperature.

By far, most time-temperature relations are investigated above the glass transition, with little if any systematic data being available on a nearly similar scale for the corresponding behavior below the glass transition. We therefore examine to what extent such a time-temperature trade-off can be accomplished in that structurally important temperature regime. In this context it is particularly interesting to note that for the structural adhesive studied this time-temperature relation conforms well to unique thermo-rheological simplicity even though the material is a two-phase (rubber filled) polymer.

II Description of the Creep Torsimeter

The essential elements of the creep torsimeter mechanism are depicted schematically in fig. 1 and a photograph of this apparatus with supporting structure is shown in fig. 2. The upper end of the creep specimen is held in a fixed grip which, prior to clamping to the upper clamp support post A, may be adjusted vertically as required by specimen length. The lower end of the specimen is held by the active grip, which is attached to the main shaft atop the main shaft thrust disk D. Both grips are constructed to tightly clamp a 14.29-mm (9/16-inch)-diameter cylindrical surface. This

assembly reacts to both downward axial and radial loads through air bearings, the fixed surfaces of which are comprised of the inside diameter of the main shaft housing Q and a disk-shaped depression in the upper surface of the test chamber base R (fig. 2). Although specimen length changes will occur as a result of temperature variation or as a secondary deformation associated with twisting, neither of these effects have been of consequence in torsionmeter creep tests to date. Tightening the gripping screws while the specimen temperature was at the high end of the range to be studied precluded specimen buckling due to thermal expansion; slight specimen shortening associated with cooling is accommodated by the main air bearing. Twist angles were never greater than 0.16 radians and the associated length changes proved unnoticeable. The loading torque is applied to the specimen via the main shaft at the loading pulley H. Two threads fastened to this pulley run over two weight pulleys on air bearings and are attached to the two weights L, which are in turn connected to the load cranks K (fig. 1). By selectively utilizing the loading cranks a positive, negative, or zero torque may be applied to the specimen.

The angular motion of the main shaft is monitored through a circumferentially grooved displacement follower J, which rests against and is driven by the rubber-covered friction disk F, attached to the lower end of the main shaft E. The follower is connected by follower arms G to an air-bearing-supported shaft M carrying the core of an LVDT, O. Thus, rotational motion of the main shaft is converted to rectilinear motion of the follower and the LVDT probe. The LVDT air bearing S as well as the LVDT body N are located in a single support block T which may be leveled by a 40 thread per inch (1.57 thread per millimeter) levelling screw U (fig. 2). Threaded extensions of the follower arms protrude through the LVDT core support shaft and permit the attachment of two counter weights P diametrically opposed to the follower

arms. This allows the LVDT shaft assembly to float in its air bearing with the follower arms G oriented vertically so that the displacement follower is free of the friction disk; levelling of the LVDT shaft assembly may then be effected by adjusting the inclination of the support block with the levelling screw. A micrometer head V located behind the LVDT core support shaft provides both for accurate positioning of this shaft, thus insuring that the LVDT operates in its linear range, and for calibration of the displacement transduction system.

The main shaft housing is attached to a levelled plate W. This plate is situated on three base-supported levelling pads X which also permit in-plane motion of the level plate to locate the main shaft housing, which protrudes through a hole in the bottom of a temperature-control cabinet (Missimers, Inc., Model FT-3.2). The main shaft housing also carries a test chamber which surrounds the specimen but which is located entirely within the Missimers cabinet. This inner test chamber is constructed of 25 to 38 mm (1 to 1.5 in.)-thick metal walls as thermal mass in order to allow close temperature control of the specimen. The compressed air supply for the main shaft air bearing, a portion of which is ultimately vented into the inner test chamber, passes through a coiled copper heat exchanger tube interior to the temperature-control cabinet prior to entering the air bearing supply passage-way which is located in the test chamber base. The configuration described provides for essentially complete mechanical isolation of the torsionmeter loading and rotation sensing components from the temperature-control (Missimers) cabinet. Furthermore, the high heat capacitance of the massive test chamber provides a highly stable test temperature, which is measured by a thermocouple and/or a mercury thermometer which protrudes through a hole in the top of the test chamber.

III Calibration of the Torsiometer

In order to establish the accuracy and limitations of the torsiometer, it was necessary to determine sources of error and their influence. A series of simple tests to accomplish this goal was conducted on the completed torsiometer.

1) Minimum torque sensitivity ("sticking"). Although air bearings are practically frictionless the motion of the torsiometer involves a small energy loss through the deformation occurring in the rubber covering of the friction disk at its contact with the displacement follower rod. While this effect may be minimized by minimizing the tracking force exerted by the displacement follower, frequency (time) response requirements place a practical lower limit on the acceptable tracking force. Thus a certain amount of friction or "sticking" is unavoidable. Without specimen but with the displacement follower in place on the friction disk, the torsiometer was first balanced using the levelling screw. Then the torque "deadband" was established by determining the rotation of the levelling screw required to produce motion in either direction. Since the mass of the LVDT shaft and follower and the geometry of the system are known, the gravity force arising from the change in inclination and hence the torque applied to the friction disk are easily calculable. The "deadband" torque was found to be less than $\pm 3.7 \times 10^{-6}$ Nm (33×10^{-6} lb in.).

It was found that although motion occurred as just described, a "potential well" effect existed wherein, once balance of the torsiometer had been established, this equilibrium position became preferred. A torque greater than the "deadband" torque to cause perceptible motion was required to produce motion through the complete range of LVDT, ± 2.54 mm (0.1 in.). The "potential well" torque was determined to be approximately 2.7×10^{-5} Nm (240×10^{-6} lb in.). This value was verified by direct loading: After

balancing, the application of a 4.9×10^{-4} N (1.1×10^{-4} lb) weight was sufficient to cause full range motions; this weight generates a torque of 2.5×10^{-5} Nm (220×10^{-6} lb in.). The potential well effect is associated with a viscoelastic settling of the LVDT follower into the rubber layer covering the friction disk. This potential well may be reduced: By placing one counterweight on the LVDT shaft, and thus reducing the tracking force between follower and friction disk from 0.21 N (0.047 lb) to 0.04 N (0.009 lb), the torque change associated with travel through the entire LVDT range was reduced to a value of $\pm 1.92 \times 10^{-6}$ Nm ($\pm 17 \times 10^{-6}$ lb in.). However, because tracking characteristics under initial loading in this configuration were only marginally satisfactory, all creep tests are run without such counterweights.

In order to explore the possible effect of electromagnetically induced forces arising at the LVDT probe, the LVDT shaft with counterweights in place, was balanced and the effects of energizing the LVDT examined. In this configuration, which was the most sensitive encountered, a gravity force change of 7.3×10^{-5} N (1.6×10^{-5} lb) along the LVDT axis (applied via the levelling screw) gave rise to a complete reversal of motion. However, the effect of LVDT energization on balance was not discernable, indicating that electromagnetic forces on the LVDT probe are insignificant in the present apparatus.

2) Twist angle resolution and repeatability. The LVDT stroke of ± 2.54 mm (0.1 in.) corresponded to ± 10 V electrical output. Since the friction disk has a radius of 25.4 ± 0.06 mm ($1 \pm .0025$ in.), the maximum specimen twist angle measurable is ± 0.1 radian. Because the LVDT itself imposes no lower resolution limit, such a limit is determined either by the electronics utilized for read-out or by the fidelity inherent in the LVDT drive mechanism. Here the latter item was found to be limiting. To evaluate this limit an arm was fixed to the torsimeter main shaft at the lower

specimen grip such that its motion was limited by the inner cabinet wall, which served as a stop and thus defined a particular main shaft orientation. With the displacement measuring system activated, the main shaft was rotated, so that the LVDT moved through its stroke, and was then returned to the stop. Repeatability of the LVDT output voltage was always within 1 mv, corresponding to an angle of less than 10^{-5} radians.

3) Frequency response limitations. The apparent coefficient of friction between the displacement follower and the friction disk was found to be approximately 1.1; along with the known masses and geometry this allows one to calculate that the follower will begin to slip at a frequency of approximately 8 Hertz. For comparison we note that in creep tests, the load is applied smoothly over a period of about 3 seconds with the aid of the loading crank. Tests with a 0.991 mm (0.039 in.) diameter steel specimen were conducted which confirm that no slip in the displacement measuring system occurs when this loading technique is employed.

4) Test chamber temperature control. After thermal equilibrium has been achieved in the test chamber, a process which takes approximately three hours, the test temperature is maintained indefinitely within $\pm 1/20^{\circ}\text{C}$ (tested for a period of more than 24 hours). The temperature control cabinet is stated to permit temperatures from -73°C to 121°C .

5) Specimen geometry. Several different specimen geometries have been utilized in the torsimeter to date. In one case the "dumbbell" shaped specimen consisted of 7.94 mm (5/16-inch) diameter by 51 mm (2-inch) long gage section with 14.29 mm (9/16-inch) diameter ends which were clamped in the torsimeter grips. In a second instance a 14.29 mm (9/16-inch) diameter cylinder (of a highly compliant material) was bonded to aluminum end pieces of the same diameter, which were then gripped. In the experiments described in the sequel strip specimens were accommodated to the torsimeter grips with

tightly fitting aluminum adaptor pieces. For the last two configurations the aluminum cylinders are easily fixed in the grips to prohibit any slipping and, furthermore, their great stiffness compared to the test materials renders them effectively rigid so that the relative rotation between the grips is, for all practical purposes, exactly that of the gage section ends. The first specimen configuration does deform somewhat in the gripped ends. The stresses, strains and displacements for this configuration were evaluated using an axisymmetric finite element code². The ratio of gage-length relative rotation to total rotation between the grips was found to be 0.94; this factor may be applied to the data as a correction.

IV Fabrication and Creep Testing of FM-73M Adhesive

In its as-received form, FM-73M adhesive* consists of a soft, sticky layer approximately 0.13 mm (0.005 in.) thick. Successive layers of this material were pressed together under vacuum to form a 102 mm (4 in.) by 102 mm (4 in.) plate of uncured FM-73M. This was then cured at a temperature of 250°C for one hour; the cured plate had a thickness of 1.30 mm (0.051 in.). Strip specimens 9.53 mm (0.375 in.) wide and 102 mm (4 in.) long were then machined from the plate and stored at ambient conditions, approximately 20°C and 50% relative humidity.

Four hemicylindrical aluminum adaptor pieces, each with a rectangular groove in the flat coaxial surface, which was slightly less than half of the specimen thickness, were fitted (snugly) in pairs at either end of the specimen; this accommodated the strip specimens to the cylindrical torsionmeter grips. The gage length for the specimen was taken to be the length between the aluminum adapting pieces; this length was measured as 62.2 mm (2.45 in.) for the data reported in the sequel. The entire sequence of creep tests reported below was conducted without

*American Cyanamid Company FM-73M neat, i.e., no scrim cloth.

once removing the specimen from the torsionmeter. This was accomplished over a period of 10 days during which time the specimen chamber remained at or below a relative humidity of 15%. This low humidity level was maintained by the continuous exhausting of dry air into the test chamber via the main air bearing, which always remained activated.

Creep tests were conducted at temperatures extending from 20.5°C to 101.3°C . The applied torque ranged from 2.61×10^{-3} Nm (23.1×10^{-3} lb in.) for the coolest run, to 6.22×10^{-4} Nm (5.51×10^{-3} lb in.) for the warmest run, respectively. The effect of previous runs was minimized by always allowing a sufficient time interval between runs so that the recovery creep was not discernible on the pre-load baseline of the strip chart record. The load direction for consecutive runs (on the same specimen) was always arranged so as to minimize potentially cumulative creep strains.

V Master Creep Curve

Figure 3 presents plots of the creep compliance $J(t)$ obtained for various test temperatures. $J(t)$ is determined from the formula*

$$J(t) = \frac{\gamma(t)}{\tau} = \frac{k_1(2a)^3(2b)}{TL} \theta(t) , \quad (1)$$

where a is the thickness, b the width, $\theta(t)$ the time dependent twist angle for the specimen whose length is L and to which torque T is applied. The parameter k_1 depends on the ratio $\frac{b}{a}$ and is tabulated in ref. 3; τ denotes the shear stress and $\gamma(t)$ the time dependent shear strain. The creep curves of fig. 3 have been combined to produce a master creep curve for FM-73. These curves were first shifted vertically (ref. 4) by a factor $b_t = \frac{T}{T_0}$, where T is the absolute temperature of the test and T_0 is the absolute reference temperature, taken as

*Since FM-73M is relatively compliant and since the cross-section of the specimen is non-circular, it is necessary to check that secondary stresses and their effects are insignificant. It turns out that for the test geometry and small deformations encountered the classical theory of elasticity may be used to calculate the stress and strain distribution (ref. 2); the maximum shear strain encountered in the present experiment was 0.34%.

293.5°K (20.5°C). The vertically shifted curves were then shifted horizontally to visually produce a "best smoothness" curve, which is presented in fig. 4.

It appears that the material is reasonably well characterized as a thermo-rheologically simple material, in spite of the fact that it is a two-phase solid. The reason for this behavior is probably that the included phase is rubbery at all test temperatures and responds little to increases in temperature when compared with the response of the matrix solid. The corresponding horizontal shift factor, a_T , relative to a temperature of 20.5°C is plotted in fig. 5. The error bars on this figure represent the possible shifting error $\delta \log a_T$ corresponding to a representative error of $\pm 2\%$ in $J(t)$. With reference to fig. 6, one establishes easily that this error can be determined from

$$\delta \log a_T = 2\delta \log J(t) \cdot \frac{\Delta \log t}{\Delta \log J(t)} . \quad (2)$$

VI Analytical Representation of Test Results

For computational purposes it is desirable and sometimes mandatory to have an analytical representation of the experimental data. Such representations can and have been achieved in different ways⁵, the most prominent ones for engineering application being the discrete spectral representation (Prony series) and the power law for the relaxation of creep properties. Schapery⁶ has suggested that below the glass transition temperature a power law representation may be appropriate for the tensile creep compliance which, for the shear compliance, would be in the form

$$J(t) = J_0(T) + A\left(\frac{t}{a_T}\right)^n , \quad (3)$$

where $J_0(t)$ is a function of temperature only. It turns out that such a power law fit does not represent our data well at all, as shown in fig. 4 for two sets of constants. In contrast the discrete spectral representation

$$J(t) = J_0 + \sum_{i=1}^{18} J_i (1 - e^{-t/\tau_i}) \quad (4)$$

gives a close representation as shown in fig. 4 for the coefficients J_i and τ_i (at 20.5°C) shown in Table 1.

TABLE 1. Coefficients for the discrete spectral representation shown in fig. 4.

$$J_0 = 1.264 \times 10^{-9} \text{ m}^2/\text{N}$$

i	τ_i (sec)	J_i (m^2/N)
1	6×10^1	4.06×10^{-11}
2	6×10^2	4.35×10^{-11}
3	6×10^3	4.64×10^{-11}
4	6×10^4	5.08×10^{-11}
5	6×10^5	5.66×10^{-11}
6	6×10^6	6.53×10^{-11}
7	6×10^7	7.55×10^{-11}
8	6×10^8	8.71×10^{-11}
9	6×10^9	1.16×10^{-10}
10	6×10^{10}	1.60×10^{-10}
11	6×10^{11}	2.47×10^{-10}
12	6×10^{12}	3.70×10^{-10}
13	6×10^{13}	5.44×10^{-10}
14	6×10^{14}	8.10×10^{-9}
15	6×10^{15}	1.33×10^{-9}
16	6×10^{16}	3.78×10^{-9}
17	6×10^{17}	6.64×10^{-9}
18	6×10^{18}	6.66×10^{-9}

From volume dilatometric data* shown in fig. 7 we derive that the glass transition temperature is about 85.6°C. Note that in fig. 5 the shift factor passes through a noticeable change in slope at that temperature. It turns out that the two branches for $T > T_g$ can, within the $\pm 2\%$ error band, be represented by the WLF equation⁽³⁾

$$\log a_{T_g} = \frac{-C_1(T - T_g)}{C_2 + (T - T_g)} \quad (5)$$

if one excepts the datum at 20.5°C; of course, there are only two data points for $T > T_g^+$ so that the representation is less firm for that temperature domain.

The constants C_1 and C_2 in equation 5 are found to be

$$\begin{array}{lll} C_1 = 7.5 & & C_1 = 12.4 \\ & T < T_g ; & T > T_g \\ C_2 = 106 & & C_2 = 24.5 \end{array}$$

These values appear reasonable in the light of data compiled for different polymers by Ferry (ref. 7, pg. 219).

We summarize this discussion by repeating the earlier observation that, in spite of the two-phase nature of the test material, thermorheological simplicity is surprisingly well preserved below the glass transition temperature.

*Obtained by Mr. Luc J. Heymans, graduate student, at the Graduate Aeronautical Laboratories, California Institute of Technology.

[†]The test geometry allowed deformation to exceed the measurement range of the torsionmeter at higher temperatures; a different test geometry would be required under these conditions.

Acknowledgments

This work was supported by the Air Force Office of Scientific Research through Grant F49620-77-C-0051 for which the authors express their thanks. The authors are also grateful to Mr. H. Chai, who initiated the construction of the torsimeter; Dr. R. Kriger of American Cyanamid Company, who willingly supplied the adhesive material; and Dr. M. Gupta, Sr. Research Fellow at Caltech, for perfecting the method of forming test specimens free of gas bubbles. Finally, we acknowledge a fruitful interaction with Dr. J. Romanko, General Dynamics Materials Laboratory, Fort Worth, in connection with the AFML sponsored program on Fatigue Behavior of Adhesively Bonded Joints.

REFERENCES

1. Plazeck, D.J., "Magnetic Bearing Torsional Creep Apparatus," *J. Polymer Science: Part A2*, Vol. 6, 621, 1968.
2. Kenner, V.H. and Knauss, W.G., "Finite Element Analysis of Circular Torsion Specimens," *GALCIT SM80-6*.
3. Timoshenko, S.P. and Goodier, J.N., Theory of Elasticity, 2nd Edition, McGraw Hill, 1951.
4. Williams, M.L., Landel, R.F. and Ferry, J.D., "The Temperature Dependence of Relaxation Mechanisms in Amorphous Polymers and Other Glass Forming Liquids," *J. Amer. Chem. Soc.* 77, 3701, 1955.
5. Williams, M.L., "Structural Analysis of Viscoelastic Materials," *AIAA J.* 2, 5, 785-808, 1964.
6. Schapery, R.A., "Viscoelastic Behavior and Analysis of Composite Materials," in Composite Materials Vol. 2 Mechanics of Composite Materials, G.P. Sendeckyi (ed.), Academic Press, New York, 1974.
7. Ferry, J.D., Viscoelastic Properties of Polymers, Wiley, 1961.

CAPTIONS FOR FIGURES

Fig. 1. Schematic diagram of the creep torsiometer.

Fig. 2. Photograph of the torsiometer. Labels A through P are defined in Fig. 1. Additional labels are: Q. main shaft housing; R. test chamber base; S. LVDT air bearing; T. support block; U. levelling screw; V. micrometer head; W. level plate; X. levelling pads.

Fig. 3. Creep compliance curves for FM-73M at several temperatures.

Fig. 4. Master creep curve for FM-73M at 20.5°C (points) and analytical fits (curves) described in the text.

Fig. 5. Experimentally obtained time-temperature shifting relationship for FM-73M (points) and separate fittings of the WLF equation to data above and below the glass transition temperature.

Fig. 6. The analysis of shifting errors between two creep curves, which are depicted only in the locality of overlap.

Fig. 7. Volume change vs. temperature for FM-73M.

CAPTIONS FOR FIGURES

Fig. 1. Schematic diagram of the creep torsiometer.

Fig. 2. Photograph of the torsiometer. Labels A through P are defined in Fig. 1. Additional labels are: Q. main shaft housing; R. test chamber base; S. LVDT air bearing; T. support block; U. levelling screw; V. micrometer head; W. level plate; X. levelling pads.

Fig. 3. Creep compliance curves for FM-73M at several temperatures.

Fig. 4. Master creep curve for FM-73M at 20.5°C (points) and analytical fits (curves) described in the text.

Fig. 5. Experimentally obtained time-temperature shifting relationship for FM-73M (points) and separate fittings of the WLF equation to data above and below the glass transition temperature.

Fig. 6. The analysis of shifting errors between two creep curves, which are depicted only in the locality of overlap.

Fig. 7. Volume change vs. temperature for FM-73M.

Abstract

A relatively inexpensive, yet precise creep torsionmeter has been developed and operation limitations for the instrument determined. Shear creep compliance measurements were then made for a thermo-setting structural adhesive at temperatures below and near this material's glass transition temperature. The time-temperature behavior of the material in this temperature regime is found to be thermorheologically simple.

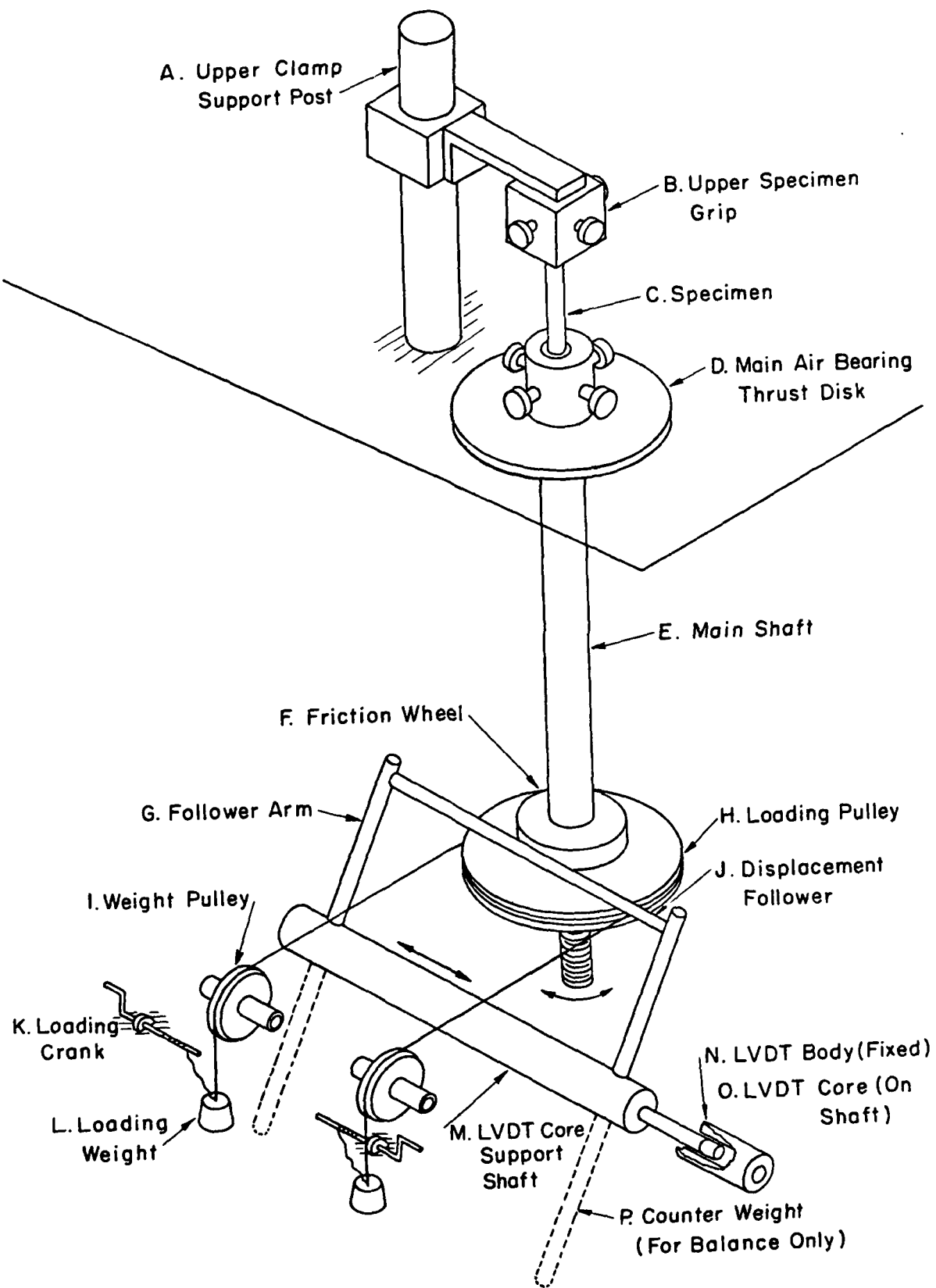


FIG 1

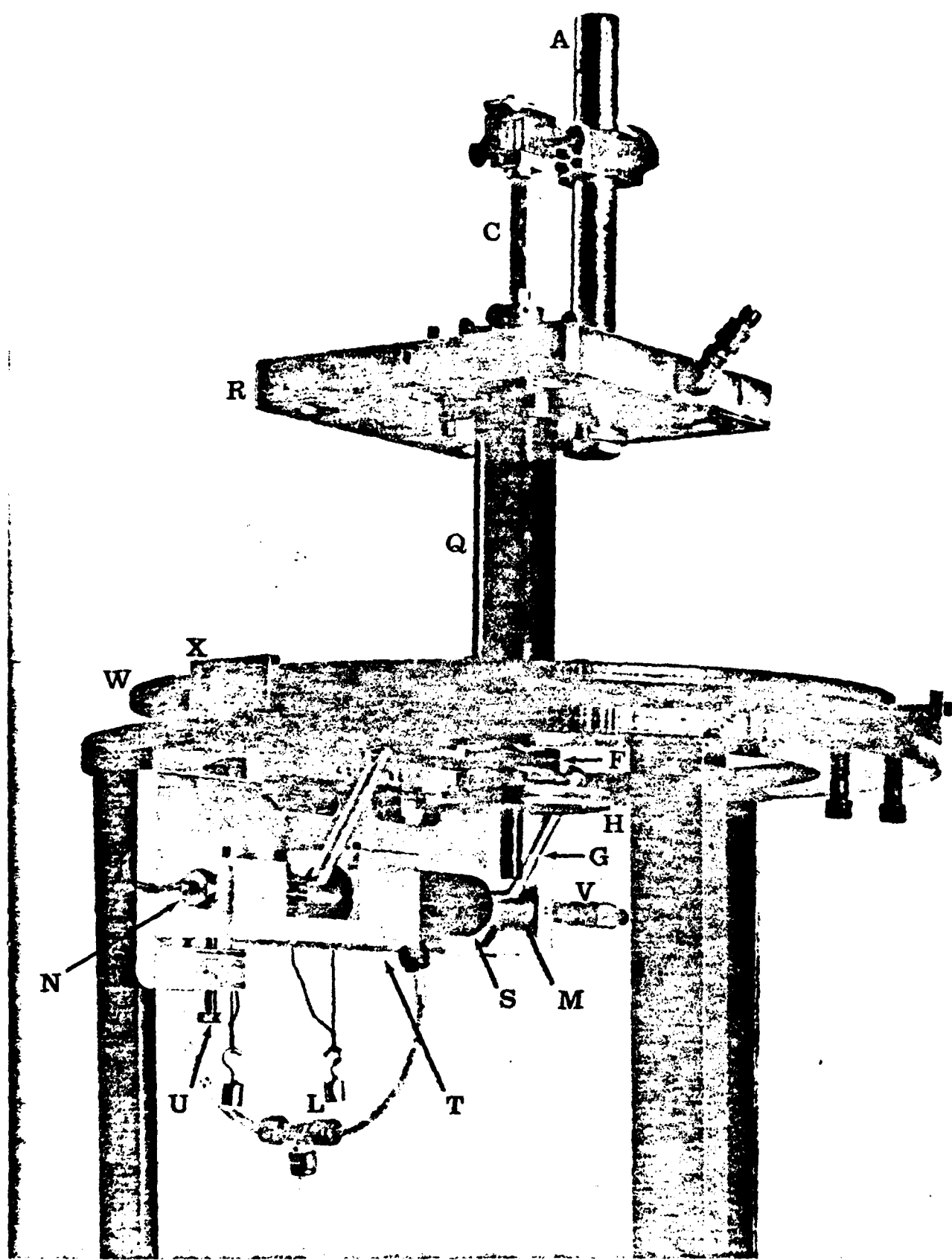


FIG. 2

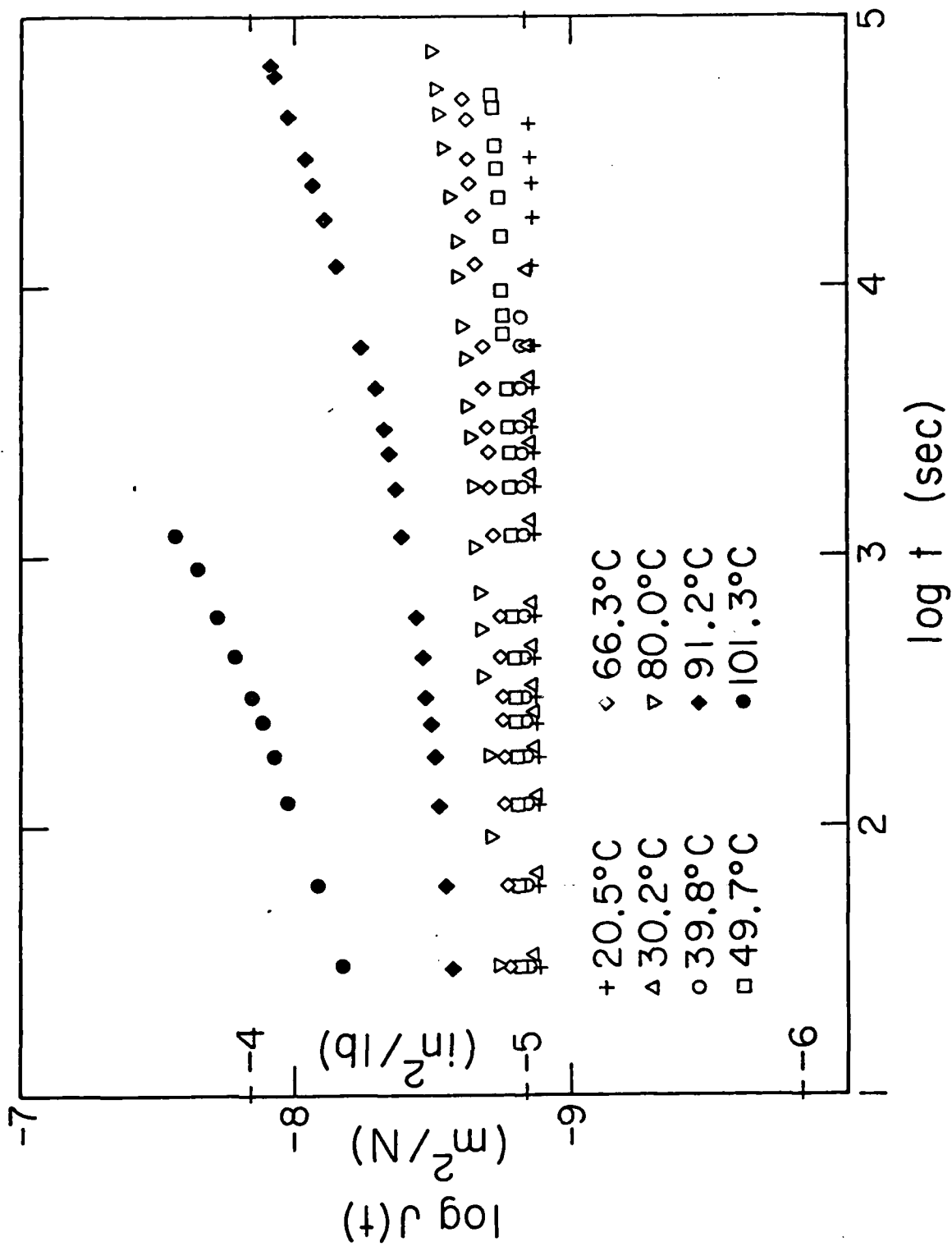
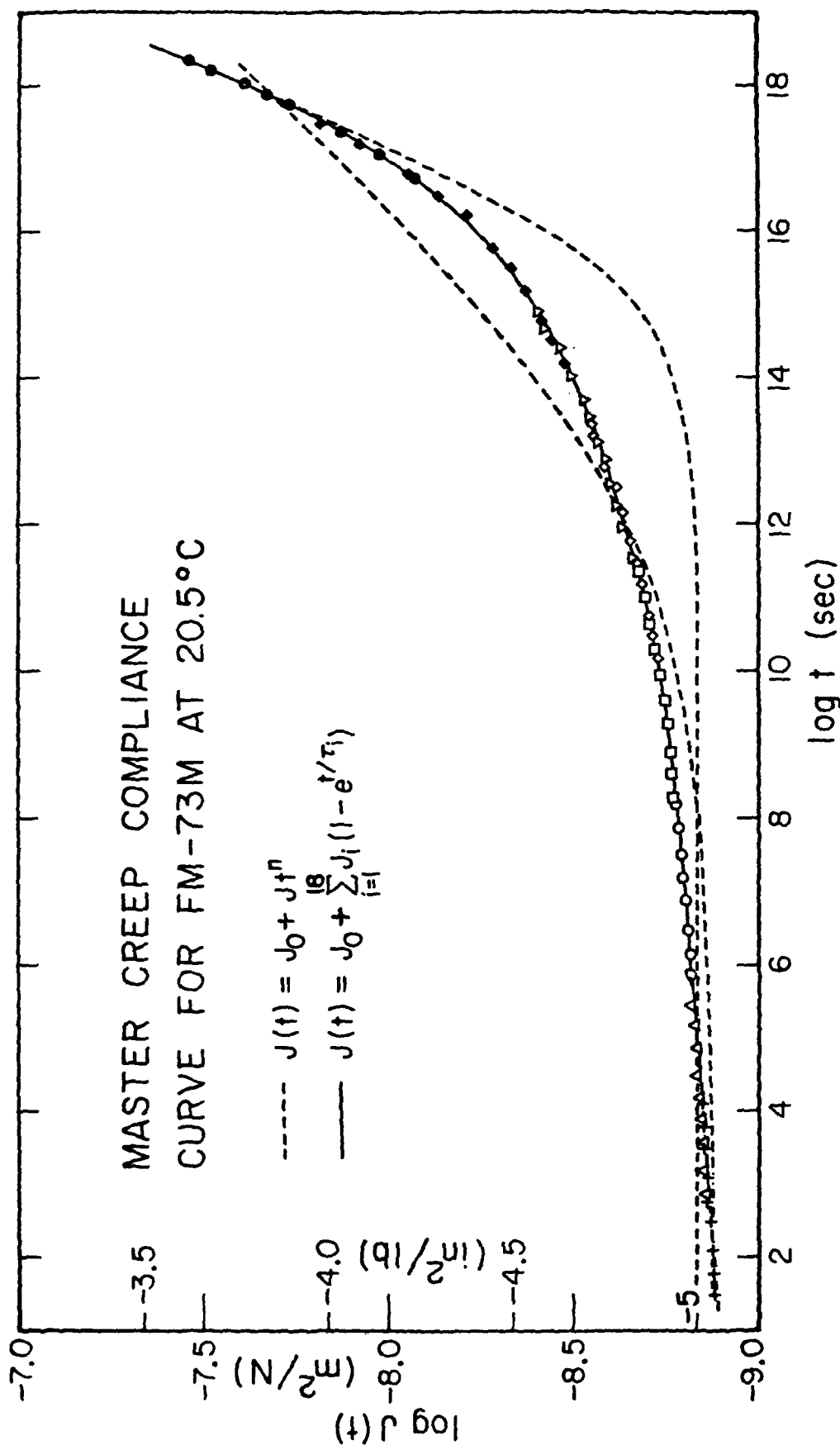


FIG. 2



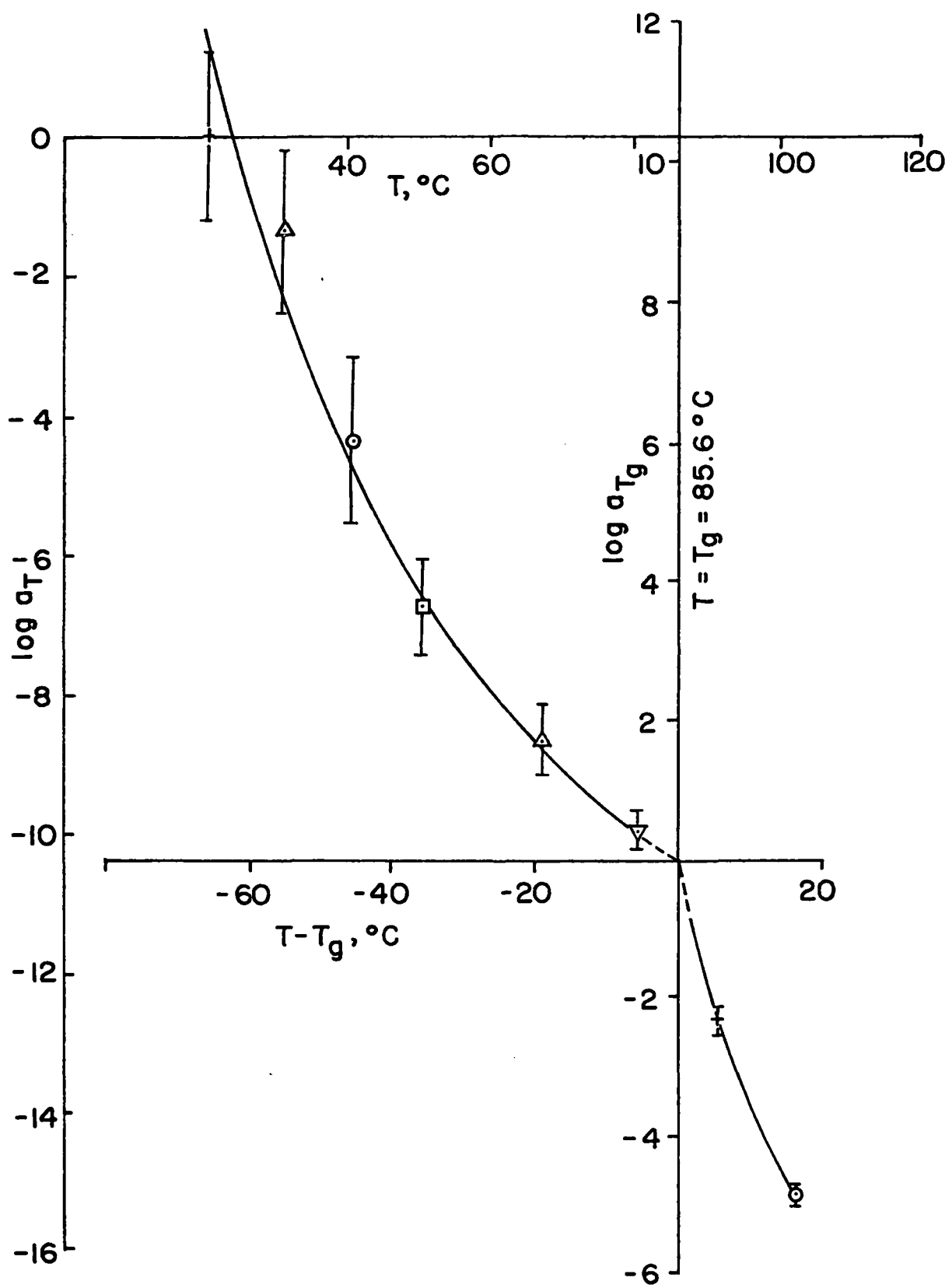
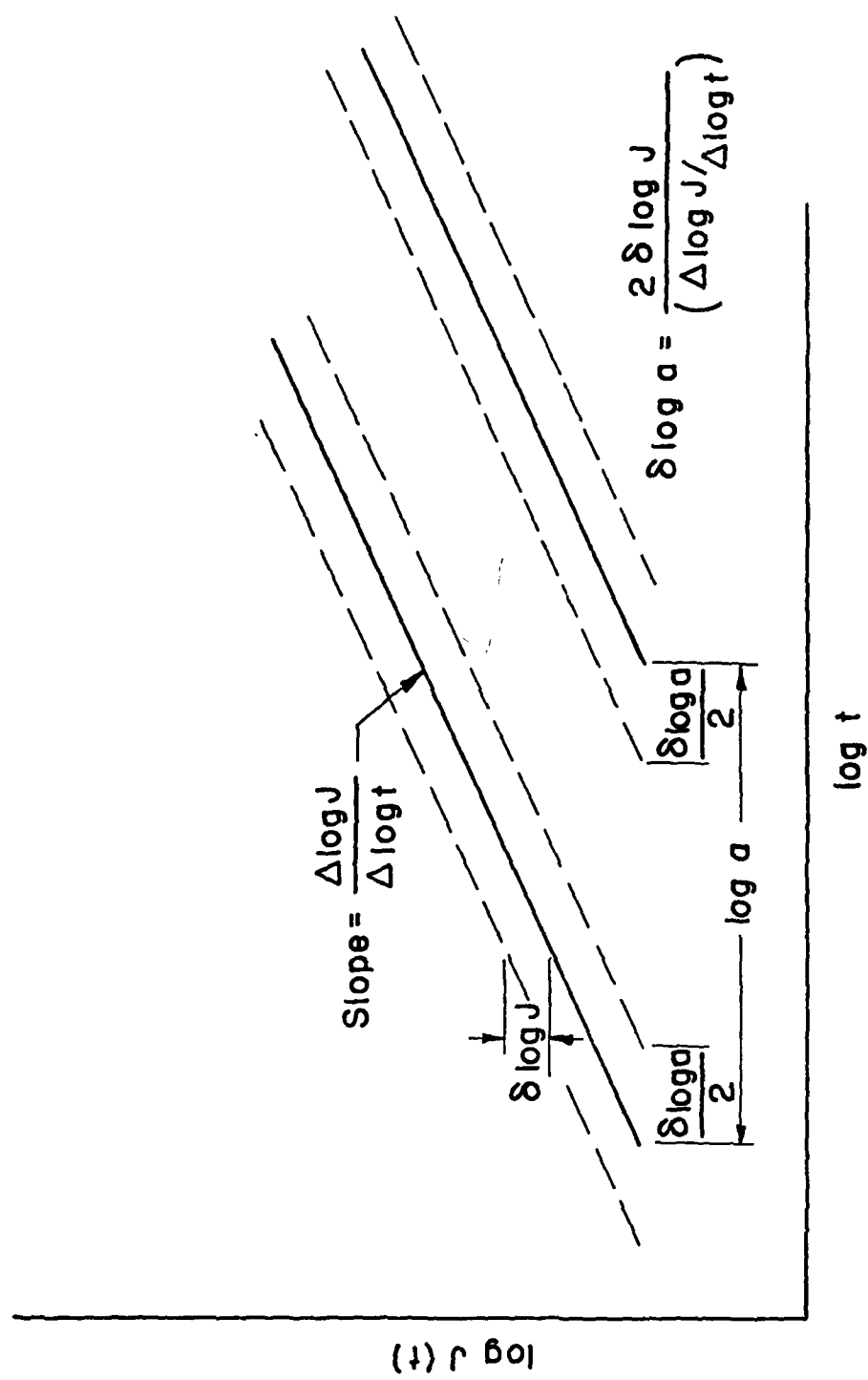
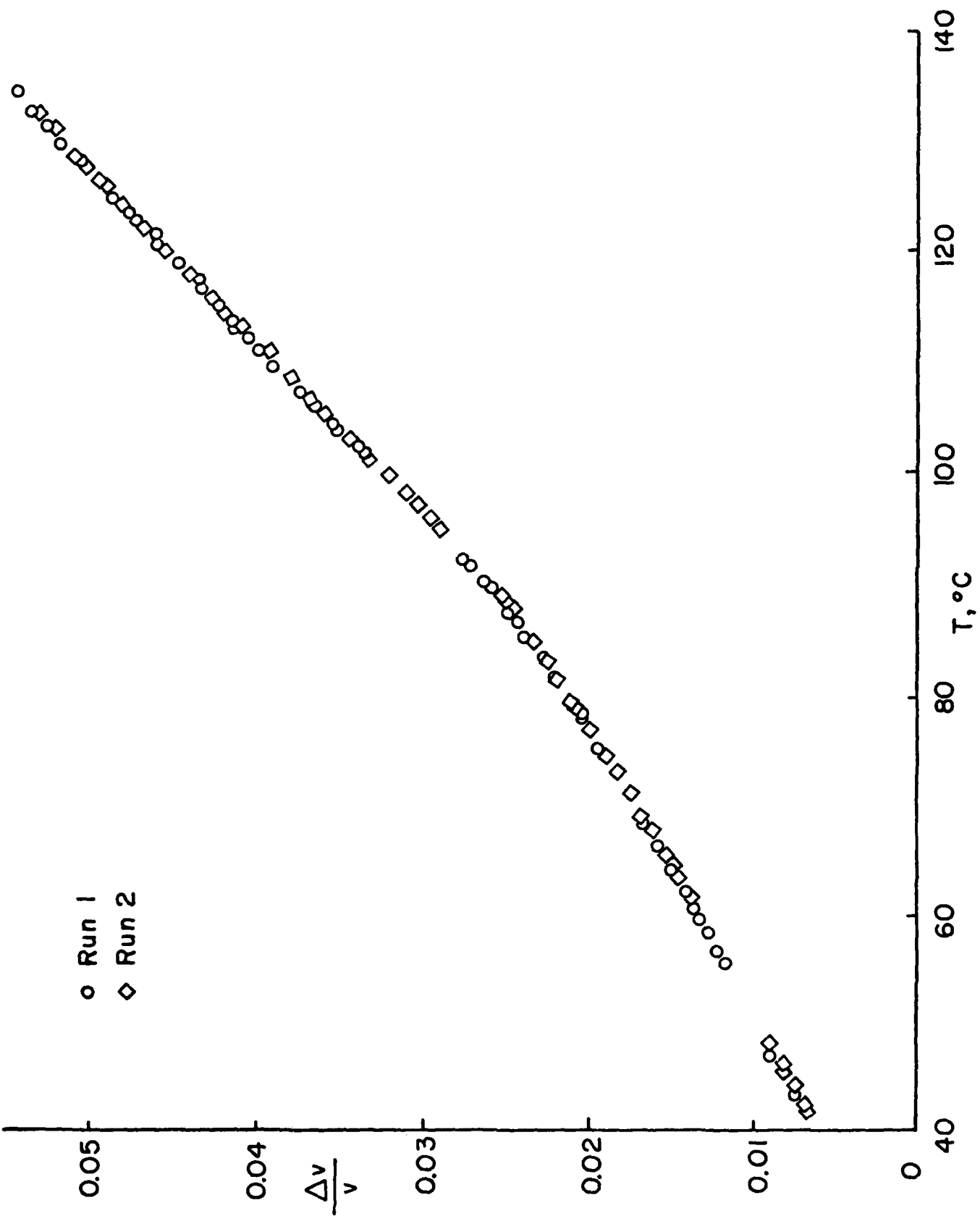


FIG 5

FIG 6





SM 80-21

APPENDIX B

This paper is on the process of
printing for SESA. Original figures
are not available.

CRACK PROPAGATION AT MATERIAL INTERFACES:

I. EXPERIMENTAL TECHNIQUE TO DETERMINE CRACK PROFILES

by

K. Liechti
W. G. Knauss

GRADUATE AERONAUTICAL LABORATORIES
CALIFORNIA INSTITUTE OF TECHNOLOGY
PASADENA, CALIFORNIA

CRACK PROPAGATION AT MATERIAL INTERFACES:

I. EXPERIMENTAL TECHNIQUE TO DETERMINE CRACK PROFILES

1.1 INTRODUCTION

The use of adhesives for structural joints promises several advantages over conventional mechanical fasteners. Substantial savings are possible through weight reduction and in manufacturing costs. Thin as well as contoured sheets can be joined more effectively under reduction of stress concentrations and galvanic corrosion. These advantages are attractive in both the aerospace and automotive industries. Sealants are finding increased use in these as well as the building industry and in a variety of encapsulation applications, including solar photovoltaic cell encapsulation.

These seeming advantages have sometimes been out-weighed in the past because of an apparent low reliability and/or durability. Yet, on closer examination, such seemingly low reliability can usually be accounted for by environmental effects and time dependent processes not considered in common engineering analysis. More thorough structural mechanics considerations, including these effects, are therefore in order.

Structural adhesives are polymers and possess viscoelastic or "time dependent" properties, thus requiring the involvement of the total load history in the life prediction of a structural element. Adhesives are also sensitive to the thermal history (from both thermal dilatational and thermorheological considerations) as well as the moisture history of their service environment. Procedures, based on experience obtained from designing with metals which are generally rate, thermorheologically and moisture insensitive, led to the notion of apparent failure of adhesive joints. This randomness in the failure process is not inherent, but

rather is the result of negligence in considering time, temperature and moisture as contributing factors.

The bonding problem is an old one and we cannot attempt to even briefly review here all the important contributions. Suffice it to point out that two approaches to characterize adhesive strength are practiced if not uniformly accepted today; peel testing and what we wish to call "thickness-averaged" fracture mechanics. Peel testing is achieved with relatively thin adherends which undergo large (often elastoplastic) deformations and yields a measure of (rate dependent) energy expenditure (1, 2, 3).

By contrast, "thickness-averaged" fracture mechanics (4,5,6,7,8), deals primarily with (2 dimensional) plate or beam-like geometries, joined along a line by an adhesive layer. Since the latter is usually thin compared to the thickness of the plates, the thickness of the adhesive layer is deemed negligible, and the plate problem is reduced to the fracture of a homogeneous or bimaterial plate containing a "weak" line, to which geometry fracture mechanics concepts may then be applied. As a result, certain fracture parameters, normally considered material parameters depend then on the bondline thickness.

We are particularly interested in studying the interactive effect of loading normal and tangential to the bondline or joint failure. We use the terminology of "mode I and mode II" for local deformations at the crack tip and reserve "normal and tangential loads" (displacements) when referring to the uniform or overall displacements of the adherends. We also recall that either purely normal or purely tangential loads produce in general both mode I and mode II deformations at the tip of an interface crack, at least when estimated within the realm of linear elasticity theory.

It is a common experimental observation that bonds tend to be very strong under tangential loading and that a relatively small amount of normal loading will seriously impair the "bond strength". (see e.g. ref. 9). The recognition that relatively small normal loads have a significant effect on bond shear carrying ability raises the question whether possibly non-linearity related mode I displacements could govern the unbonding process. Expressed in an extreme way one might ask whether a crack-opening mode properly accounting for non-linear materials behavior and kinematics could control interface crack growth.

The definition of what constitutes an interface crack is not generally clear, for often, if not always, a layer of molecular dimensions may adhere to one of the separated parts. We are here not concerned with such full detail and consider that interface fracture occurs whenever observation with the unaided eye or with low power magnification reveals no substantial residue of adhesive on the adherend. That such interface fracture occurs has been observed recently for low frequency cycle deformation history by Romanko (10) as well as Sykes et al (11) in dry environments.

Our interest in pursuing this work derives then from two considerations; first we are concerned with the detailed mechanics of time-dependent unbonding at interfaces under mode I and II deformations and second we ask specifically for information on the presence of non-linear phenomena and their possible effects on crack propagation. We choose to accomplish this without recourse to analyses that depend on an assumed or approximate constitutive law. We are, consequently, limited to measuring displacement fields. In view of our interest in non-linear phenomena excessively large scale models are ruled out by modelling considerations so that the only appropriate investigative tool is optical interferometry. Crack opening observation by this technique has been previously demonstrated in monolithic fracture specimens (12, 13, 14); however, our unique desire to avoid data that depend on constitutive behavior analyses requires us to control boundary displacements instead of forces to at least the same accuracy as the measurement of the crack opening displacement. Thus, if a bond line of 0.5 μm thickness is used a 1% normal average strain corresponds to 5 μm , and if a resolution of at least 10% is desired one has to be able to contend with displacements on the order of 0.5 μm . This is slightly smaller than the wave length of helium-neon (laser) light (0.63 μm) so that a resolution of 2-4% is feasible. Displacement control needs to be accomplished, therefore, also via optical interferometry.

In this paper we describe primarily the apparatus and techniques required to accomplish these refined measurements and controls. In a second paper (16) we delineate the results on the relative importance of non-linear effects and the measurement evaluation for a crack growth criterion.

2. Loading Frame

In view of the just mentioned requirements on the edge displacements of a bonded joint and their control we now describe the construction of an orthogonal loading device. In fracture testing it is desirable to deal with stiff loading devices in order to avoid energy release from the frame into a fracturing specimen. Therefore, it seemed desirable to design the frame rigidly enough so that 1% energy could be released into the specimen if a high strength bond were effected with a brittle adhesive. For this reason a hydraulic system appeared unsuitable though its control would have been relatively easy while a screw type design presented overpowering backlash problems. However, the use of thermal dilatation provided just the right "mechanical" advantage for absolute control of the required displacements.

Figure 1 shows the device which is constructed of 5x5 H I-beams and the mounting of the model joint. Motion normal to and tangential to the bondline is independently controlled in the following way. Each normal displacement actuator tube is connected to a tangential actuator tube by connecting plates which also serve as specimen grips. The normal actuator tubes are heated or cooled independently from the tangential actuator tubes. Because the tubes are connected, they will bend slightly and will, in general, cause a rotation of the adherends. However, the symmetry of the arrangement and equal heating or cooling within each pair of normal and tangential actuator tubes ensures that the adherends rotate to the same degree, thus leaving the adherend edges which define the bond thickness parallel. This bending of the tubes gives rise to small secondary normal and tangential displacements in addition to the primary thermal dilatation displacements; they are, however, two orders of magnitude smaller and are easily corrected for in the control feedback loop described later.

The actuator tubes are made of stainless steel tubes three inches in external diameter having a half-inch wall thickness. Heating of the actuator tubes is provided by band heaters wrapped around their outside. Cooling is achieved through spraying vaporized liquid nitrogen uniformly onto their inside. Because of the thermal mass involved and the need to provide uniform temperature fields, the rate of relative displacements was limited to 1 $\mu\text{m/sec}$, (5 sec/%strain) which turned out to be sufficient for the small displacements encountered in this study.

3. Control of Adherend Displacements

The displacements of the adherends are monitored by two Michelson interferometers mounted on the specimen close to the bondline. Pickup points of the interferometers were epoxied into holes drilled into this 1/4 inch thick glass adherends (see figure 2 for location). The interferometers are arranged such that one measures displacements normal to the bondline while the other measures tangential displacements. The compact arrangement of the double interferometers is shown in figures 5 and 6.

The Michelson interferometer produces a fringe pattern of concentric light and dark circles. As the path difference between the split beams changes (beams A and B in figure 5, for example), these circular fringes expand or contract as the path difference increases or decreases. If the circles are expanding, a new circle appears at the center each time the path difference changes by a half-wavelength of the monochromatic light source. For a contracting pattern, circles disappear at the center. A stationary, centrally placed photodiode converts this varying light intensity (as the path difference changes) into a sinusoidally varying voltage signal when suitably amplified. A second photodiode placed somewhat less than a quarter of a fringe spacing from the center produces a similar voltage signal which is, however, out of phase with the centrally located photodiode signal by less than $\pi/2$. The sign of the phase difference is used to determine the direction of the path difference change and therefore whether to count up or down, i.e. whether the adherends are separating or moving together in the normal displacement case with a like logic applying to the tangential displacements.

The amplified signal of the photodiodes is sampled by an analog-to-digital converter module in an 8-bit microprocessor. Data sampling and conversion, phase comparison and fringe counting, displacement history prescription and control decisions

in a closed feedback loop are all software controlled. The control program is arranged such that most of the time is spent sampling the photodiode signals, awaiting the occurrence of a fringe. As soon as the fringe is registered, the sign of the phase difference between the photodiode signals is checked, and the fringe accordingly counted up or down. This current count (or displacement) is then compared with the prescribed displacement (set point) for that instant. The difference between the current and prescribed displacement is then used to decide whether to activate returns to the data sampling. The time spent in phase comparison, set point comparison and signalling the heaters or coolers is very much smaller than that spent in the sampling of the photodiode signal so that the chances of missing a fringe are very small.

It was necessary to develop an algorithm for effectively counting fringes. The main difficulty arose because the fringe rates varied over a large range, namely from about 10^{-4} Hz (nearly steady state) to 2 Hz. The use of slope changes to detect maxima in order to count fringes turned out to be very noise sensitive. A zero crossing amplitude based algorithm was therefore developed which was much less noise sensitive, more efficient and gave a one half fringe resolution ($\lambda/4 = 0.16 \mu\text{m}$).

A real time module in the microprocessor allows us to prescribe time-varying applied displacement histories. Any prescribed displacement history can be preprogrammed into the computer, limited only by the thermal response (0.2% strain/sec) of the actuator tubes, sampling rate and measurement and control resolution.

The heaters are proportionally controlled by TRIAC solid state relays which, in turn, are controlled by the analog signals (0 to 10 volts corresponding to 0 to 100% power) derived from the microprocessor. The coolers are controlled in an on-off

mode by solenoids activated by the control program. In view of the small displacements involved, it turned out that proportional control of the heaters was sufficient to guarantee the stability of the system. Some development was necessary to determine optimum heating rates in order to minimize overshoot but the flexibility of software control was really emphasized here. The set point can be controlled to within 6.25×10^{-6} (0.16 μm), the resolution limit imposed by counting every half fringe. All factors combined to provide a maximum displacement rate of 1 $\mu\text{m/s}$.

4. Specimen Preparation

The specimen configuration developed under a series of constraints relating to compatibility with the loading frame, surface finish and flatness as well as availability; the final form is shown in figure 2. The adherends are of pyrex glass (BK7) and the adhesive is a polyurethane elastomer, Solithane 113*. This choice evolved from several considerations. The crack profile measurement technique required optically clear and flawless adherends, the adhesive faces of which would be ground flat to within a quarter wavelength of light per inch. Plexiglass does not fulfill this requirement. The adhesive used does not exhibit objectionable irreversible deformations and its index of refraction is close to that of the adherends, this latter property aided significantly in determining the location of the crack front. Further advantage of the material combination derived from the low adhesive strength between them which ensured ready interfacial separation, the object of our study. Moreover, the adhesive could be cured at room temperature to eliminate stresses due to thermal shrinkage although those associated with 1% volume shrinkage during cure could not be eliminated except through testing at elevated temperature. (see below).

* Composition 60% prepolymer, 40% catalyst by weight (17).

However, in spite of extensive experience with this polymer in our laboratory we arrived at this choice only after rather extensive experimentation with polymers of higher glass transitions, notably Araldite. Yet the dominant requirement virtually dictated the choice of an elastomeric adhesive for this study. Recall from the introduction that we wish to check the validity of current linear stress analyses and that we wish to take no recourse to any analysis for data reduction (such as, eg, in compliance measurements of cracked bodies). Measurements are therefore to be made of the crack profile as well as the relative displacements of the adherends. The latter measurements are made at the pick-up locations of the Michelson Interferometers, located 0.093 inches from the bondline. These displacements are assumed to be those actually occurring along the whole bondline which statement is equivalent to assuming that the adherends are rigid compared to the adhesive. To assess the relative order of magnitude of material stiffness so as to justify this assumption, the specimen geometry was examined through a finite element analysis*. Because the analysis provided only a guide for the design of the experiment through suitable material choices, it does not therefore compromise the independence of the experiment from an incomplete constitutive characterisation. The crack profile measurements per se required no material assumptions and were therefore completely independent of this analysis.

In this numerical examination the boundary conditions imposed by the loading frame were closely followed. It was found that, for a ratio of adherend to adhesive modulus of 10^4 , an error on the order of 4% was incurred at the specimen center if one assumed that the interferometer indication represented the same constant displacement along the entire edge of the adherend. For the case where

* We wish to thank Professors E.B. Becker and M. Stern for the use of the finite element code, TEXGAP, at the University of Texas at Austin as well as their helpful advice.

the specimen is fully gripped along its width, the error is reduced to 0.5%.

The glass/Solithane material combination chose results in a sufficiently large modulus ratio of 2×10^4 so that the assumption of rigid adhered displacements appears justified. We also point out in passing that the glass adherends were ground with a 42° wedge angle (figure 2) to eliminate extraneous light interference that might result from nearly parallel adherend faces.

Room temperature cure avoided thermal shrinkage stresses but required long cure times. Multiple specimens were therefore cast in a fixture as shown in figure 3; two adherends are clamped across the specimen thickness by two flat jig plates with the gap between the adherends set by spacers defining the bond thickness. Once the adherends are clamped, the spacers are removed and injector nozzles attached to the jig plates, the nozzles being aligned with the bond thickness. Teflon tape is attached to one of the adherends on the face defining the adhesive adherend interface prior to casting. The Solithane mixture is thoroughly mixed, degassed and then pressure injected into the gap, sealed and cured at room temperature for one week. Casting four specimens simultaneously from the same mixture decreased the possibility of material property and adhesive strength variations between specimens. For avoiding bubbles in the bond line, pressurized injection was found to be far superior to pouring or sucking the Solithane into the gap.

Once the specimen has cured it is glued to the loading device grips while still being held in the casting jig using a plastic steel epoxy (Devcon). Since the specimen is held fixed by the casting jig, the cure shrinkage of the plastic steel cannot introduce any initial loading. However, to facilitate specimen removal from the test frame following a test, mold release is applied to the sides of the adherends so that the steel epoxy forms a less than perfect bond. The glass

adherends could then be reused.

The steel epoxy is allowed to cure only (at room temperature) for a minimum of 8 hours; only then is the casting jig removed.

To initiate a crack, a 0.003 inch diameter wire is pulled along the Solithane - Teflon tape interface like a cheese cutter a small amount beyond the end of the tape and then the wire is removed. This procedure assured a clean interface separation beyond the end of the Teflon inserts. The Teflon tape serves to protect the glass adherend surface from scratching by the wire as well as to indicate the initial crack length. (Figure 4).

It was sometimes found that, when a crack was initiated from only one side, another crack started from the opposite edge of the specimen anyway, but always on the opposite interface. Worse still, it sometimes grew in preference to the wire-initiated crack, causing loss of a specimen. Therefore, cracks are initiated from both ends of the specimen along the Glass - Solithane interface close to the profile measurement device as indicated in figure 4. It should be remembered that the crack surface on the adhesive side is a curved surface while the glass adherend side is flat. This "cutting" procedure guaranteed thus also that the incident light beam penetrated the distortion free, glass-to-air surface first.

5. Crack Profile Measurement System

Crack opening interferometry has been used to measure directly the normal deformations in the crack front regions of cracked monolithic bodies (12). These measurements quantify features of fracture processes occurring over very small dimensions. The crack face separation can be resolved to within at least half a

wavelength of the viewing light at any point in the field of view (for sufficiently small profile gradients). In linearly elastic monolithic fracture studies, this technique has been employed to study the relationship between the opening mode displacement and stress intensity factors of complex fracture problems where analysis is not tractable (13, 15). However, the technique can also be applied to fundamental fracture studies to relate loading and crack propagation effects as well as time dependent aspects to changes in crack profile. A practical problem with the method is that the crack faces need to be quite planar for interference effects to occur, a situation which does not often arise in the fracture of monolithic materials. The method is, however, particularly suited to the study of interfacial cracks because the adherend surface forming one of the crack faces can be carefully controlled for flatness.

For convenience, a laser light source separate from the Michelson interferometers is used to measure the adherend displacements. Extensive mirror arrangements channel the incident laser beam to the specimen and beams reflected at the crack faces into a microscope. A closed-circuit T.V. camera is mounted on the microscope and the changing fringe patterns are then recorded on video tape and displayed on a monitor. The microscope is mounted on an orthogonal micrometer traverse arrangement which allows tracking of the crack motion. Figure 7 shows a schematic of the crack profile measurement system.

When the coherent and monochromatic beams reflected by each crack face are combined, an interference pattern is formed which consists of light and dark fringes corresponding to loci of constructive and destructive interference, respectively. In general, for normal incidence and an airfilled crack, each consecutive fringe of extinction corresponds to a change in crack face separation of a half wavelength for the incident light. At a given fringe of extinction, m say, counted from the crack tip, the crack face separation distance, h , along that fringe is given by

$$h = m \lambda/2 \quad m = 1, 2, \dots$$

For sufficiently small angles between the crack faces, fringes can be observed with the naked eye. A microscope is necessary to resolve the higher fringe densities produced by larger angles. It should be noted here that manual evaluation and reduction of the fringe patterns is a slow and painful task. However, the expected incorporation of a video digitizer to the crack profile measurement system will greatly alleviate the data reduction task and allow the generation of the full three-dimensional shape of the crack rather than generating the profile along a single central, lengthwise scan of the crack, the procedure used to date.

In connection with interpreting crack opening interferograms two issues need to be discussed: (1) crack front location and (2) fringe resolution and crack profile slope limits.

(1) Crack front location

Figures 8a and 8b depict two possible cases for the location of the crack front ($x = 0$). Note that the shaded areas correspond to the area ahead of the crack front which is still bonded and also to fringes of extinction and further that the fringe spacing, f_s , is the distance between a light and dark fringe. Assume the fringe thickness is the same as the fringe spacing (a limiting assumption). In figure 13a, where the crack front lies in an area of forming but not yet fully formed bright fringe (i.e. the crack front is less than $1.5 f_s$ away from the first fringe of extinction) there is no ambiguity in the determination of the crack front location. If the crack front lies in an area of the forming zero order fringe of extinction (figure 8b), it cannot be seen because destructive interference is occurring and its location is therefore uncertain. The crack front could be as much as $2.5 f_s$ away from the first order fringe of extinction (assuming the worst case of a linear crack profile; the crack front would be closer for a power law profile). In taking the crack front to be at the boundary of the zero and half order fringe, the error in crack front location could be as much as one fringe spacing. In cases where the fringe spacing is equal to the critical fringe spacing (or minimum resolvable fringe spacing) the error is on the same order as the fringe location resolution. For lower gradients, either at low load levels or for stiff adhesives, this could be considerable. In order to avoid this uncertainty,

determination of the crack front location is only made under the conditions of the case illustrated in figure 8a.

2. Resolution limits

The spatial resolution in the crack plane provided by the microscope is $6.50 \mu\text{m}$ (256×10^{-4} inches). This dimension defines the resolution of the fringe and crack tip location. Fringes which are less than $16.26 \mu\text{m}$ (64×10^{-4} inches) apart cannot be distinguished from one another and we call this fringe spacing the "minimum fringe spacing" because the crack profile cannot be determined in areas where the fringe spacing is less than this minimum. The change in crack profile height between a light and a dark fringe is $\lambda/4 = 0.16 \mu\text{m}$ (6.25×10^{-6} inches). The minimum fringe spacing therefore determines the maximum profile gradient α_c that can be measured. In the present set up, then, $\alpha_c = 33.5$ minutes, a value which could be increased only by decreasing the working distance and increasing the magnification of the microscope.

The gradient of a parabolic crack profile, predicted by linear elastic fracture mechanics close to the crack front approaches angles of $\pi/2$. The crack profile measurement system here is limited to angles of 33.5 minutes, making its applicability, at first sight, questionable. However, it must be remembered that the crack face separation is very small (on the order of a few wavelengths of light). Thus, if a parabola does indeed describe the crack profile, then it is very long and thin with large changes in profile gradients occurring within a small distance from the crack front. In fact, this large change in profile gradient must occur between the first order fringe of extinction, corresponding to a crack face separation of $0.32 \mu\text{m}$ (1.25×10^{-5} inches) and the crack tip.

The question needs to be raised, therefore, as to whether the first order fringe of extinction corresponds to a crack face separation of $\lambda/2$. The underlying assumption there is that the crack profile does not have the profile shown in figure 13c. In that case, there could be a very steep front effectively providing a step discontinuity in the crack face separation, h_0 say. To check this possibility, observations of crack closure under a normal compressive applied displacement were made. Crack closure occurred through a decrease in length rather than through a simultaneous total contact of the two crack faces. The fringes were easily resolved

right up to the crack front. It is unlikely that the profile depicted in figure 13c could be supported under a compressive load and this type of closure. We therefore deduce that the first observable fringe does indeed correspond to the first order fringe and a crack face separation of $\lambda/2$.

We make a distinction here between the "first observable fringe" and the "first resolvable fringe". The first observable fringe is taken to be the first order fringe of extinction. Under conditions of crack closure, sufficiently low loads or a stiff adhesive, the first observable fringe and the first resolvable fringe are the same. However, under higher loads the fringe density can become so high that fringes near the crack front cannot be resolved by the microscope. Thus while the crack front can be clearly discerned, there is an area of brightness behind the crack front where the fringe spacing is less than the minimum fringe spacing and appear to be superimposed on one another. The first fringe of extinction behind this bright area is taken to be the first resolvable fringe and is not the first order fringe. The question then arises as to how to determine the order of the first resolvable fringe in these high fringe density cases. Loading is always commenced from a situation in which a first observable fringe is identified. The changing fringe patterns under loading are continuously recorded on the video system. The order of the first resolvable fringe at any time can then be determined by counting the number of fringes that pass a given location, well removed from the crack front, during that time.

Figure 9 shows a series of photographs of a stationary crack in a glass-Solithane joint taken at different normal load levels. The width of the picture covers slightly more than a third of the specimen thickness. The crack, having the finger-like outline is centered on the specimen mid-thickness. The dark area surrounding this finger indicates the region which is still bonded. Thus the crack does not extend all the way through the thickness but rather displays a finger or tunnelling mode of fracture. The interference pattern used to generate the profile is a series of fringes contained within the crack outline. The fringe density increases as the applied normal displacement is increased to the extent that fringes are no longer distinguishable immediately behind the crack front.

A single, central scan behind the crack front produces a profile along that line. A series of such scans for different levels of applied displacement is shown in figure 10. The profile data show the fringe location resolution of $6.5 \mu\text{m}$ (2.50×10^{-4} inches) are very consistent and allow precise measurement and evaluation. The distance from the crack front to the first resolvable fringe varies from 0.076 mm (0.003 inches) at zero load (its order was established by scanning further behind the crack front than one field of view allows) to 0.159 mm (0.00625 inches) for an applied normal displacement of $6 \mu\text{m}$ (2.375×10^{-4} inches).

Concluding Remarks

Let us summarize the findings of the applicability of the crack opening interference method to the measurement of the unbond profiles in adhesive joints and the requirements it places on the measurement and control of the displacements applied to the joint. While the resolution of the method is insufficient to fully resolve the high deformation gradients when the adhesive has low modulus and is hardly compressible, the restriction is not severe, and the method has been successfully developed for the measurement of unbond profiles in carefully prepared adhesive joints. The loading device constructed to independently apply orthogonal boundary displacements does so to within $0.16 \mu\text{m}$, making it completely compatible with the displacements measured by the crack opening interference method. Due to the high precision of the measurements that are possible, a sound basis for examining and modelling the failure response of adhesive joints is provided. The exploitation of that capability is discussed in a companion paper (16).

REFERENCES

1. Bikerman, J.J.: Experiments in Peeling, *J. Appl. Poly. Sci.*, 2 (1959) pp. 216-224
2. Kaelble, D.H.: Peel Adhesion, *Adhesives Age*, May 1960, pp. 37-42
3. Kobatake, Y. and Inoue, Y.: Mechanics of Adhesive Joints, Part IV: Peeling Test, *Applied Scientific Research (A)*, 8 (1959) pp. 321-338.
4. Ripling, E.J.; Mostovoy, S. and Patrick, R.L.: Measuring Fracture Toughness of Adhesive Joints, *Material Research and Standards*, March 1964, pp. 129-134
5. Williams, M.L.: The Centinuum Interpretation for Fracture and Adhesion, *J. Appl. Poly. Sci.* 13 (1969) pp. 29-40.
6. Jemain, W.A. and Ventrice, M.B.: The Fracture Toughness of Adhesive-Bonded Joints, *J. Adhesion*, 2 (1971) p. 106.
7. Ripling, E.J.: Corten and Mostovoy, S.: Fracture Mechanics: A Tool for Evaluating Structural Adhesives, *J. Adhesion*, 3 (1971) pp. 107-123.
8. Mostovoy, S., Bersch, C.R and Ripling, E.J.: Fracture Toughness of Adhesive Joints, *J. Adhesion*, 3 (1971) pp. 125-144.
9. Stone, S.E.: Westmann, R.A. and Fourney, M.E.: Analytical and Experimental Studies in Adhesive Mechanics, UCLA-ENG-7556 (1975), Univ. of Calif., Los Angeles.
10. Romanko, J.: Behavior of Adhesively Bonded Joints under Cyclic Loading, AGARD-LS-102- Bonded Joints and Preparation of Bonding 4-1 (1979).
11. Sykes, J.L.: Greene, G.W. and Chow, C.L.: Experimental Techniques and the Mixed-Mode Fracture of Adhesive Joints, *VDI Berichte*, 313 (1978) pp. 503-509.
12. Sommer, E.: An Optical Method for Determining the Crack Tip Stress Intensity Factor, *Engng. Fract. Mech.* 1 (1970) p. 705.
13. Packman, P.F.: The Role of Interferometry in Fracture Studies, in Experimental Techniques in Fracture Mechanics 2, ed. Kobayashi, SESA Monograph Series (1975).
14. Patoniak F.J., Grandt, A.F., Montulli, L.T., Packman, P.F.: Fatigue Crack Retardation in the Closure in Polymethylmethacrylate, *Engineering Fracture Mechanics*, Vol. 6, No. 4, 1974, pp. 663-670.
15. Crosley, P.B., Mostovoy, S. and Ripling, E.J.: An Optical Interference Method for Experimental Stress Analysis of Cracked Structures, *Engng. Fract. Mech.*, 1 (1971) pp. 421-433.

16. Liechti, K. and Knauss, W.G.: "Crack Propagation at Material Interfaces: Experiments on Mode Interaction", California Institute of Technology, Pasadena, California, 91125, GALCIT Report SM 80-21.
17. Mueller, H.K. and Knauss, W.G.: "The Fracture Energy and Some Mechanical/Properties of a Polyurethane Elastomer", GALCIT SM 69-4, California Institute of Technology, Pasadena, CA 91125 (1969).

LIST OF FIGURES

- 1a. 1b. Thermally Actuated Servo Loading Device
2. Specimen Mounting
3. Specimen Casting System
4. Crack Initiation Procedure
5. Michelson Interferometer Arrangement
6. Michelson Interferometers
7. Crack Profile Measurement System
8. Crack Front Location
9. Interference Fringe Patterns of an Interface Crack
at Successive Normal Load Levels
10. Crack Profiles for Different Applied Normal
Displacement

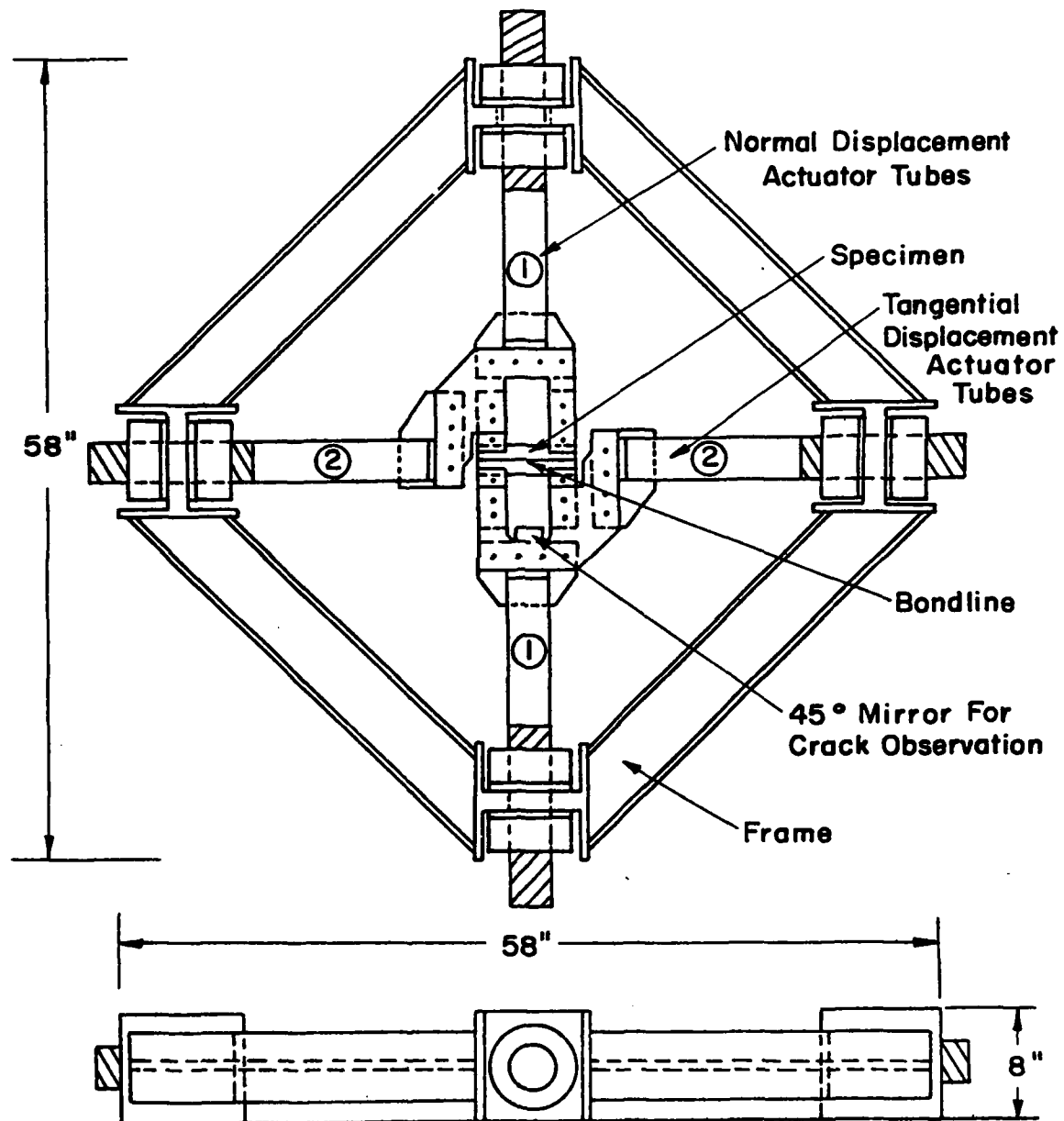


Figure 1a

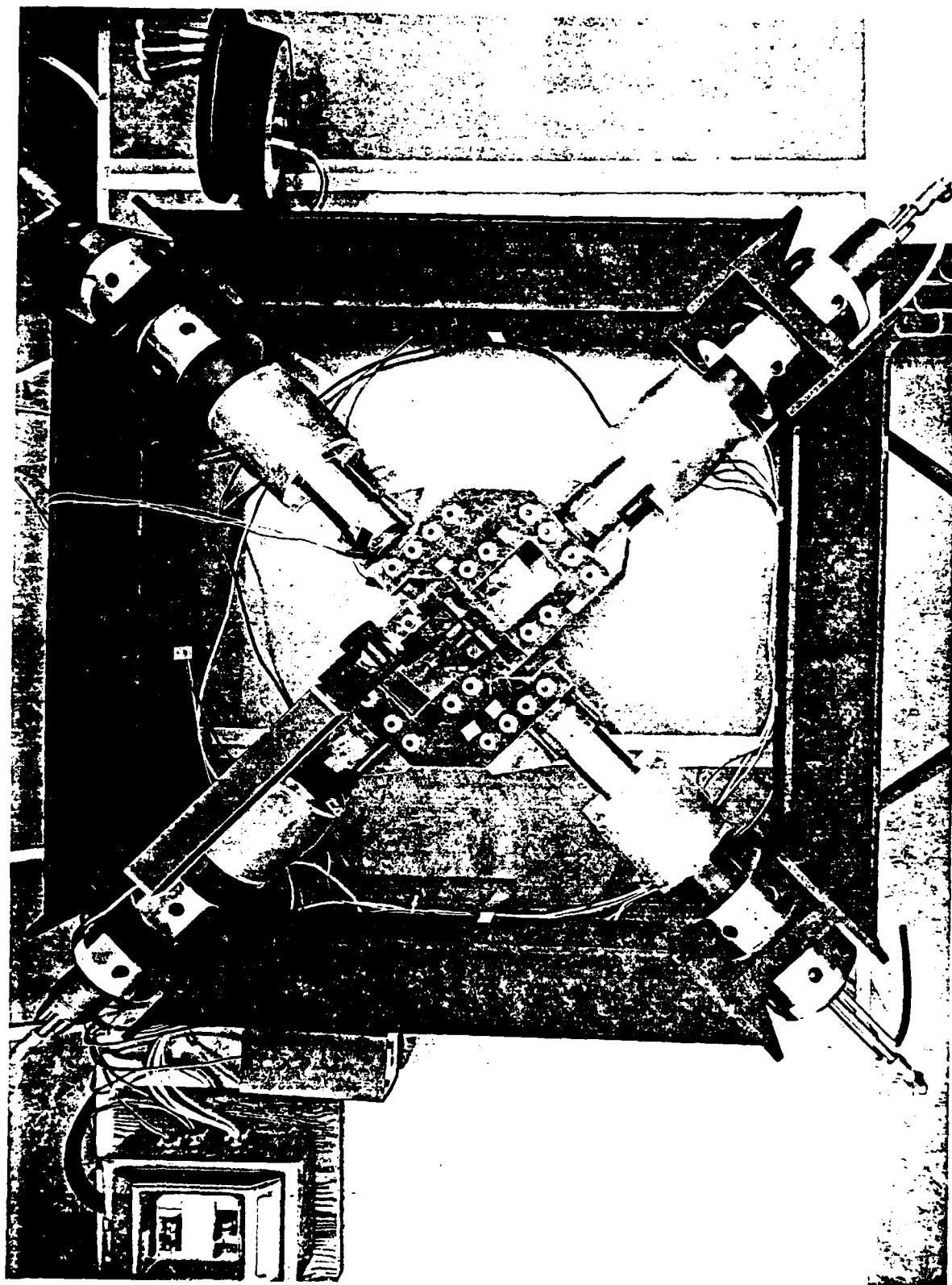


Figure 1b

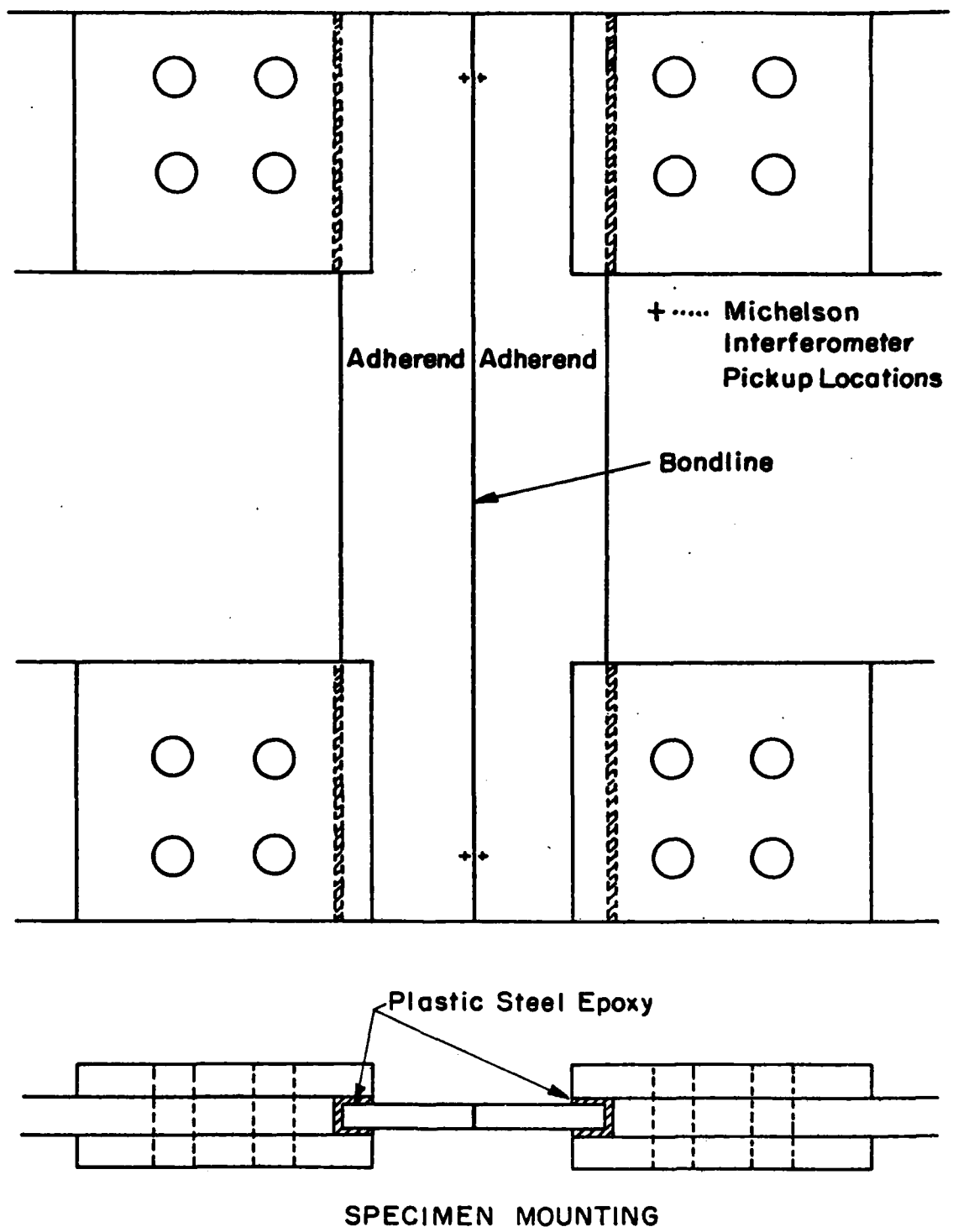


Figure 2

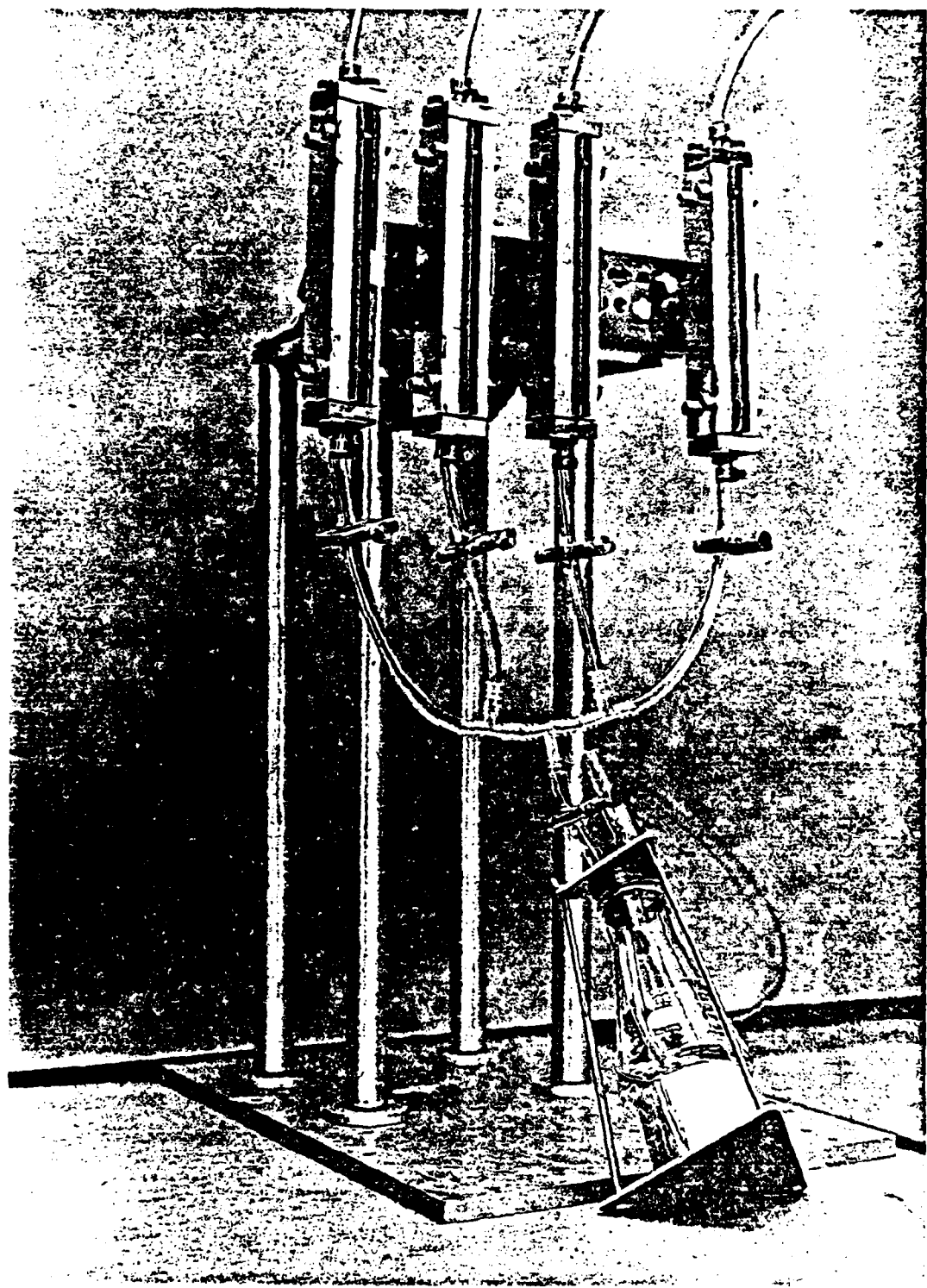
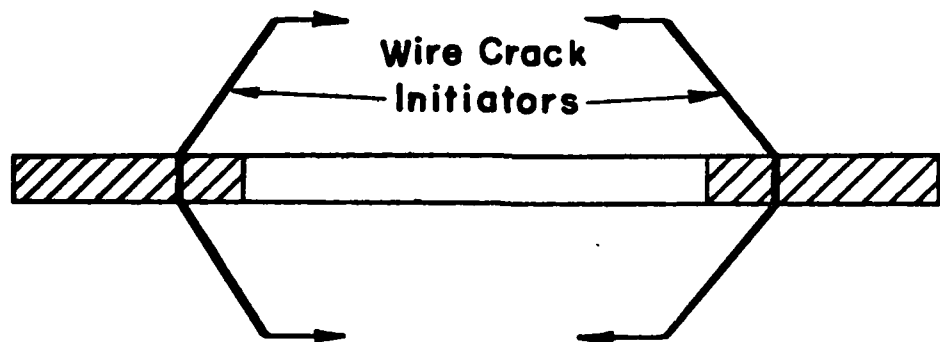
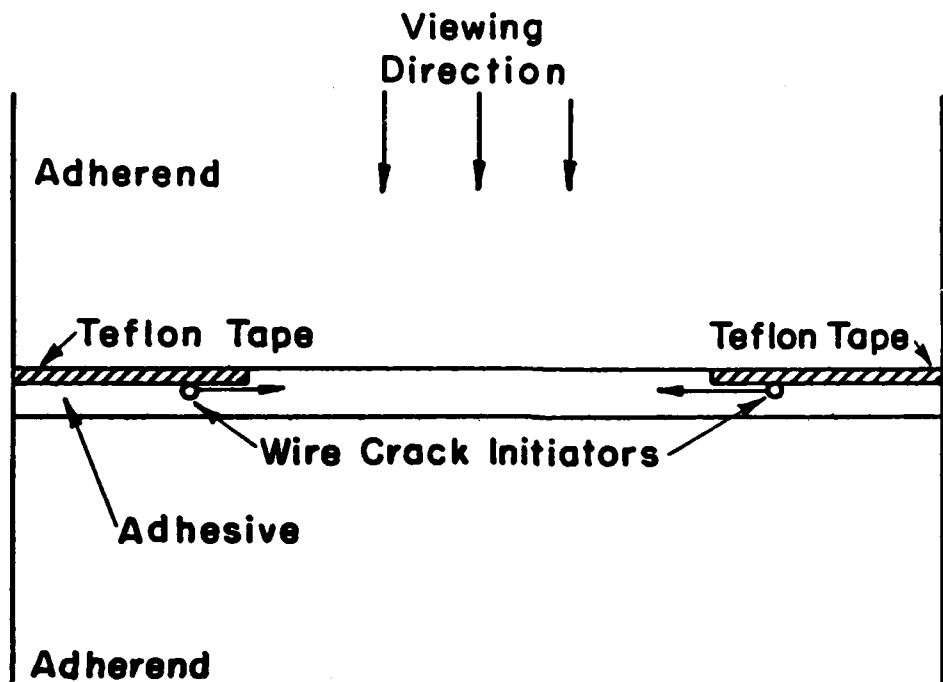


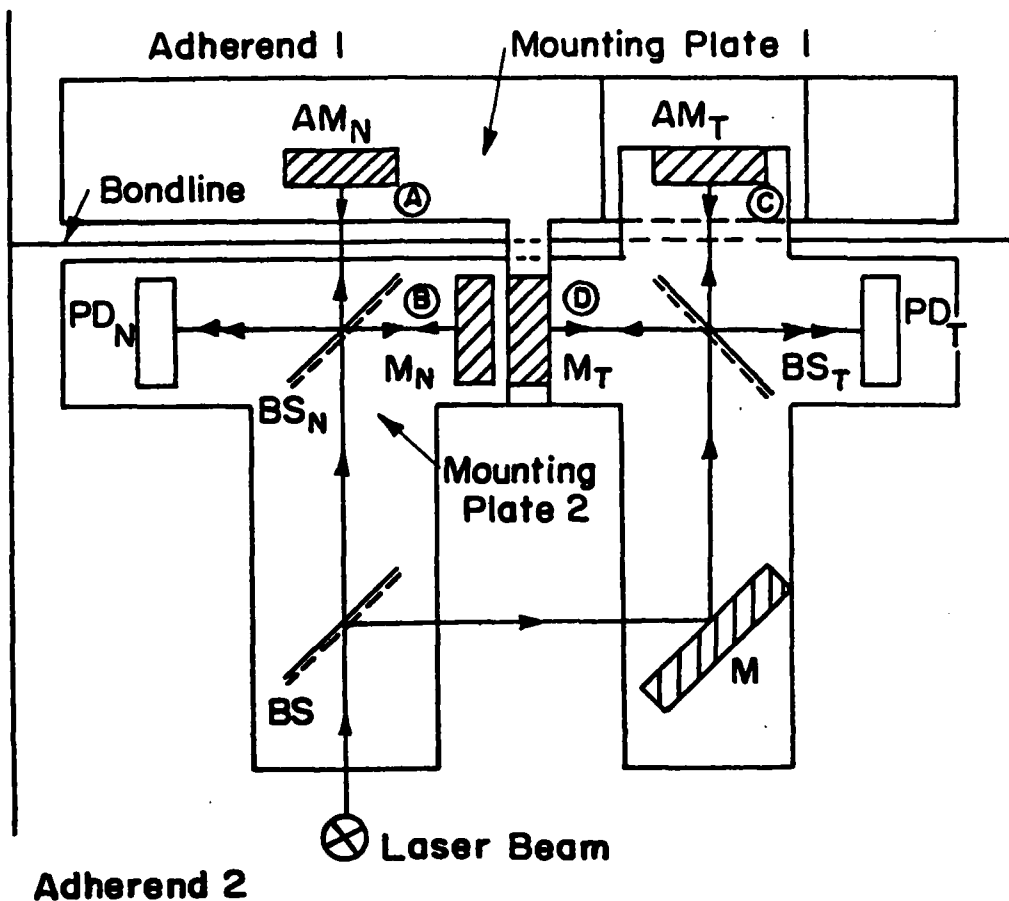
Figure 3



**To Initiate A Crack From Each Edge Of The Specimen,
A 0.003 " Diameter Wire Is Inserted At The Teflon
Adhesive Interface At The Specimen Edge And Pulled
Towards The Centre, Stopping At The End Of The Teflon.**

CRACK INITIATION PROCEDURE

Figure 4



MICHELSON INTERFEROMETER ARRANGEMENT

Abbreviations: M = Mirror, AM = Adjustable Mirror, BS = Beam Splitter, PD = Photodiode Pair. Subscripts "N" and "T" refer to elements of the interferometers measuring displacements normal to and tangential to the bondline, respectively. Elements AM_N and M_T are attached to adherend 1 through mounting plate 1. Mounting plate 2 connects all other elements to adherend 2. Any displacement is resolved into its components normal to and tangential to the bondline by changes in path difference occurring between beams (A) and (B) and beams (C) and (D), respectively.

Figure 5

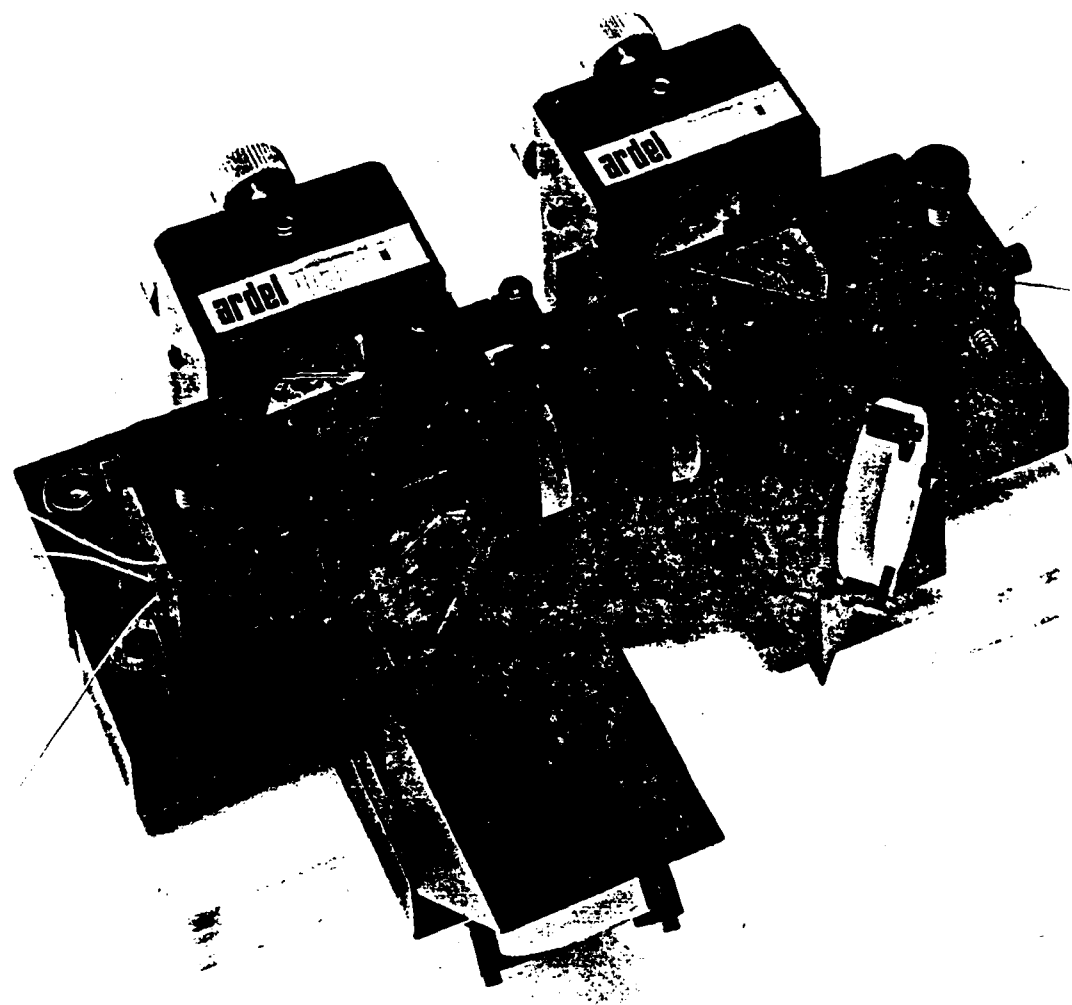
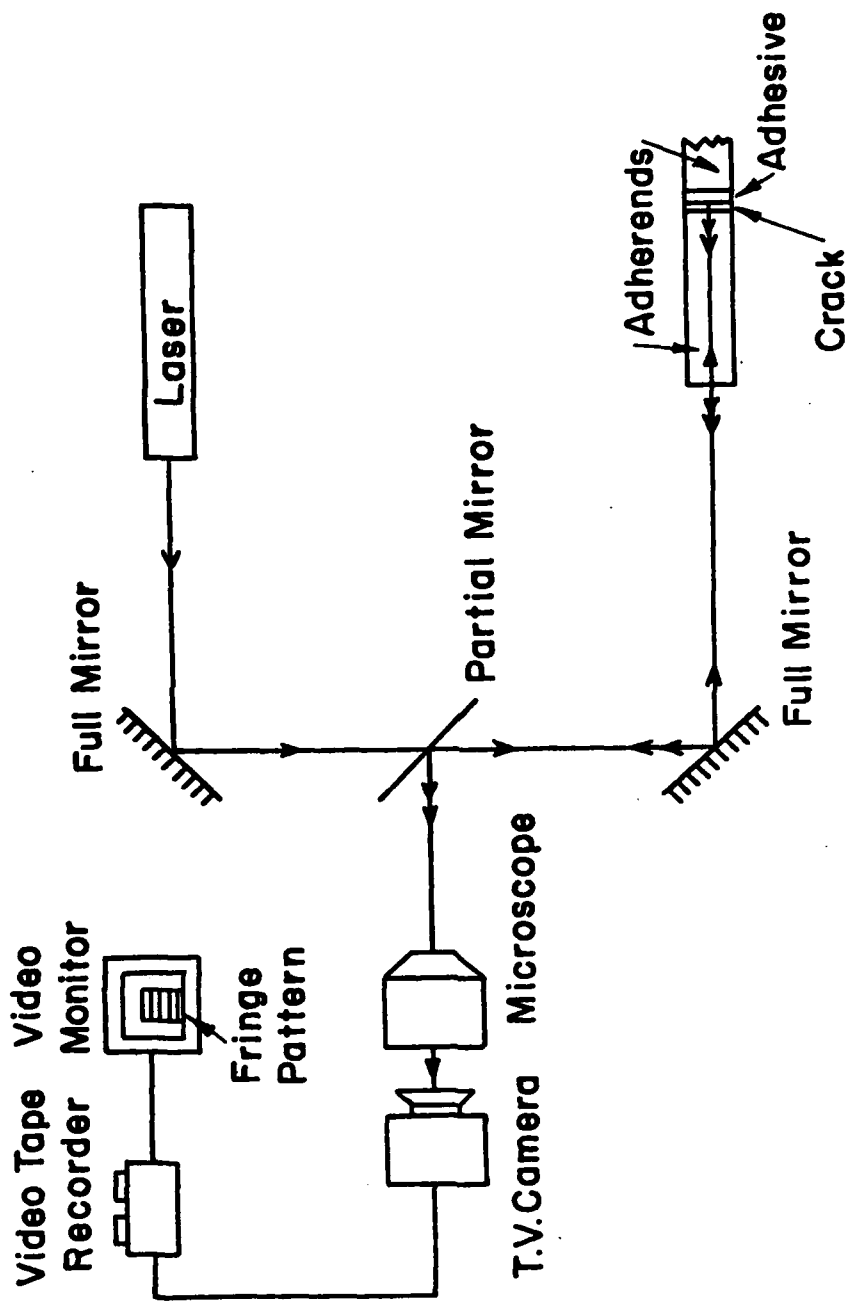
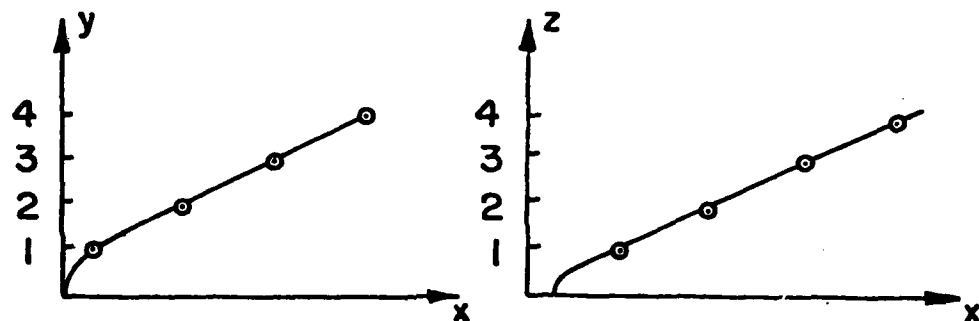
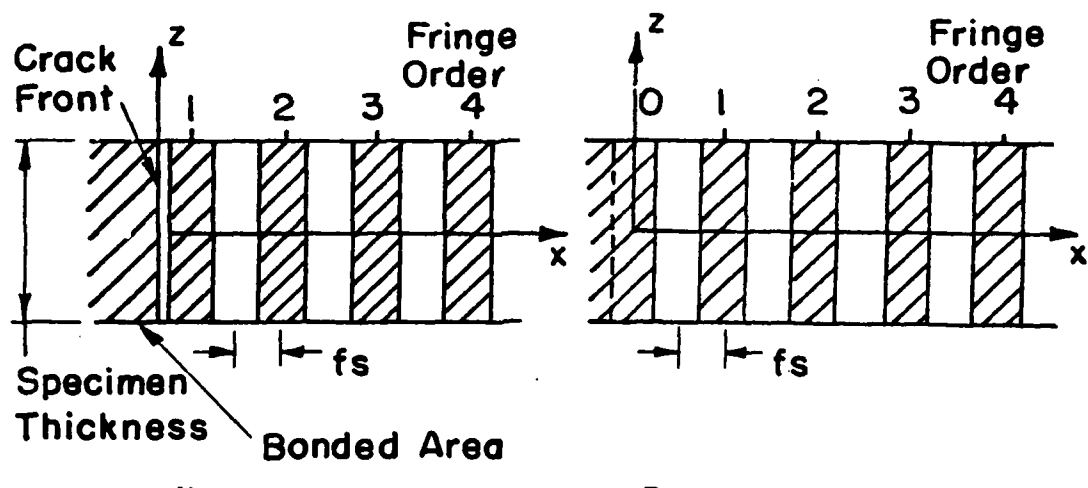


Figure 6



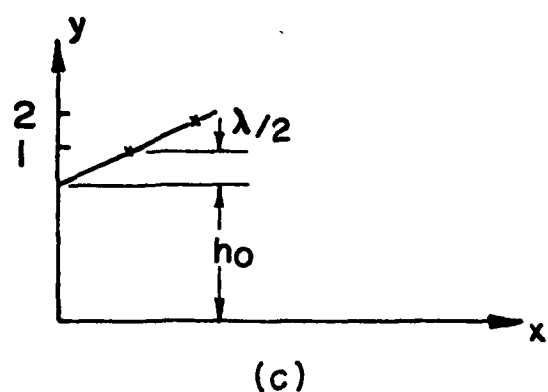
CRACK PROFILE MEASUREMENT SYSTEM

Figure 7



(a)

(b)



CRACK FRONT LOCATION

Figure 8

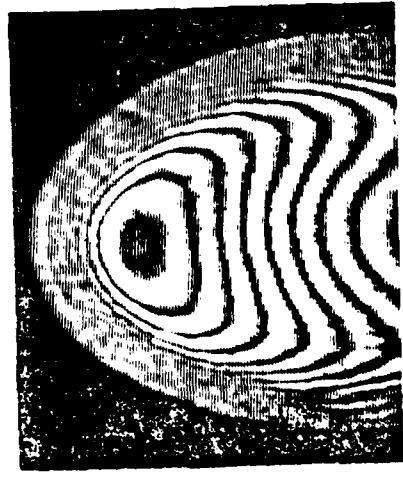
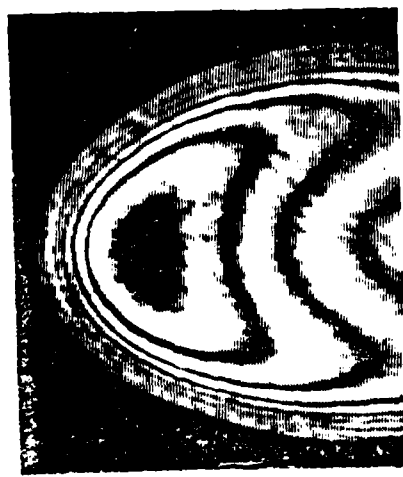
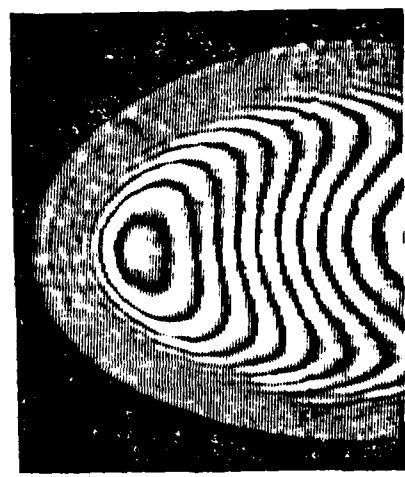
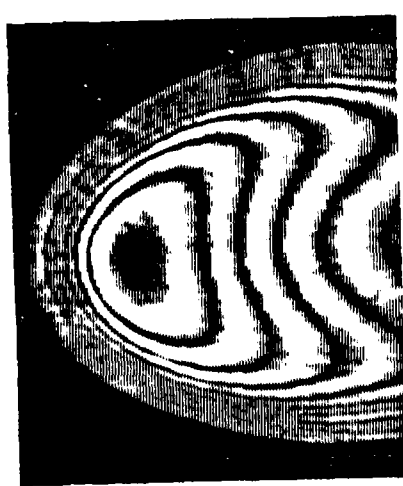
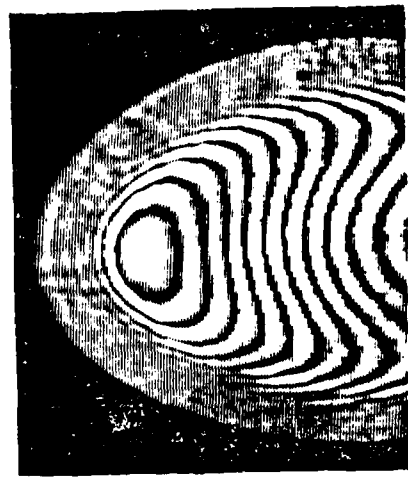
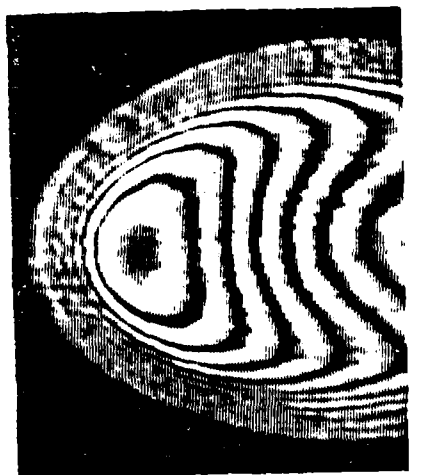


Figure 9

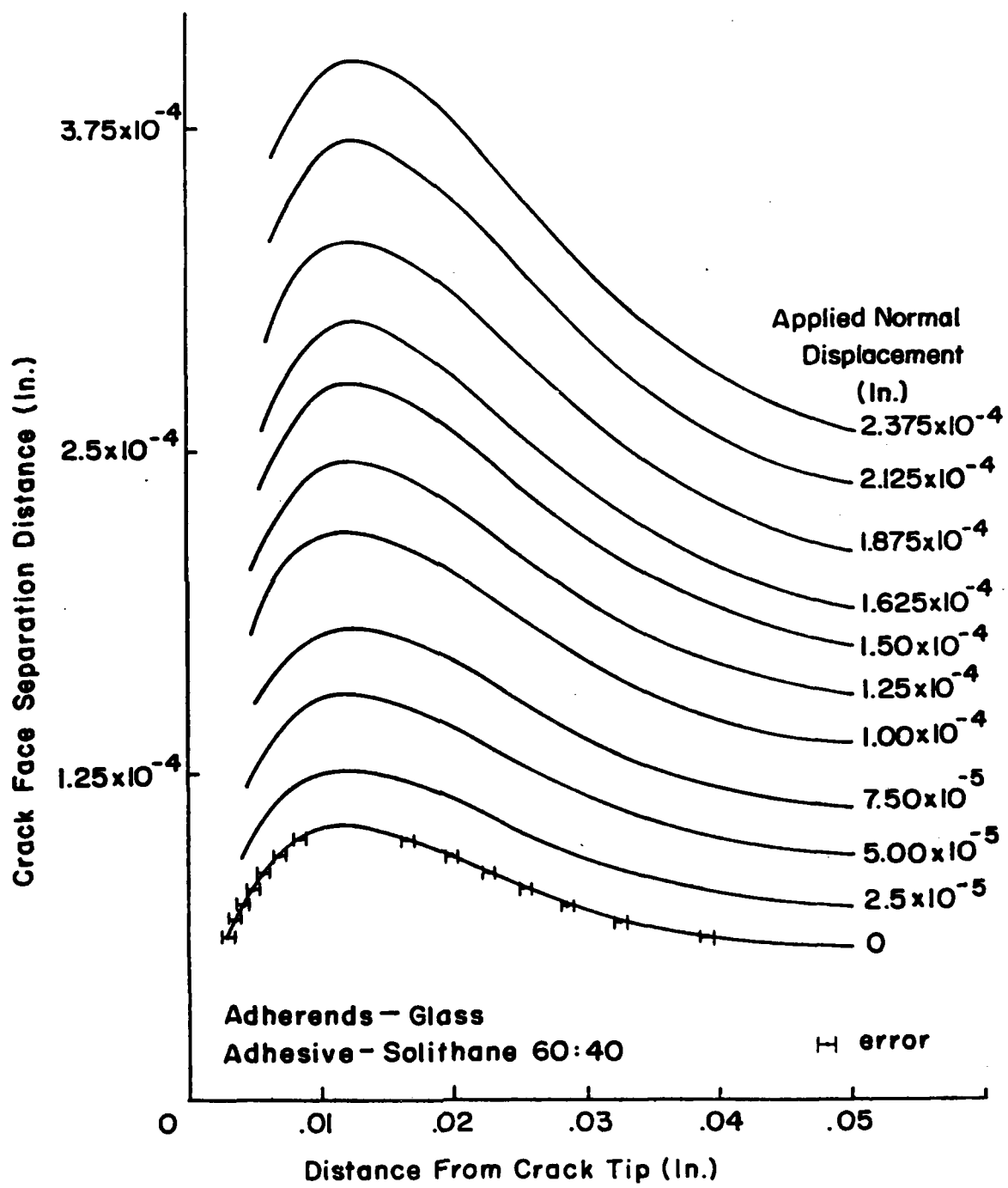


Figure 10

AD-A102 367

CALIFORNIA INST OF TECH PASADENA GRADUATE AERONAUTIC--ETC F/G 11/4
A STUDY OF THE TIME DEPENDENCE IN FRACTURE PROCESSES RELATING T--ETC(U)
APR 81 W G KNAUSS F49620-77-C-0051

UNCLASSIFIED

GALCIT-SM-81-3

AFOSR-TR-81-0590

NL

202
20367



END
10
1000
8 8 8
DTIC

APPENDIX C

On the hygrothermomechanical characterization of polyvinyl acetate

W. G. Knauss and V. H. Kenner

Graduate Aeronautical Laboratories, California Institute of Technology, Pasadena, California 91125

As a part of a program to understand the mechanisms of failure in time-dependent adhesion and film bonding, the creep compliance of polyvinyl acetate (PVAc) in shear has been determined both as a function of temperature and absorbed moisture. Volumetric expansion as a function of temperature or moisture takeup was also measured. We find that practically realizable changes in moisture content affect both the creep compliance and the swelling of PVAc to a degree comparable to that resulting from realistic changes in temperature. For example, the creep rates (histories) at corresponding times for PVAc subjected to 92% relative humidity storage are accelerated by approximately four orders of magnitude over those found for the dry material. Moreover, we find within reasonable experimental error that water concentration affects the time scale of creep like temperature through a concentration-dependent shift factor. An attempt is made at discussing the interrelation of temperature- and moisture-induced volume changes.

PACS numbers: 62.20.Hg

I. INTRODUCTION

In our recent investigations into the fundamental driving mechanisms which produce time-dependent failure in adhesive joints and bi-material laminates, the need for a thoroughly characterized model material has arisen. The modeling of material systems requires that this characterization include the following features: (1) the effects of hot (polymeric) film deposition or bond formation with subsequent cooling through the glass-transition temperature T_g ; (2) the effects of operation at elevated and/or cyclic temperatures; and (3) the effects of water, or moisture content.

The first feature will permit assessment of the role which residual stresses incurred during fabrication may play in the failure process. The latter two features translate into an ability to analyze the stresses induced by changes in ambient temperature or moisture level. The history of these stresses depends on viscoelastic material functions which themselves vary with temperature or moisture content. Furthermore, crack-propagation rates in viscoelastic materials depend explicitly on these material functions.¹ Thus, any analysis of stress history and debond growth requires not only a knowledge of the time-dependent material properties but also the temperature or moisture dependence that these functions exhibit.

We have chosen polyvinyl acetate (PVAc) as a model material. Dilatometrically, this material has a single well-defined glass-transition temperature at approximately 29 °C, and its material properties prove to be suitably temperature and moisture sensitive. Accordingly, we have conducted and report here creep tests in torsion to determine the shear creep compliance $J(t)$ for PVAc both for different levels of temperature and moisture content. The volumetric expansion of PVAc has also been determined both as a function of temperature and absorbed moisture. Finally, we consider the effects which temperature changes and moisture absorption have on the time scale for creep by relating both the moisture and the temperature dependence to the volumetric changes (free-volume change) associated with these variables.

II. SPECIMEN PREPARATION AND MEASUREMENTS

A. Specimen preparation

All PVAc specimens were derived from medium-molecular-weight PVAc, which is obtained from the manufacturer² in the form of clear spherical beads of approximately 0.8-mm average diameter. These beads were molded at elevated temperature and pressure in a cylindrical cavity 152 × 15.9 mm in diameter formed between two steel mold halves. The cylindrical cavity was sealed at one end and fitted with a piston at the other end. After some experimentation, we settled on the molding technique of filling the cavity with PVAc beads at room temperature, heating in a 125 °C oven for 2 h, inserting the (also heated) piston, and pressurizing the sample via the piston at approximately 68.9 MPa for 5 min in a hydraulic press. Then the mold was returned to the oven for an additional 2 h, the pressurization was repeated, and the mold was cooled under ambient conditions with piston displacement fixed. This recipe produced uniform cylindrical blanks approximately 102 mm long, which, while slightly yellowed, exhibited a smooth and glassy fracture surface under microscopic examination at 30× without revealing the nascent bead structure.

In order to determine the degree to which the molding process produced deterioration of the PVAc, an analysis of molecular weight for both the as-received PVAc beads and the molded blanks was carried out using liquid chromatography. The number average and weight average molecular weights for the beads were found to be 126 000 and 353 000, respectively, while corresponding quantities for the molded blanks were 85 000 and 268 000, respectively. The decrease in molecular weight during the molding process was accompanied by the appearance of ultraviolet (254-nm wavelength) absorbing species of very low molecular weight. Although these observations indicate a definite change of the PVAc during molding, the procedure outlined above produced consistent specimens which proved to have repeatable mechanical properties. Furthermore, the knowledge that no greater changes in molecular weight were encountered un-

der the relatively harsh molding conditions gave assurance that material changes under the much lower temperature used for subsequent creep measurements would be insignificant.

Torsion creep specimens were machined from the molded cylinders which had a gauge section diameter and length of 7.94 and 51 mm, respectively, and a grip-end diameter of 14.2 mm. Since, as noted above, the glass-transition temperature of 29 °C for PVAc is only slightly above room temperature, it was found necessary to cool the specimens with compressed air to prevent softening during machining. In a series of preliminary torsion tests, it was found that the machined specimens contained residual stresses which resulted in highly nonuniform test results according to whether the applied torque was in the same or the opposite direction as the torque imposed during the machining (i.e., turning in a lathe). We found that this specimen asymmetry could be removed by annealing the specimen at 40 °C for 3 h or more; this was subsequently done with all specimens reported upon.

B. Creep measurements

All creep testing utilized a creep torsionometer.³ This device provides for both the application of either "positive" or "negative" constant torques as low as 6.2×10^{-4} Nm and for the continuous measurement of specimen twist angle. The specimen is housed in an inner chamber which is constructed of 25-mm-thick brass or aluminum walls, floor, and ceiling. This chamber is itself contained in a temperature-controlled cabinet so that after thermal equilibrium is established (about 3 h) the specimen temperature may be maintained within $\pm 1^\circ\text{C}$ indefinitely. In addition to air vented into the chamber through an air bearing which supports the specimen, a provision is made for injecting additional gas, e.g., dry nitrogen or moist air, into the specimen environment. Thermocouples in the inner chamber measure both dry-bulb and, as necessary, wet bulb temperatures.

Two series of creep tests were conducted on PVAc torsion samples. The first utilized a single specimen which was maintained in the dry state by continuous storage under vacuum except during machining and annealing as described above. Creep test at temperatures ranging from -5 to $+38.6$ °C were carried out over a period of 14 days. Throughout this period the specimen remained in the torsionometer test chamber, which was ventilated continuously with either dry air or dry nitrogen. The creep behavior at 24 °C was used as a "base-line." This response remained substantially the same for testing at the beginning and at the end of the 14-day period. This practical indication of unchanged specimen properties throughout the test series is consistent with the modest cooling rates used in specimen preparation ($10^\circ\text{C}/\text{h}$ or less), which should produce a stably equilibrated material. Since the torsionometer allows loading in either of two directions, each new test, after the initial one, was conducted with load applied so as to reduce the cumulative specimen deformation. After each test the specimen was unloaded and allowed to undergo recovery so that the recovery creep superposed on a succeeding test was inconsequential.

($< 1\%$). This was facilitated by proceeding from the lowest to successively higher temperatures.

The second series of creep tests was conducted using five torsion specimens which were preconditioned at storage relative humidity levels of 32, 51, 66, 81, and 92% over suitable saturated salt solutions. Prior to conditioning, each of these specimens was desiccated, annealed, and creep tested at 24 °C under dry conditions to ensure consistency with the results of the dry-test series. Specimens were weighed in the dry state and intermittently thereafter until the weight stabilized (approximately 10 days). They were then placed in the torsionometer with the test environment maintained at the storage relative humidity level by injecting an appropriate combination of saturated air and dry air into the test chamber at 24 °C. The specimen was weighed immediately after testing to verify that no appreciable weight change had occurred during testing. In the worst instance, the difference between pre-test and post-test weights amounted to 0.049% of the specimen's dry weight.

C. Dilatometric measurements

PVAc strip specimens $70 \times 1.6 \times 12.7$ mm thick, which were formed between polished steel plates in a hot press, were first desiccated and then stored over saturated salt solutions to give both the equilibrium linear dimension increase and the equilibrium mass gain as a function of storage relative humidity. The measurement of dimension changes was made using an optical comparator whose least count was 25×10^{-4} mm, while specimen-weight-change measurement utilized an electronic balance with a least count of 0.1 mg.

The thermal expansion characteristics of PVAc were determined using a mercury dilatometer.^{4,5} In this apparatus, a cylindrical sample of PVAc, 35 mm long and 6.35 mm

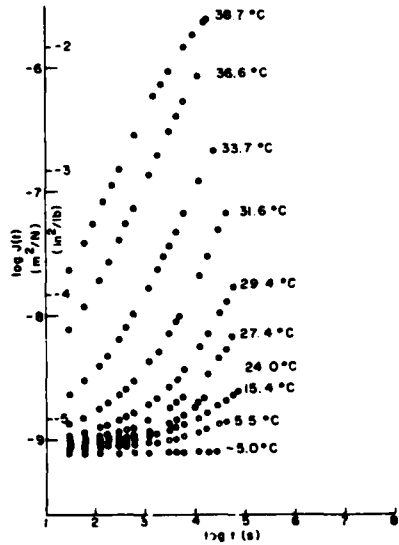


FIG. 1. Creep curves for dry PVAc at several temperatures.

in diameter, is contained in a small chamber which is otherwise filled with mercury and which is connected to a capillary tube in which the mercury level changes as specimen volume changes due to controlled heating and cooling.

III. EXPERIMENTAL RESULTS

Plots of creep compliance $J(t)$ versus time t were derived from the experimental data through the classical relations for torsion of circular cross sections, which give

$$J(t) = \frac{\gamma(t)}{\tau} = \frac{\pi d^4 \theta(t)}{32 L T}, \quad (1)$$

where $\gamma(t)$ and τ are the time-dependent shear strain and constant shear stress, respectively, and d , $\theta(t)$, L , and T are the specimen diameter, measured twist angle, specimen gauge length, and applied torque, respectively. Figure 1 presents the creep compliance for dry PVAc with the test temperature as a parameter, while Fig. 2 presents the creep compliance for PVAc at 24 °C with the moisture weight-gain fraction $\Delta m/m$ as a parameter. The normal error level for these curves is evaluated to be approximately $\pm 2\%$. Equilibrium swelling and mass gain for PVAc are plotted in Fig. 3 as a function of relative humidity. The thermally induced dilatation for PVAc is exhibited in Fig. 4.

IV. ANALYSIS AND DISCUSSION

A. Thermomechanical behavior of PVAc

A master creep curve for PVAc was generated from the data of Fig. 1. First, test temperature was accounted for by shifting each curve vertically by amount T/T_0 , where T_0 was taken to be 297 K (24 °C), according to the notion of the statistical theory of rubber elasticity. Then horizontal shifting was effected relative to the data for 24 °C to produce the

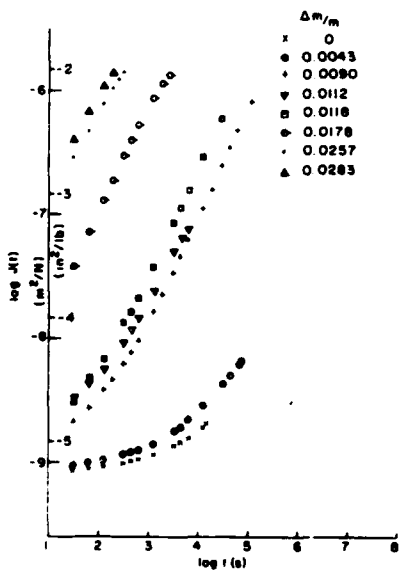


FIG. 2 Creep curves for PVAc at 24 °C at several absorbed moisture levels.

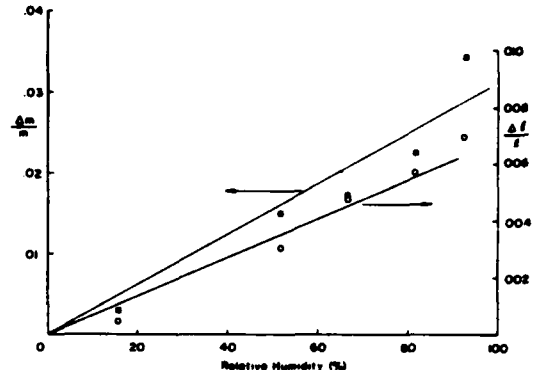


FIG. 3. Moisture takeup and elongation for PVAc as a function of storage relative humidity.

smoothest composite curve from the individual curves; this master curve is presented in Fig. 5.

As Fig. 5 shows, the shifting of creep data to form a master creep curve was accomplished with a good degree of consistency. Thus, we consider PVAc to be reasonably characterized as a thermorheologically simple material so that

$$J(T,t) = (T_0/T)J(T_0[t/a_T(T)]). \quad (2)$$

Here $a_T(T)$ is the temperature-dependent shift factor, which is given in Fig. 6 for dry PVAc. The error bars shown in Fig. 6 represent the shifting uncertainty corresponding to a $\pm 2\%$ error level for $J(t)$, which is considered representative. The glass-transition temperature of 28.9 °C, determined from the results of the dilatometric measurements presented in Fig. 4, is also shown in Fig. 6. It is seen that at this temperature a change in slope of the shift factor versus temperature data occurs; this slope "discontinuity" has also been observed at the glass transition for a filled epoxy.³ Due to the limited data for temperatures above T_g , it was found that no significant fitting of the WLF⁶ equation was possible. However, the slope of the shift function approaching T_g from $T > T_g$ was found to be $-0.45/^\circ\text{C}$, which is equal to $-C_1/C_2$, the WLF constants C_1 and C_2 being referenced to

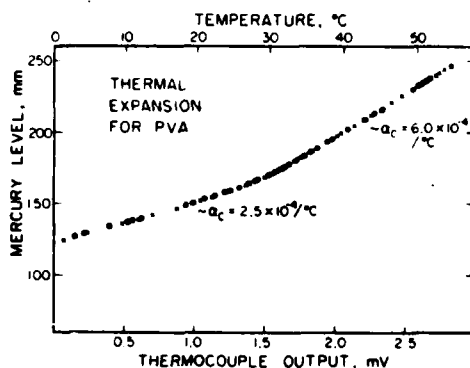


FIG. 4 Thermal-expansion characteristics for PVAc. A change in level of 1 mm corresponds to a specimen volume change of 13×10^{-6} ml.

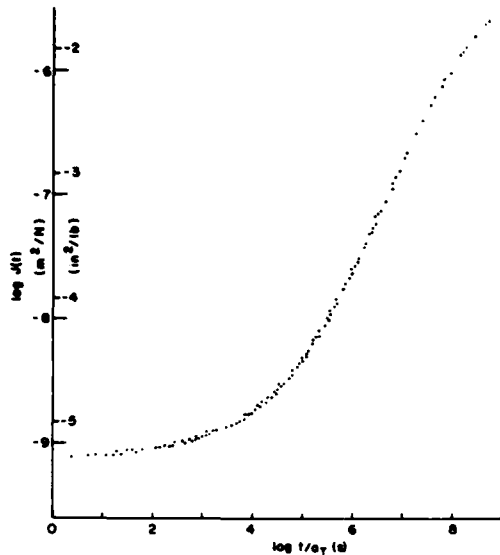


FIG. 5. Master creep curve for dry PVAc at 24 °C, derived from Fig. 1.

the glass-transition temperature.⁷ This value compares to the value of $-0.33/^\circ\text{C}$ calculated from data presented by Ferry.⁸

Figures 5 and 6 may be compared to the experimental results recently presented by Plazek.⁹ These torsional experiments utilized PVAc of molecular weight 6.5×10^5 and were conducted over the temperature range from 37.5 to 154 °C. The recoverable creep compliance curves for both experiments correspond closely in shape, although Plazek's results are shifted approximately $\frac{1}{2}$ decade toward longer time. This difference is qualitatively constants with previous experimental results¹⁰ and the predictions of entanglement theories¹¹ in view of the greater molecular weight of Plazek's PVAc. In addition, we note that our specimen was desiccated but not tested *in vacuo*; we suspect that a difference in

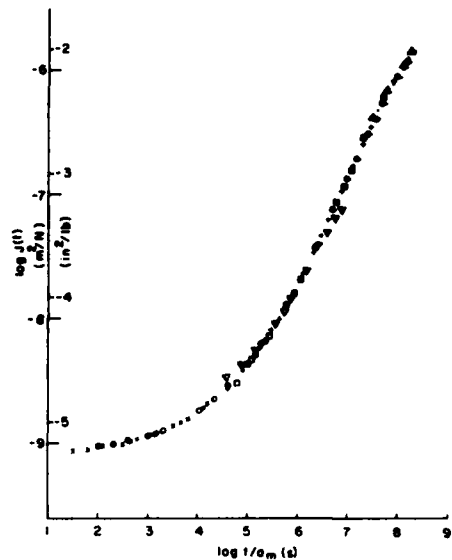


FIG. 7. Master creep curve for dry PVAc at 24 °C derived from Fig. 2.

"base-line" moisture levels may contribute to the difference. As shown in the sequel, a moisture content change of approximately $\frac{1}{4}\%$ would account for the entire discrepancy. In view of the close temperature control afforded by both our and Plazek's apparatus, we tend to believe that the difference is indeed due to residual moisture which could not be extracted during the period of *in vacuo* storage.

B. Hygromechanical behavior of PVAc

The creep curve from Fig. 2 for PVAc at several absorbed moisture levels were shifted horizontally relative to the dry creep curve to produce the master creep curve presented in Fig. 7. With the exception of one slightly irregular run, this procedure resulted in excellent construction of a master curve. The shift factors a_m corresponding to Fig. 7 are plotted as a function of the fractional mass gain in Fig. 8. The error bars shown in Fig. 8 again represent shifting errors corresponding to a $\pm 2\%$ uncertainty in $J(t)$. There is an

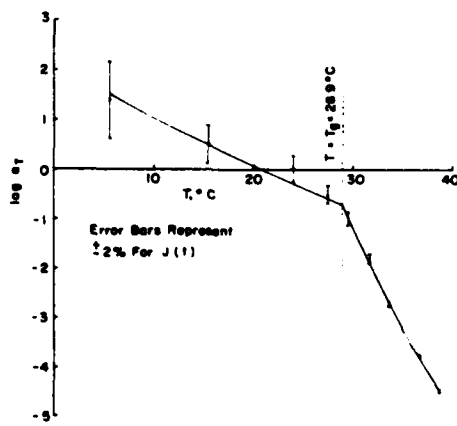


FIG. 6. Temperature shift factor for dry PVAc relative to 24 °C.

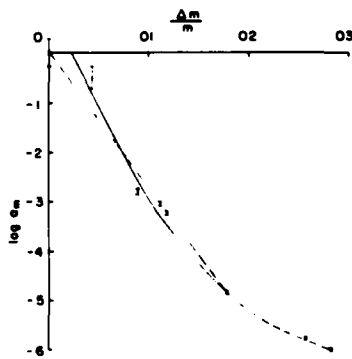


FIG. 8. Moisture absorption shift factor for 24 °C relative to the dry state.

inconsistency in the first two data points on this curve, and we show two fits in Fig. 8 according to whether the point at the origin is accepted (dashed curve) or the next point is considered accurate (solid curve). This ambiguity near the origin reflects, first, uncertainty as to the definition of "dry" and, second, increased errors inherent in the shifting procedure for the short-time regime of the master curve.

Horizontal shifting procedures a master curve which represents creep at several moisture absorption levels with dependence on $\Delta m/m$ entirely incorporated in $a_m(\Delta m/m)$; therefore, we use the term "hygro rheologically simple material (HSM)" in analogy to the words used in temperature-time shifting. We thus describe a material for which the moisture dependence is expressible through (in the case of shear creep compliance)

$$J(\Delta m/m, t) = J_0 \{ (\Delta m/m)_0 [t/a_m(\Delta m/m)] \}. \quad (3)$$

C. Hygrothermomechanical behavior

Since both the master curve derived from the dry temperature-varied series of tests (Fig. 5) and that derived from the 24 °C moisture-varied tests (Fig. 7) are referenced to the dry material at 24 °C, they should, in principle, be identical, i.e., each should predict the extended time creep behavior of dry PVAc at 24 °C. Indeed, when both creep curves are plotted together, as in Fig. 9, one observes that they are essentially identical, the difference between the two being within limits of experimental and plotting errors. Shifting of temperature-and/or moisture-test creep data to produce a single master creep curve has also been accomplished for other polymers.^{12,13}

Since the material response to increased temperature corresponds closely to that resulting from the absorption of moisture, there is a strong indication that the basic mechan-

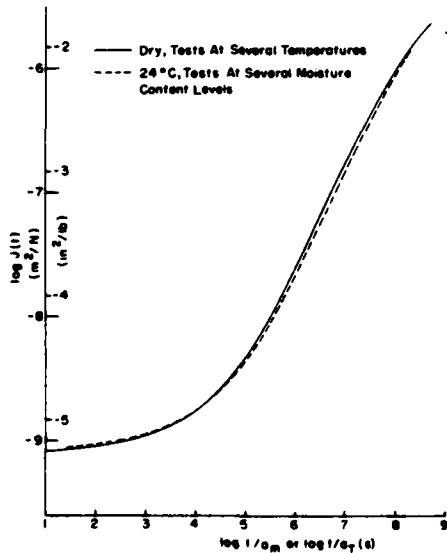


FIG. 9. Comparison of master creep curves for PVAc.

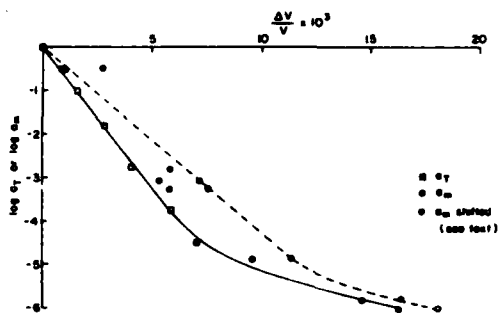


FIG. 10. Shift data from moisture and temperature experiments presented in terms of fractional volume changes.

ics underlying both responses are the same. For example, in view of Fig. 9, it seems unlikely that chemical changes which might occur with moisture absorption have resulted in changed mechanical behavior. Following the relationship between the so-called "free volume" and the time-temperature shift factor a_T ,⁷ we now attempt to establish a commonality between the two sets of creep data on the basis of volume change. Since several representations of free volume have been correlated with experimental observations of various physical phenomena,^{12,14,15} the present comparison is effected simply on the basis of net volume gain relative to the reference state, i.e., relative to dry PVAc at 24 °C.

The volume change due to temperature increase may be calculated from the results of the dilatometric measurements in Fig. 4. The two linear segments of the curve below and above the glass-transition temperature correspond to coefficients of volume expansion of $2.5 \times 10^{-4}/^{\circ}\text{C}$ and $6.0 \times 10^{-4}/^{\circ}\text{C}$, respectively. From these values we readily calculate the fractional volume increase $\Delta v/v$. The data of Fig. 3 may be used to obtain the relation between mass gain due to moisture absorption $\Delta m/m$ and the corresponding volume increases $\Delta v/v$. In this case, the straight-line fits shown in Fig. 3 correspond to a ratio

$$\frac{\Delta v/v}{\Delta m/m} = 0.64 = \frac{1}{\rho} \frac{\Delta v}{\Delta m}, \quad (4)$$

where ρ is the density of PVAc, which we have determined to be 1.17 g/cm^3 . The second equality gives $\Delta v/\Delta m = 0.75 \text{ cm}^3/\text{g}$, i.e., the volume increase in the water absorption measurements is equal to three-quarters of the volume of the added water.

Let us now plot the shift factor data of both Figs. 6 and 8 in terms of the fractional volume increase $\Delta v/v$ relative to dry PVAc at 24 °C in Fig. 10. In the case of a_m , the degree of linearity of the $\log a_m$ -vs- $\Delta v/v$ curve simply corresponds to that exhibited by the $\log a_m$ -vs- $\Delta m/m$ data presented in Fig. 8. However, the linearity exhibited by $\log a_T$ in Fig. 10 represents a "straightening" from the antecedent data of Fig. 6. Thus, we emphasize that while shift data in the trans- T_g range exhibit a discontinuity of slope at T_g , these data are continuous when recast in terms of volume change.

Disregarding, for the moment, the possibility that the "dry" specimen was not entirely free of water,¹⁶ one obtains

the relation shown dotted in Fig. 10 for the shift function α_m . The shift function derived from temperature variations is plotted by squares. By comparing these two relations one would be led to confirm that volume dilatation by water leads to less "free volume" for molecular motion than dilatation through temperature would provide.

Alternately, if our so-called "dry" material was not truly free of water in spite of prolonged desiccation, then a correction of water content by an initial small amount of about 0.27%¹⁷ would bring the temperature and moisture shift data into good agreement (solid circles and square, Fig. 10).

Clearly, the necessity of further work on preparation of water-free specimens is indicated to completely resolve this uncertainty. However, it emerges fairly clearly already that changes in rheological behavior resulting from changes in temperature and moisture are coupled through the free volume of the material.

The present PVAc is similar to the nylon reported on by Williams and Bender¹² in the sense that $\Delta v/\Delta m$ is initially equal to 0.75 cm³/g for water absorption in both materials. If the view that free volume consists of voids is taken,¹² then the free volume decreases as absorbed water fills voids. The presence of water in these voids makes either no or only slight difference according to the current results. Thus, for purposes of determining changed creep compliance, we consider all volume increases due to absorption to represent "effective free volume." This seems consistent with a notion of ease of movement of large molecules being dependent on space between them, with relatively very small water molecules providing little, if any, change from void insofar as the present quasistatic and equivoluminal motion is concerned.

Consider now the usual representation⁷ of the shift factor as a function of free volume fraction f through

$$\log a = c(1/f - 1/f_0), \quad (5)$$

where c is constant and f_0 represents the fraction of free volume at reference conditions. If, in view of the above discussion, we suppose that volume change governs shifting regardless of its origin, then the fractional free volume f would, to first order, change additively due to temperature and moisture. Thus, if f_T and f_m represent the free-volume frac-

tion due to temperature and moisture, respectively, then $f = f_T + f_m$. One concludes then from Eq. (5) that a combined shift factor a is not merely a product of the separate shift factors a_T and a_m , i.e., that shifting (on a log-log plot) will not be simply the sum of moisture and temperatures shifts. This is consistent with the empirical representation of the temperature- and moisture-dependent shift factor observed by Maksimov *et al.*¹³ for polyester resin.

ACKNOWLEDGMENTS

The authors wish to express their gratitude to the Air Force Office of Scientific Research (Lt. Col. J. Morgan), and the Jet Propulsion Laboratory (Dr. J. Moacanin) and the Department of Energy, who supported this work through Contracts F49620-77-C-0051 and 49-767-1D002-0-3460, respectively. We also gratefully acknowledge the assistance of M. Sarbolouki of JPL for performing the liquid chromatography and I. Emri and L. Heymans of Caltech for conducting the measurements leading to Figs. 3 and 4, respectively.

¹W. G. Knauss, in *Deformation and Fracture of High Polymers*, edited by H. H. Rausch, J. A. Haswell, and R. I. Jaffee (Plenum, New York, 1974), p. 501; in particular comment 4, p. 538.

²Polysciences, Inc., Warrington, Pa.

³V. H. Kenner and W. G. Knauss (unpublished).

⁴W. G. Knauss, V. H. Kenner, and L. J. Heymans, GALCIT SM 78-12 (California Institute of Technology) (unpublished).

⁵N. Bekkedahl, J. Res. Natl. Bur. Stand. 42, 145 (1949).

⁶M. L. Williams, R. F. Landel, and J. D. Ferry, J. Am. Chem. Soc. 77, 3701 (1955).

⁷J. D. Ferry, *Viscoelastic Properties of Polymers* (Wiley, New York, 1961).

⁸See Ferry's (Ref. 7) discussion, p. 218.

⁹D. J. Piazek, Soc. Rheol. 1979 Fall Meeting.

¹⁰K. Ninomiya, J. Colloid Sci. 14, 49 (1959).

¹¹S. D. Hong, J. Appl. Phys. 48, 4019 (1977).

¹²M. L. Williams and M. F. Bender, J. Appl. Phys. 36, 3044 (1965).

¹³R. D. Maksimov, E. A. Sokolov, and V. P. Mochalov, Polym. Mech. 11, 334 (1976).

¹⁴F. N. Kelley and F. Bueche, J. Polym. Sci. 50, 549 (1961).

¹⁵W. Brostow, Research Conference in Chemical Engineering at California Institute of Technology, 1980 (unpublished).

¹⁶See Sec. IV A.

¹⁷Corresponding to a volume change of 0.18%.

APPENDIX D

NON-LINEAR VISCOELASTICITY BASED ON FREE VOLUME CONSIDERATION

W. G. Knauss and I. J. Emri

Graduate Aeronautical Laboratories, California Institute of Technology, Pasadena, CA 91125, U.S.A.

(Received 17 May 1980)

Abstract—Many advanced engineering problems suffer from inadequate solution because the appropriate constitutive behavior for the materials involved is not available. This is certainly true where polymers are concerned because in many situations involving failure analysis the non-linear viscoelastic material properties become important.

In this paper a non-linear viscoelastic constitutive law is considered. It starts from the assumption that linear viscoelasticity is appropriate under infinitesimal strains and that the material description must revert to this case. The non-linearity of this development is derived from the stress dependent time response in the deformation process. The physical basis for the description derives from the observation that stress induced dilatation effects the mobility of molecular chains through changing the free volume in the polymer. Test data for polyvinyl acetate are compared with computations under conditions of relaxation and constant strain rate deformation. Excellent agreement is obtained between the proposed model and experiments. This agreement would indicate that the free volume model is definitely a possible way of describing non-linear viscoelastic behavior under small to moderate strains.

1. INTRODUCTION

The use of high speed computers in mechanics has removed a great many obstacles to scientific and design problem solving. In solid mechanics and structural engineering finite element techniques have made great strides in solving problems that were considered extremely complex by the earlier standards. These advances were made possible by the discretization of the well known field equations for virtually arbitrary geometries. The exploitation of these methods has become often more a matter of finances than of basic ability.

Besides possibly finances, a severe limitation on physically realistic problem solving arises from our lack of knowledge of material constitutive behavior. By far most structural or "continuum" codes incorporate linearly elastic material behavior with only some possessing capability of modelling non-linearly elastic and plastically deforming solids. With regard to time or rate sensitive materials only the (physically unrealistic) rudiments of linear viscoelasticity seem to be considered. In connection with today's increased use of structural polymers in advanced engineering designs, these material descriptions pose severe limitations. All the power of computational mechanics developed so far is compromised critically if the constitutive behavior of the structure is modelled insufficiently well.

In this presentation we are concerned with non-linearly viscoelastic material behavior. There are several physical reasons why materials behave in a non-linear manner. We distinguish polymeric solids as being single-phase or filled with soft or stiff inclusions in the form of particulates or continuous and chopped fibers. Examples are solid propellant rocket fuels, impact toughened polystyrene, tire tread shock, glass and graphite fiber reinforced plastic and structural adhesives.

Macroscopic non-linear material response in such materials may be associated with the development of discontinuities such as (micro) cracks and separation of

the phases. On the other hand, grossly non-linear behavior in single phase materials may be the result of the appearance of crazes which qualitatively have the same effect as the generation of multiple cracks.

Here we wish to address non-linearly viscoelastic behavior from more molecular forces which do not occur as the result of such internal damage. Thus, this type of non-linearity is (possibly) present before damage mechanisms become operative.

Specifically, we are concerned here with the effect of stress or strain induced changes in the rate of relaxation or creep. In related work [1] we have noted that the intrinsic time scale of a material can be modified by moisture in the same manner as by temperature. In fact, we observed that the time scale was affected by the volume dilatation whether the latter was occasioned thermally or by swelling. The deduction is then close at hand that also stress induced volume dilatation will affect the intrinsic time scale of the material.

The effect of pressure on rheological behavior has been studied by several authors, first with a change in the glass transition behavior in mind [2-4] and later with rheological implications [5]. There seems to be no systematic study involving the effect of stress state on rheological behavior as a result of associated volume changes. Gent has attributed the crazing phenomenon in glassy plastic to stress-induced softening and void formation in the craze [14]. Very recently Bernstein and Shokoh [7] have considered the phenomenological concept of a "stress clock" which concept is akin to the physical basis underlying Gent's considerations and those of volume increase developed here in the sequel. It should be mentioned that in connection with fibrous and particulate composite thermodynamic reasoning led Schapery and Lou [8, 9] to examine modification of the relaxation or creep rate through a "strain dependent" shift factor.

For our present purposes we confine ourselves to relatively small strains which seems appropriate for the deformation of rigid polymers. We thus exclude spec-

ifically considerations of the large deformations [10] associated with rubber elasticity and viscoelasticity. Therefore, we may feel justified to begin our considerations with the linearly viscoelastic behavior of an isotropic solid which must describe its constitution under truly small strains or stresses; in other words, the non-linear description of material behavior reduces then automatically to linear viscoelasticity in the limit of vanishing stresses and strains.

2 THEORETICAL BACKGROUND

As mentioned in the introduction, several investigators have studied the effect of temperature and pressure on the thermorheology of high polymers [2-5, 11-15]. These effects are commonly associated with changes in the free volume of the material. According to our experimental studies mentioned in the introduction and involving parametric variations in temperature and in water concentration, the (free) volume offers a unifying parameter to describe changes in the time scale of the material response. We proceed now to enlarge this concept by including the effect of mechanically (stress) induced volume dilatation.

The time dependence or viscosity of the rheological response is modified by a time-multiplying factor a which depends on the temperature, solvent concentration and mechanical dilatation,

$$a = a(T, c, \theta). \quad (1)$$

Doolittle expressed this factor in terms of the free volume by

$$\log a = \frac{B}{2.303} \left(\frac{1}{f} - \frac{1}{f_0} \right), \quad (2)$$

where f is the fractional free volume defined in terms of the total volume v_0 of the solid and the free volume v_f as

$$f = \frac{v_f}{v_f + v_0} \approx \frac{v_f}{v_0}. \quad (3)$$

and denotes f_0 the fractional free volume at some reference conditions. We consider the fractional free volume to depend on three variables: temperature T , solvent concentration c , and mechanically induced dilatation θ , or

$$f = f(T, c, \theta). \quad (4)$$

Let us assume that the change in fractional free volume due to any one of the three variables is additive. This assumption appears entirely adequate for our present purposes since an examination of the partial derivatives of f with respect to T , c and θ reveals that only a small error results for ranges of the variables encountered normally. We then have differentially

$$df = x dT + \gamma dc + \delta d\theta, \quad (5)$$

where x , γ and δ are, in general, functions of T , c and θ . Let us assume further that x , γ and δ are constants, a condition that does not seem poor if we remain below the glass transition temperature and below the boiling point of the solvent. Then

$$f = f_0 + x \cdot \Delta T + \gamma \cdot c + \delta \cdot \theta, \quad (6)$$

where we allow for zero solvent concentration and zero mechanical dilatation in stress free reference conditions. In terms of (6) eqn (1) becomes then

$$\log a(T, c, \theta) = - \frac{B}{2.303 f_0} \frac{\alpha \cdot \Delta T + \gamma \cdot c + \delta \cdot \theta}{f_0 + \alpha \cdot \Delta T + \gamma \cdot c + \delta \cdot \theta}. \quad (7)$$

Through its dependence on the stress induced volume changes this shift factor $a(T, c, \theta)$ becomes instrumental in the non-linear material response described below.

Let us consider first the linearly viscoelastic constitutive description of an isotropic solid under infinitesimal deformations, in terms of the deviatoric stress and strain components (S_{ij} , e_{ij}) which are derived from the components of stress, τ_{ij} and (infinitesimal) strains ε_{ij} through the relations

$$S_{ij} = \tau_{ij} - \frac{1}{3} \tau_{kk} \delta_{ij}, \quad (8a)$$

$$e_{ij} = \varepsilon_{ij} - \frac{1}{3} \theta \delta_{ij} \quad \theta = \varepsilon_{kk}. \quad (8b)$$

Let $\mu(t)$ and $K(t)$ be, respectively, the relaxation moduli in shear and volume deformation. We have then at reference conditions

$$S_{ij} = 2 \int_{-\infty}^t \mu(t - \xi) \frac{\partial e_{ij}}{\partial \xi} d\xi, \quad (9)$$

$$\tau_{kk} = 3 \int_{-\infty}^t K(t - \xi) \frac{\partial}{\partial \xi} (\theta + \alpha^* \Delta T + \gamma^* c) d\xi. \quad (10)$$

If all macroscopic change in volume equal the change in free volume then $\alpha = \alpha^*$, $\gamma = \gamma^*$ and $\delta = 1$; we are not prepared to make that assertion now, nor is such an assertion absolutely necessary at this time for our later development. However, we point out that the comparison of our analysis with that data produces that $\delta = 1 (= 0.98)$. Also we note that for comparison of our computation with that data the terms $\alpha^* \Delta T$ and $\gamma^* c$ shall not enter our considerations.

Generalizing Lee's suggestions [16-18] that the time-temperature shifting under non-isothermal conditions be valid instantaneously, i.e. the temperature reduced time t' relates to the actual time t by the differential relation

$$dt' = \frac{dt}{a[T(t)]}. \quad (11)$$

We have, more generally, in view of (7)

$$t' = \int_0^t \frac{d\xi}{a[T(\xi), c(\xi), \theta(\xi)]}; \quad \xi = \int_0^t \frac{d\xi}{a[T(\xi), c(\xi), \theta(\xi)]}. \quad (12)$$

Under conditions of time varying temperature, solvent concentration and stress dilatation

$$S_{ij}(t) = 2 \int_{-\infty}^t \mu(t' - \xi) \frac{\partial e_{ij}}{\partial \xi} d\xi, \quad (13)$$

$$\tau_{kk}(t) = 3 \int_{-\infty}^t K(t' - \xi) \frac{\partial}{\partial \xi} (\theta + \alpha^* \Delta T + \gamma^* c) d\xi. \quad (14)$$

Inasmuch as the reduced time in the argument of the relaxation function depends on the total stress or strain history, these relations no longer represent linear operations that connect stresses with deformations. Thus while the appearance of a linearly viscoelastic material behavior appears preserved considerable deviation from small strain linearity will become apparent.

[†]Repeated indices indicate summation.

3. EXAMPLES FOR TWO SPECIAL LOAD HISTORIES

From eqn (12) it is apparent that holding the temperature, concentration and dilatation constant during a test would produce a time independent shift of the test result since thus $t' = \text{constant} \cdot t$. Experimentally such a condition is extremely difficult, if not impossible, to impose. The next constraint is posed by available test equipment. With a view toward later comparison of test data with the evaluations of eqns (13) and (14) we therefore consider, for the present, the problems of stress relaxation and monotonic loading by a history of constant strain rate.

(1) Relaxation at constant temperature and concentration

We consider a uniaxial tensile specimen and impose the Heaviside strain history

$$\varepsilon_{11} = \varepsilon_0 H(t), \quad (15)$$

while all stresses except τ_{11} vanish. The pertinent equations become then

$$\frac{2}{3}\sigma_{11} = \tau_{11} = 2 \int_{-\infty}^t \mu(t-\xi) \frac{\partial}{\partial \xi} (\varepsilon_{11} - \varepsilon_{22}), \quad (16)$$

$$\frac{1}{3}\tau_{11} = \int_{-\infty}^t K(t-\xi) \frac{\partial}{\partial \xi} (\varepsilon_{11} + 2\varepsilon_{22}), \quad (17)$$

Since these relations constitute non-linear operations between τ_{11} and the strains ε_{11} and ε_{22} there is no direct analytical way of eliminating ε_{22} in order to obtain a relation between τ_{11} and ε_{11} only, except for infinitesimal strains ($a(T, c, \theta) = \text{constant}$). In this case

$$\tau_{11} = \int_{-\infty}^t E(t-\xi) \frac{\partial \varepsilon_{11}}{\partial \xi} d\xi, \quad (18)$$

$$\theta = \int_{-\infty}^t \frac{1}{3} K^{-1}(t-\xi) \frac{\partial \tau_{11}}{\partial \xi} d\xi, \quad (19)$$

where the tensile relaxation modulus $E(t)$ is achieved by

$$E = \frac{9K\bar{\mu}}{3K + \bar{\mu}}, \quad (20)$$

bars denoting Laplace transformed quantities.

The increase $K^{-1}(t)$ of the bulk modulus $K(t)$ is determined by

$$\int_0^t \frac{1}{3} K^{-1}(t-\xi) K(\xi) d\xi = t. \quad (21)$$

Because the non-linear effects considered here are due to the stress induced changes in the scale of relaxation times, it is reasonable to assume that the same effect is prevalent in the simple tensile test. We therefore generalize the eqns (18) and (19) by applying the time reduction (12) to render

$$\tau_{11} = \int_{-\infty}^t E(t-\xi) \frac{\partial \varepsilon_{11}}{\partial \xi} d\xi, \quad (22)$$

$$\theta = \int_{-\infty}^t K^{-1}(t-\xi) \frac{\partial \tau_{11}}{\partial \xi} d\xi. \quad (23)$$

We note once more that (22, 23) do not follow directly from (16, 17); however, since the representation of linearly viscoelastic behavior can be given in several ways, each of which involves two independent material functions, it seems justifiable to start with the representations (18) and (19) in order to lead to stress induced non-linear behavior.

We now specialize (22) and (23) for step strain loading according to (15) to obtain

$$\tau_{11} = \varepsilon_0 \int_{-\infty}^t E(t-\xi) \delta(\xi) d\xi, \quad (24)$$

with $\delta(\xi)$ denoting the delta function; this reduces further to

$$\tau_{11} = \varepsilon_0 E(t'), \quad t' = \int_0^t \frac{d\xi}{a[T(\xi), c(\xi), \theta(\xi)]}, \quad (25)$$

which, for infinitesimal strains ($\theta \rightarrow 0$) render

$$\tau_{11} = \varepsilon_0 E(t), \quad (26)$$

where $E(t)$ is the relaxation modulus for infinitesimal strains. Note that (25) represents a decaying stress history; however, because t' depends on the stress history, which in turn depends on the applied strain ε_0 , the decay history will vary with the applied strain. Nevertheless, for short times the same glassy limit modulus will be achieved.

We particularize (17) now to the case of constant temperature and zero solvent concentration. There results then

$$\log a(\theta) = - \frac{B}{2.303f_0} \frac{\delta \cdot \theta}{f_0 - \delta \cdot \theta}, \quad (27)$$

with θ being given by (23). In order to evaluate (27) we need to specify the bulk modulus $K(t)$ or its inverse $K^{-1}(t)$. We started this investigation by assuming a constant bulk modulus, but when we effected a comparison with the experimental data found that a time dependent description in the form of a standard linear solid yielded much better results. Accordingly, we chose

$$K^{-1}(t) = M_0 + M_1(1 - e^{-\theta t}). \quad (28)$$

The complete set of equations governing $\tau_{11}(t)$ is then, with $E(t)$ as the relaxation modulus at infinitesimal strain

$$\tau_{11} = \varepsilon_0 E(t'), \quad (25a)$$

$$t' = \int_0^t \frac{d\xi}{a[T_0, \varepsilon_0, \theta(\xi)]} \quad (25b)$$

$$\log a = - \frac{B}{2.303f_0} \frac{\delta \cdot \theta}{f_0 + \delta \cdot \theta}, \quad (27a)$$

$$3\theta = (M_0 + M_1)\tau_{11} - \int_0^t e^{-t'-\xi} \frac{\partial \tau_{11}}{\partial \xi} d\xi. \quad (29)$$

These equations are solved numerically. In order to avoid extensive iteration in their solution, we approximated (29) by replacing $t' - \xi$ with $t - \xi$, since we believe that difference to be relatively unimportant. In fact, for our experimental study we have no information on $K(t)$, so that M_0 , M and τ must be extracted by data fit; the physical reasonableness of the values so determined would then constitute a further test of the present considerations.

(2) Constant rate of strain extension

Prescription of constant rate of straining in the form of

$$\varepsilon_{11} = \dot{\varepsilon}t \quad (30)$$

results in the full set of response equations, analogous to (25a, b), (27a) and (29) as

$$\tau_{11}(t) = \dot{\varepsilon} \int_0^t E(t-\xi) d\xi, \quad (31a)$$

$$r - \zeta = \int_{\zeta}^r \frac{ds}{a[T, \sigma, \theta(s)]} \quad (31b)$$

$$\log a = \frac{-B}{2.303 f_0} \frac{x_r \Delta T + \delta \cdot \theta(t)}{f_0 + x_r \Delta T + \delta \cdot \theta(t)} \quad (31c)$$

$$3\theta(t) = (M_0 + M_1) r_{11}(t) - \int_0^t e^{-t-\zeta} \frac{\partial r_{11}}{\partial \zeta} d\zeta. \quad (31d)$$

Again, according to the remarks following eqn (29) we have replaced $t - \zeta$ by $t - \zeta$ in (31d). For later reference when we compare the evaluation of (31a-d) with test data we point out that the experiments with constant strain rates involve relatively short times; the transition behavior of the bulk modulus is not involved and it is entirely adequate to consider the bulk modulus to be constant at its glassy or short time value. Also, because test data were obtained at different temperatures, we include here the effect of different but constant temperatures. Since all test temperatures are below the glass transition temperature we allow only for the simple proportionality of the free volume to the temperature change.

4. COMPARISON WITH EXPERIMENTAL DATA

In order to test the proposed theory we compare the computations with data from measurements on polyvinyl acetate. In the interest of brevity we do not account here the method of specimen preparation but content ourselves with stating that the specimens were machined in a cylindrical shape with a test section 0.8 cm (0.312 in.) in diameter and a test section of 5 cm (2 in.). The measurements were made with the aid of an Instron tensile tester[†]. Measurements of strain in the relaxation tests were accomplished via bench marks on the specimen test section, the relative distance of which was monitored with an Optron. Such direct strain measurement also allowed continued monitoring of whether specimen slippage occurred in the grips.

(1) Relaxation tests

Relaxation tests were conducted at uniaxial tensile strains of 1, 3 and 5%. While the method of strain measurement allows an accuracy of a fraction of a percent the prescription of the applied strain through the mechanism of the straining machine was difficult. We were therefore not able to prescribe small strains well though it could be measured well; as a consequence, we lack precise data at "infinitesimal" strains.

Relaxation tests were conducted at different temperatures at each of the indicated strains. For each of the latter a master curve was prepared by shifting the segments for a best fit as a master curve. Strictly speaking this temperature shifting should not be independent of the strain at which measurements are made; however, as a first approximation we assume that procedure to be adequate.

The experimental master curves are compared with those calculated in Fig. 1. Note that a 1% strain produces a high stress and thus a significant dilatation. As a result the 1% relaxation data should not agree well with the relaxation behavior for infinitesimal strain. Accordingly, we have also calculated the relaxation behavior of

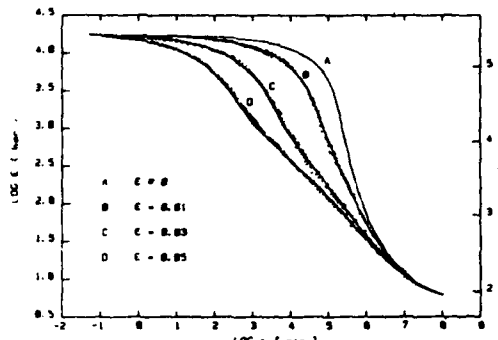


Fig. 1. Relaxation behavior of polyvinyl acetate in uniaxial tension at different strain levels. Dots represent experimental results; solid lines indicate non-linear analysis.

infinitesimal strain, shown as curve A in Fig. 1.

The calculated curves exhibit some apparent "un-evenness" which is the result of our uncertainty of the true bulk behavior. Apart from this blemish it is clear, however, that the general response of the specimens is well followed by the calculations, provided we let

$$K(t) = [1.34 + 2.01 \exp(-t/\tau)] \cdot 10^3 \text{ bar}$$

$$\tau = 4 \cdot 10^5 \text{ min.}$$

Note that at least a partial check on the validity of the representation of $K(t)$ is given by comparing the computation of Section 3 with appropriate and independent experiments, as described next, as long as the same bulk representation is used.

(2) Constant rate of strain test

Tensile specimens were strained in a closely controlled (dry) thermal environment to produce typical "stress-strain" response curves. Since we found that the discrepancy between theory and experiment was on the order of 5% we saw no urgency to compensate for changes in specimen cross section. Accordingly, the stress is referred to the original, undeformed cross section.

In Figs. 2(a-c) we show experimental results (dotted curves) together with the responses computed from eqns (31a-d) (solid lines). Also shown are the responses which a linearly viscoelastic solid would produce if linear viscoelasticity were valid at non-infinitesimal strains. It is apparent from eqn (7) and how the instantaneous shift factor affects the stress-strain response (27a) and (31c) that the apparently non-linear behavior is noticeably affected by the environmental temperature. The polyvinyl acetate used possesses a glass transition temperature of 28-29°C. To illustrate the effect of change in temperature on the stress-strain behavior we show in Fig. 2(a) and 2(b) the response at two temperatures (24.3 and 26.5°C). The difference is so noticeable because the higher temperature is fairly close to the glass transition temperature. To illustrate the effect of strain rate we include Fig. 2(c) which results from an increase in strain rate by a factor of 10 over that in Fig. 2(b). Here it is interesting to note that the range of apparent agreement with the linearly viscoelastic behavior extends to higher stresses or strains than for the slower strain rate, thus emphasizing the fact that the non-linear behavior is a rate or time related non-linearity.

[†]We gratefully acknowledge Professor Tschoegl's assistance, in whose laboratory we could perform the relaxation measurements.

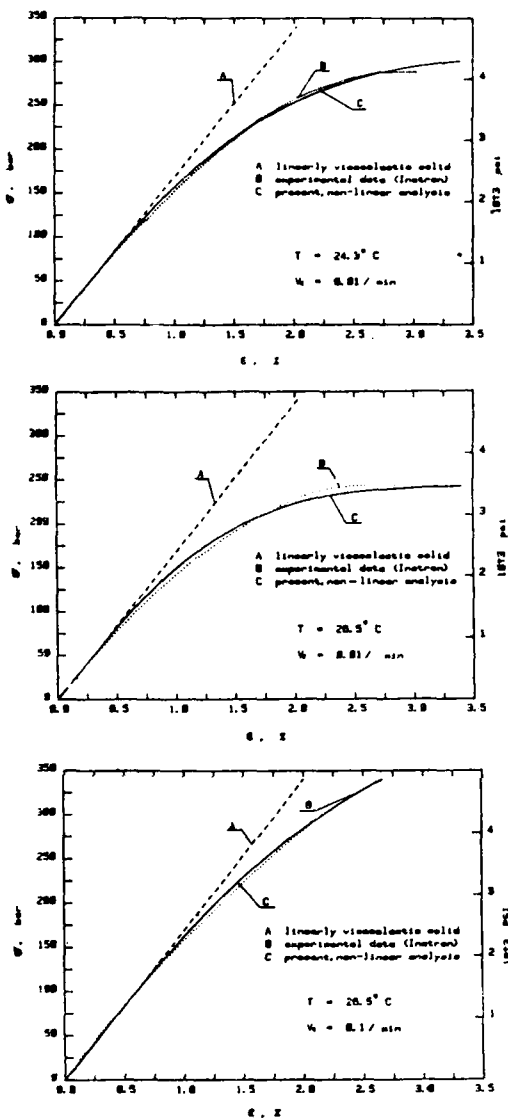


Fig. 2. Uniaxial tensile stress as a function of strain in constant rate of strain test. (a) and (b) illustrate different temperatures at the same strain rate. (b) and (c) illustrate the effect of different strain rate at constant temperature.

CONCLUSIONS

We have presented a theory of non-linearly viscoelastic behavior which is based on the concept of how the free volume affects the internal time scale of the material. We have demonstrated that a formulation consistent with linearly viscoelastic behavior for infinitesimal strains leads to good agreement with the test data in uniaxial tension. The computation requires numerical evaluation and can be incorporated into numerical stress analysis codes.

While it is not our primary purpose to have to justify the polymer physical aspects of the problem, it is of

interest to note that the constants required for the evaluation of the model are either determined by measurements independent from those reported here

$$B = 0.16 \dagger$$

$$f_0 = 0.01 \dagger$$

$$\alpha_T = 5.98 \times 10^{-4}/^\circ\text{C}$$
 (coefficient of thermal volume expansion) \dagger

and by fitting the theory to the test data with the bulk representation of eqn (28). Note also that, as mentioned before the constant $\delta = 1$; this means that the mechanically (stress) induced dilatation is equal to the increase of the free volume.

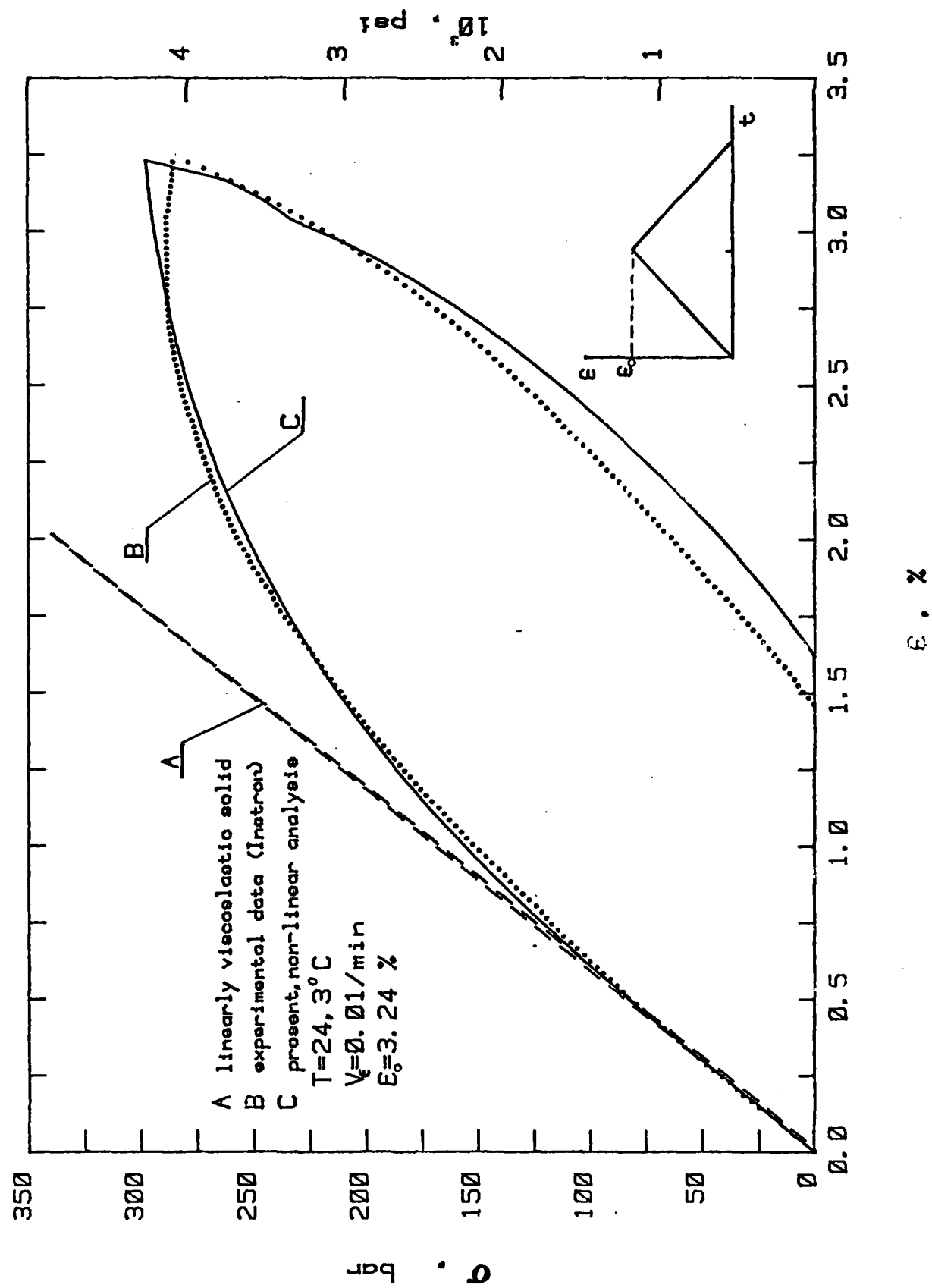
Acknowledgements—The authors wish to acknowledge the support of the Office of Naval Research under Contract N00014-78-C-0634 and are grateful for the support of Dr. R. S. Miller. We also acknowledge the support of Air Force Office of Scientific Research Contract F49620-77-C-0051 and are grateful for the personal support of Lt. Col. J. D. Morgan, who was associated with this program until very recently.

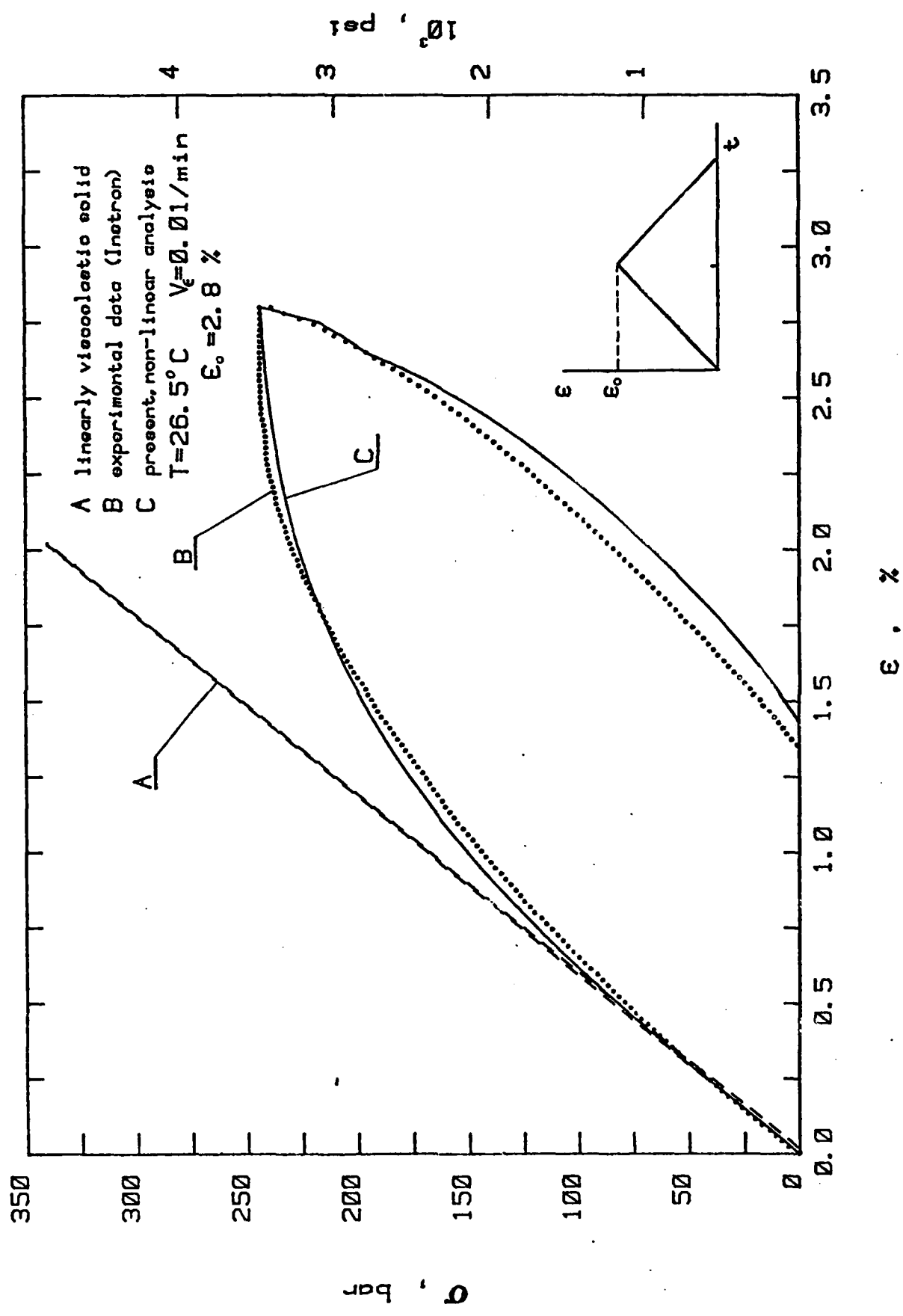
REFERENCES

1. W. G. Knauss and V. H. Kenner, On the hydrothermomechanical characterization of polyvinyl acetate. California Institute of Technology, Graduate Aeronautical Laboratories, GAL CIT SM 80-8.
2. J. D. Ferry and R. A. Stratton, The free volume interpretation of the dependence of viscosities and viscoelastic relaxation times on concentration, pressure and tensile strain, *Kolloid-Z* 171(2), 107-111 (1960).
3. D. Turnbull and M. H. Cohen, Free-volume model of the amorphous phase-glass transition. *J. Chem. Phys.* 38(1), 120 (1961).
4. A. Quach and R. Simha, Pressure-volume-temperature properties and transitions of amorphous polymers; polystyrene and poly (orthomethylstyrene). *J. Appl. Phys.* 42(12), 4592-4606 (1971).
5. R. W. Fillers and N. W. Tschoegl, The effect of pressure on the mechanical properties of polymers. *Trans. Soc. Rheology* 21(1), 51-100 (1977).
6. A. N. Gent, Hypothetical mechanism of crazing in glassy plastic. *J. Mater. Sci.* 325-932 (1970).
7. B. Bernstein and A. Shokoh, The stress clock function in viscoelasticity. *J. Rheology* 28(2), 189-211 (1980).
8. R. A. Schapery, An engineering theory of nonlinear viscoelasticity with applications. *Int. J. Solids Structures* 2, 407-425 (1966). See also
R. A. Schapery, On the characterization of nonlinear viscoelastic materials. *Polymer Engng Sci.* 9(4) (1969).
9. Y. C. Lou and R. A. Schapery, Viscoelastic characterization of a nonlinear fiber-reinforced plastic. *J. Composite Mater.* 5 (1971).
10. W. V. Chang, R. Bloch and T. W. Tschoegl, Study of the viscoelastic behavior of uncrosslinked (gum) rubbers in moderately large deformations. *J. Polymer Sci.* 15, 923-944 (1977).
11. H. Leaderman, Elastic and creep properties of filamentous materials and other high polymers. The Textile Foundation, Washington (1943).
12. J. D. Ferry, M. L. Williams and R. F. Landel, The temperature dependence of relaxation mechanisms in amorphous polymers and other glass-forming liquids. *J. Am. Chem. Soc.* 77, 3701 (1955).
13. J. D. Ferry and R. F. Landel, Molecular friction coefficients in polymers and their temperature dependence. *Kolloid-Z* 184(1/2), 1 (1956).
14. M. L. Williams, Free volume approach to polystyrene melt viscosity. *J. Appl. Phys.* 23(10), 1395 (1958).

\dagger Determined at our laboratory by Mr. Luc Heymans, graduate student.

15. K. H. Hellwege, W. Knappe and P. Lehmann, Die Isotherme Kompressibilität Einiger Amorphen und Teilkristalliner Hochpolymerer im Temperaturbereich von 20–25° C und bei Drucken bis zu 2000 kp/cm². *Kolloid-Z* 143(2), 110 (1961).
16. M. L. Morland and E. H. Lee, Stress analysis for linear viscoelastic materials with temperature variation. *Trans. Soc. Rheology* 8, 233–263 (1960).
17. E. H. Lee, Some recent developments in linear viscoelastic stress analysis. *Proc. 11th Int. Cong. of Applied Mechanics*, Munich (Germany), Springer-Verlag, Berlin (1964).
18. E. H. Lee and T. G. Roberts, On the generation of residual stresses in thermoviscoelastic bodies, *J. Appl. Mech.* No. 65, APMW-8 (1965).





APPENDIX E

SM 80-21

Preliminary Version

CRACK PROPAGATION AT MATERIAL INTERFACES:

II EXPERIMENTS ON MODE INTERACTION

by

K.M. Liechti

W.G. Knauss

California Institute of Technology
Graduate Aeronautical Laboratories
Pasadena, California

I INTRODUCTION

The adhesives used to manufacture structural joints are polymeric and potentially viscoelastic. In contrast to structures made of rate insensitive material properties it has been found in the fracture of monolithic materials^[1], that failure of structural elements having viscoelastic properties need not be due to catastrophic crack growth increase in crack length of an existing flaw. Instead, the element may fail after a rather long period of time due to very slow crack growth which is dictated by the viscoelasticity of the material. We expect the time dependent material properties of the adhesive layer in an adhesive joint can under proper circumstances produce similar effects in the growth history of an interfacial unbond.

The growth history of an interface crack will clearly be affected by the constraint offered by the adherends, particularly through different combinations of displacements of the adherends normal and/or tangential to the bondline. Furthermore, the local stresses in the crack front region may be high enough to induce a nonlinear kinematic and material response, features not normally considered in joint analyses which are mostly based on the linearized theory of elasticity.

These considerations have motivated two initial sets of experiments in what is expected to be a continuing study. The first, for stationary cracks, concerns the linearity of the response

of the crack flank displacements resulting from adherend displacements normal and tangential to the bondline. In the second study, the effects of loading direction on the crack profile and crack propagation rate are determined for steadily propagating cracks.

The tools developed for these experiments as documented in reference 1, allowed the independent prescription of displacements normal to and tangential to the bondline. In addition, that reference delineates how optical interferometry is employed to measure the crack velocity and changes in crack profile of an interfacial debond in a cracked butt joint. The local fracture processes were observed and measured crack opening displacement profile directly through displacement measurements with a resolution of $0.16 \mu\text{m}$. These direct measurements, free of any theoretical stress analysis and its underlying assumptions, provide the basis for exposing nonlinear effects in the adhesive joints under study as well as for investigating various crack propagation criteria.

We turn first to the examination of non-linear phenomena in the next section and follow that development by the description of the crack propagation experiments and examination of failure criteria in section 3.

2 EXAMINATION OF NON-LINEAR DISPLACEMENT RESPONSE FOR A STATIONARY CRACK

The analyses used preferentially today for estimating bond strength average out the effect of the adhesive layer. This procedure ignores the details of the fracture processes in the region of the crack front and assumes the thickness adhesive layer to be negligible small. Fracture mechanics parameters thus become functions of bond thickness and the joint is then considered to be a monolithic body. (See discussion in ref. 2.)

The neglect of the local fracture processes has not, in general, been confined to analysis but also to experimental investigations because it is much easier to measure global rather than local effects. Experiments making the same a priori assumptions as theoretical analysis are therefore conducted which thus may not clarify deficiencies in the modelling. However, serious deficiencies have been exposed in service environments where factors such as temperature and humidity variations (which affect the local fracture processes) produce an apparent randomness to joint failure, when failure is characterized only in terms of global parameters.

Before presenting the results for these two cases, we discuss the general crack profile and shapes obtained in these examinations. The specimens, as described in ref. 2 were composed of glass adherends and a polyurethane elastomer, Solithane 113,

a Thiokol product as the adhesive. Figure 1 shows a sequence of video recordings of an interface separation recorded under increasing applied, (normal) displacement levels. The field of view covered in these pictures corresponds to approximately 0.6 mm, the pictures being centered on the specimen through the thickness. Clearly the crack does not extend completely through the thickness, but has a finger-like shape. The separation of the crack faces is given by the order and location of the fringes in the interference pattern. This finger phenomenon or tunnelling mode of fracture always developed from the through-the-thickness initial crack generated as described in Ref.1. The width of this "finger" was found to change with the type of loading. For displacements applied normal to the bondline, it is approximately $W_n = 0.45$ mm wide, whereas a purely tangential applied displacement produces widths on the order of $W_t = 2$ mm. However, the crack front still retains considerable curvature in this case. A detailed explanation of the finger fracture appears in Ref.2.

Let it suffice for the present purposes to characterize the crack profile by a single lengthwise scan along the center line of the crack (cf. fig.1). The full three dimensional shape of the crack could be generated by a series of scans spanning the full crack width. However, because of the immense use labor for the requisite data acquisition and reduction in our current non-automated system this additional information was not

developed; it would add little to the observations we make here in principle.

A sequence of profiles for increasing displacements applied normal to the bond line is shown in figure 2. The fact that the crack faces are separated when no displacement has been applied indicates the presence of residual stresses. Thermal stresses were eliminated by curing the specimens at room temperature. The initial non-zero crack face separation is therefore due to cure stresses only. It was found [2] that this cure shrinkage is equal to that resulting from a 25°C drop in temperature.

The resulting high deformation gradients in the crack front region cannot be resolved fully to the crack front region by the present crack profile measurement arrangement [1]. The profiles shown in figure 2 are therefore incomplete near the crack front, although the crack front location itself is well identified. Nonetheless, in the regions where the profile can be resolved, the resolution and consistency of the data is extremely good. The error bars on the profiles correspond to the spatial resolution of the microscope (6.5 μm). That is, the location of the crack front and fringes can be determined to within 6.5 μm . We are therefore able to make definitive statements on the linearity of the response in the crack front region due to the globally applied loading.

2.1 Crack Profile Response Displacements Applied Normal to the Bondline

The incremental response at various locations behind the crack front due to applied displacements is obtained by determining the change in crack face separation from the initial (or zero load) profile. We call this change in the crack face separation (on the centerline of the crack) the crack flank normal displacements, record it for various locations behind the crack front as a function of the normal applied displacement in figures 3 and 4. Figure 3 shows the response curves for locations as far behind the crack front as the location of the profile maximum; figure 4 for locations beyond that in order not to confuse the clarity of their presentation.

We see that for normal applied displacements up to about $0.5 \mu\text{m}$ (0.1% average strain across the bond thickness) the response is nearly the same for all locations and fairly linear. At higher levels of normal applied displacement the response is no longer the same for all locations, nor is it linear with respect to the applied displacements

2.2 Crack Profile Response to Displacement Applied Tangentially to the Bondline

We next determine the profile of the normal crack flank displacements resulting from displacements applied tangentially

to the bondline.

In order to examine to what degree the opening displacement depends linearly on the applied displacement parallel to the bonding the following concern must be resolved: A point "A" on the crack surface of the adhesive experiences displacements both normal and tangential to the interface (cf. figure 5). Because the crack profile is measured in the deformed state it could appear, therefore, that any non-linear dependence of the normal displacement u_n could be due to the kinematic involvement of the local tangential displacement u_b . This effect could be pronounced only if the gradient of the crack profile were large. However, as discussed in ref [1] the interferometric fringes can be resolved only where the profile gradients are less than 33 minutes. We, therefore, conclude that the tangential crack surface displacement does not influence the measurement if the crack opening displacement significantly.

Figure 5 shows that a sequence of tangentially applied displacements do indeed produce crack flank normal displacement. Furthermore, the crack develops a finite length with a maximum in the crack face separation occurring near the "leading crack front" (defined in figure 5) decreasing with much smaller profile gradients towards the "lagging crack front". As the tangentially applied displacements are increased in the direction defined by the insert of figure 5, the profile gradients near the loading crack front increase. At the lagging crack periphery,

the gradients remain much the same but there crack closure occurs. In fact, the profile could be fully resolved there within half a wavelength ($0.3 \mu\text{m}$) of separation from the adherend surface. The steepening of the profile and maximum at the leading crack front as well as the smooth crack closure at the lagging crack front has been predicted theoretically by Comninou and Schmueser [3] for an interface crack at a bimaterial interface of two semi-infinite linearly elastic bodies. Although we are dealing here with an adhesive joint geometry of finite thickness, the qualitative behavior could be similar. It is also of interest to note that, if the direction of the applied displacements is reversed, the lagging and leading crack fronts are interchanged such that the maximum in the crack face separation moves to what was the lagging crack front [2].

The crack flank normal displacements at various locations from the leading crack front are shown in figure 6 as a function of the applied tangential displacement. In contrast to the case for normal applied displacements, one observes a pronounced non-linear response even for small applied tangential displacements (less than 0.5% strain). For the purpose of comparing the crack opening displacements resulting from the two deformation modes we draw attention to the differences in the scales of figures 3-4 and 6: Opening displacements resulting from normal applied displacements are on the order of 20 times as large as those

induced by tangentially applied displacements approximately twenty times higher.

2.3 Linearity Analysis - Conclusion

We have been able to consistently and precisely characterize the response of the region close to the crack front due to globally applied loading. Ultimately, it is the local crack tip response which determines the onset of fracture. Measures of the local response have hitherto been unavailable and analyses have therefore characterized joint failure in terms of global parameters under assumptions of a linearised theory. The results show that for normal displacements the linearity assumptions are indeed valid (for strains less than 0.1%), at least to engineering accuracy. However, in the case of displacements applied tangential to the bondline, the local response is highly nonlinear. Linear modelling in this case must therefore be suspect. Since even amounts of tangentially applied displacements produce a nonlinear response, this suspicion must also be extended to cases of combined loading. Most joints will experience combined loads and any realistic modelling and analysis of failure should incorporate measurements of the local failure processes.

SUMMARY OF THE NON-LINEARITY ANALYSIS

In view of the refined resolution of displacement measurements we are able to identify the range of relative adherend displacements (or thickness averaged normal and shear strains) in which non-linear phenomena became appreciable. The measurements are limited to monitor only normal or crack opening displacement profiles. However, we are able to establish the relative order of magnitude of normal displacements derived from applied normal and from tangential displacements. The assumption is thus near at hand that the relative difference in the crack flank tangential displacements resulting from normal and tangential applied displacements is also on the same order. These order estimates become important in our subsequent analysis (section III) of interfacial crack propagation and the search for an appropriate crack growth criterion.

3 INTERFACIAL CRACK PROPAGATION

We turn now to phenomena associated with the growth of an interfacial crack with the intent to examine criteria for crack growth. Similar to the fracture of monolithic viscoelastic solids the failure of bonded joints involving viscoelastic adhesives is described in terms of crack growth rates which depend on the viscoelastic material behavior and on the history of the applied loads (or displacements) in any particular

geometry. Any structural failure is thus the result of the crack size accumulated during the past service of the structure.

We consider first some general observations of crack growth behavior and discuss the experimental limitations on determining the crack propagation velocities.

INITIAL CRACK GROWTH RESPONSE

Again, we distinguish response to normal and tangentially applied displacements; the more general case involving their combinations was excluded from consideration in this study. In either case displacements of the adherends were prescribed to follow the incremental time history illustrated in the upper part of figure 3, each increment lasting about 500 sec. The response of the crack was distinctly different for the two types of applied displacements, with respect to crack opening and the development or change in the crack plan form. Using for the present purposes the normal displacement at the maximum as an indicator one finds that the displacement decreases while the externally applied normal displacements are held constant; the converse is true for tangentially applied displacements. This observation is illustrated in figure 8 where ΔV_N and ΔV_T refers to changes in the crack opening displacement at the profile maximum during the time when the applied displacements are held constant.

This time dependent response is somewhat surprising since in view of the uniaxial creep behavior of the model adhesive shown in figure 7 (note that this representation is appropriate at a temperature of 0°C). Bearing in mind that the present measurement were performed at 60°C (corresponding to a shift factor of 4 decades) it is indeed surprising that easily measurable viscoelastic effects would still be present.

When the applied displacements are increased to the point where crack propagation occurs a steady state condition is achieved after about 10 minutes. During this time the crack grows (expectedly) in a distinctly different manner: Under applied normal displacements the crack would propagate in the original finger mode (cf. middle of figure 8); under tangentially applied displacements the initial finger geometry first widened at the crack mouth away from the "finger tip" (cf. bottom of figure 8). The crack would not propagate until this widening had reached its tip or front. Afterwards the crack would propagate with trailing end closure as discussed in section 2, somewhat in the form of a "bubble", the volume of which was, however in communication with the surrounding air.

Crack propagation velocities could be measured in the range from 10^{-6} to 10^{-3} in/sec. The lower limit was dictated essentially by the experimenter's patience to determine the crack front location for a velocity computation with about 20% accuracy. The upper limit was determined by the field of view in the microscope

and relative error in time measurement. At room temperature crack propagation speeds were exceedingly slow, therefore the specimens were heated uniformly to 60°C. Since the elastomeric adhesive is thermorheologically simple the velocities at other temperatures can be readily determined with the aid of the shift factor in figure

3 INTERFACIAL CRACK PROPAGATION AT CONSTANT RATE

We expect the failure of adhesive joints using polymeric adhesives to occur in a gradual way and, in general, under initially very small crack propagation rates. Only in the final stages of failure is fracture expected to occur catastrophically. Thus it becomes necessary to examine the relationship between critical fracture parameters and the rate of unbonding. The life of a joint can then be estimated from a knowledge of the load (and environmental) history to which it is to be subjected and the resultant crack propagation rates. The number of fracture parameters to be related to the unbonding rate will depend on how the fracture process is to be modelled. In engineering applications, simplicity of modelling has obvious attractions. The optimum model is that which uses the minimum of parameters to capture the essentials of the process. Again, one may propose to model crack growth on the local fracture processes or by averaging out local effects and considering only global parameters.

Our experimental tools allow us to measure directly the local crack profile at a particular crack propagation rate as well as the globally applied loading which produced them. We are therefore in a position to compare local and global crack propagation criteria.

Some remarks on the nature of the adhesive material Solithane are presented by way of introduction in Section 3.1. The experimental procedure is described and some initial observations are made in section 3.2. In sections 3.3 and 3.4 the data is presented and analyzed in order to develop and compare global and local fracture criteria, respectively.

3.1 Solithane Material Properties

Solithane 113 is a polyurethane elastomer marketed by the Thiokol Chemical Corporation. It is obtained by mixing a liquid prepolymer with a catalyst. The ratio of the two components can be varied to provide a considerable range of material properties. In the present study, a mixture of 60% prepolymer to 40% by weight catalyst was used. Reasons for using Solithane as the adhesive material were discussed in [1].

We further note here that it fractures under relatively small strains (1.0%), making comparison with fracture models based on small deformation theory more valid. The fracture surface is featureless even at low crack propagation rates,

indicating a brittle type of fracture. Analysis is thus simplified by not having to account for plasticity effects. The master creep curve, obtained in [4], is shown in figure 7. Solithane is thermorheologically simple and its time temperature shift curve is also shown in figure 7. Time-temperature shifting can therefore be used to extend the range of experimentally acceptable time scales.

3.2 Experimental Procedure and Some Initial Observations

a) Applied Displacement History

Again, two separate experiments consisting of purely normal and purely tangential displacements were applied to the joints. Temporal considerations limited us to these two extremes of a range of possible combinations of normal and tangential applied displacements. The applied displacement history in these crack propagation tests is illustrated in figure 8. The displacements were applied to the joint in a sequence of discrete increments (ΔV , fig. 8), each of which was held constant for 500 seconds. Since the crack profile measurement system includes a video tape recorder, the crack front velocity could be monitored continuously. In the interests of simplicity, crack profile measurements were made only after the crack propagation rate became constant (the average of at least three measurements) at each load level.

b) Crack Velocity

The crack propagation rates that could be measured ranged from 10^{-6} to 10^{-3} in/sec. The lower limit was dictated by the length of time needed to achieve a crack front extension such that the relative error in crack front displacement measurement was less than 20%. The upper limit was determined by the field of view in the microscope and relative error in time measurement. The crack velocities obtainable at room temperature were increased by heating the specimens to 60°C. These velocities can be compared with tests at other temperatures using the appropriate time-temperature shift factor for Solithane.

c) Crack Profile Measurement

Crack profile measurements clearly lend themselves to the development of local fracture parameters such as the crack opening displacement and crack opening gradients. While there is a lack of uniqueness in defining just how far behind the crack front such parameters should be defined, we had hoped to be able to obtain such measurements as close as 2.54 μm from the crack front, corresponding to the spatial resolution of the microscope used to view the interference fringes. However, the first resolvable fringes were usually on the order of 254 μm from the crack front. We therefore sought to fit any available data to an analytically obtained profile so as to determine local fracture parameters closer to the crack front than 0.254 mm.

The choice of profiles to which to fit the data is rather limited. There are no nonlinear analyses of the full three dimensional cracked adhesive joint geometry. The best alternative is provided by findings of Knowles and Sternberg [5] in the nonlinear analysis of crack face deformations in two dimensional monolithic solids. They found for harmonic materials that the crack profile near the crack tip followed a combination linear and power law of the form

$$y = a x^{\frac{1}{2}} + b x \quad (1)$$

where y is the crack face separation and x the distance from the crack tip. The locations of the crack tip and the first two resolvable fringes were used in a curve fit to determine the coefficients a and b . This allowed the local fracture parameters to be determined much closer to the crack tip ($2.54 \mu\text{m}$ was chosen).

d) Initial Observations

Cracks were initiated from both edges of the specimen. Under normal applied displacements, both initial cracks grew to meet eventually at the center of the specimen. As noted earlier, the cracks did not extend completely through the thickness, but grew in a finger or tunnelling mode, with a consistent finger plan form thickness which was approximately one third of the specimen thickness. However, the cracks did not meet in a catastrophic manner. Instead, they stopped, leaving an as yet

unbonded region on the order of the bond thickness between them. The plan form thickness of the finger then increased until the cracks did extend completely through the specimen thickness.

The narrow initial crack, which was first brought into the field of view of the microscope with a small normal applied displacement from the wire-initiated location, widened under a tangential applied displacement. The widening propagated towards the still stationary crack front. The crack propagated only when this widening reached the crack front. Furthermore, the crack propagated as a bubble rather than growing in length.

Finally, it should be noted here that the crack profiles, which were measured only when the crack propagation rates were constant, indicated a change in crack face separation during this time period. For normal applied displacements, the crack face separation decreased slightly, whereas it increased slightly under tangential applied displacements. The time dependence of these local crack face separations during periods of constant applied displacement imply a viscoelastic response in the bulk material and not just in the local crack front region; a common assumption.

While not all the effects noted here are included in the analyses presented in the following sections, it should be clear that they would not have been noticed in an experiment measuring only such global parameters as the applied load.

3.3 A Global Fracture Criterion

The global parameters measured in this series of experiments conducted for steadily propagating cracks are the displacements applied normal to or tangential to the bondline. Figure 9 shows the relationship between the applied displacements and the resultant crack propagation rates for the two loading cases. A slight velocity dependence is indicated and it can also be seen that the displacement level required to produce a given crack propagation rate is greater in the tangential loading case. This latter observation confirms the rule of thumb or designing adhesive joints in sheer and also the findings of Stone et.al.[6].

In formulating a global fracture criterion, we wish to relate the applied displacements to the crack propagation rate. One convenient method is through the strain energy release rate, defined as the rate of change of strain energy with respect to the change in crack length. Crack propagation occurs when the strain energy release rate is greater than or equal to the fracture (surface) energy.

The evaluation of the strain energy release rate requires the knowledge of the stresses and strains in the adhesive layer. An apparent modulus, reflecting the constraint of the stiff adherends was determined on the basis of the thickness averaged normal stress in an uncracked adhesive layer [2]. It is the apparent modulus rather than simply the Young's modulus that is

used here to calculate the thickness-averaged strain energy due to a displacement applied normal to the bondline. The calculation of the strain energy due to a displacement applied tangential to the bondline is straightforward.

The displacements applied normal to the bondline were such that the normal strains in the bulk of the adhesive layer were less than 0.1%. The shear strain in the bulk of the adhesive layer due to the displacements applied tangential to the bondline were less than 1%. Such low strains are normally sufficient to justify the use of linearised viscoelasticity. The change in strain energy density is considered in regions well away from the crack front. Further simplification to the use of linearized elasticity was therefore allowed by the fact that the strain rates were low enough to preclude any viscoelastic response in the bulk material far removed from the crack front region. Note that a viscoelastic response in the material in the crack front region is expected due to the high strain rates induced by the propagation of the crack. This is reflected in a velocity dependent fracture surface energy.

Under a displacement applied normal to the bondline, the loss in energy due to a unit crack advance was found to be [2]

$$\Delta U_N = \frac{E_\infty}{3} [a_s(a_s^2 + 2) - 2a_N(a_N^2 + 2)] U_N^2 \quad (2)$$

where

E_∞ is the rubbery modulus of Solithane,

$a_s = t_s/h$ is the aspect ratio of the bonded region ahead of the crack

$a_N = t_N/h$ is the aspect ratio of the bonded region ahead of the crack front

and, with reference to figure 10.

$2t_s$ = specimen thickness,

$2t_N$ = "leg" thickness under normal loading

$2h$ = bond thickness.

Notice here that we have been able to make a small improvement on most global approaches in that we have accounted for the different crack surface areas in the different loading cases.

Similarly, under a given tangential displacement, U_T , the loss in strain energy due to a unit crack advance is

$$\Delta U_T = \frac{E_\infty}{b} (a_s - a_T) U_T^2 \quad (3)$$

For crack propagation to occur, the fracture surface energy must be equal to or exceed the rate of change of strain energy. Since the crack length can be considered infinite with respect to the bond thickness, and the displacements are uniformly applied, we assume that the change in strain energy per unit crack advance is the same as an incremental change in strain energy for

an infinitely small crack advance. We also note that S is the rate dependent fracture surface energy comprising the constant, intrinsic fracture energy. (T in Ref.[4]) and the rheological response of the material around the crack front.

Thus

$$S(\dot{c}) = \Delta U_N + \Delta U_T$$

From (2) and (3) we obtain

$$S(\dot{c}) = \frac{E_\infty}{b} [\{ 2a_s (a_s^2 + 2) - 4a_N (a_N^2 + 2) \} U_N^2 + (a_s - a_T) U_T^2] \quad (4)$$

For our particular geometry [2], (4) simplifies to

$$S(\dot{c}) = \frac{E_\infty}{b} [1332 U_N^2 = 5.92 U_T^2] \quad (5)$$

and, for the present experiments, where either U_N or U_T are zero we have either

$$S(\dot{c}) \approx 222 E_\infty U_N^2 \quad \text{or} \quad (6a)$$

$$S(\dot{c}) \approx E_\infty U_T^2 \quad (6b)$$

The square root of $S(\dot{c})$ is plotted verus the crack velocity in figure 11 by determining the applied displacements which caused the crack to run at that particular rate. The fracture energy is consistently greater, for a given velocity, for the normal loading case. The greater scatter in the normal loading case is due to the fact that different steps in applied displacement were used in some of those tests whereas as in the tangential applied displacement tests the loading history was

the same in all respect and, furthermore, that the bulk visco-elastic response (noted earlier) was dependent on the size of the load step.

In [2] an attempt was made to account for the difference in the two curves presented in figure 11 by using a time-shift on the basis of a difference in cohesive zone sizes for the two loading cases. However, the analysis showed that the cohesive zone sizes were approximately the same. The difference was certainly not enough to produce the shift in the curves in figure 11. Achenbach et.al. [7] also determined that the cohesive zone size was insensitive to load direction.

These results suggest that a critical cohesive zone size might provide a unifying fracture criterion for all possible combinations of applied displacements. It is clear, however, that the global fracture criterion, incorporating the applied displacements, does not.

3.4 Fracture Criteria

We distinguish between global and local criteria: We refer to a global criterion when the stresses or displacements acting on the test geometry are used to describe the fracture behavior. In this case such a global criterion might relate crack growth behavior to the energy released from the adhesive during crack growth. It is us trivial matter to compute the energy release rate for the crack shapes encountered here. Even if this

computation could be performed adequately these would be little sense in doing so because in the end one would only be verifying the first laws of thermodynamics, a somewhat fertile exercise.

Instead we shall concern ourselves with evaluating our experimentally derived displacement data to examine local criteria that draw on the deformations in the crack front region.

3.5 Local Fracture Criteria

The local fracture parameters developed in this section are obtained from measurements of the crack profile at a given crack velocity. We evaluate three possible criteria, namely:

- (a) critical crack profile gradient
- (b) critical normal crack opening displacement (NCOD)
- and (c) critical vectorial crack opening displacement (VCOD)

(a) Critical Crack Profile Gradient

Based on linear viscoelasticity, the local crack profile gradient can be shown to be proportional to the stress intensity factor. Since any local mode I and mode II deformations should contribute to the local profile gradient and also remembering its association with the stress intensity factor (albeit through linearized theory), the local profile gradient might be viewed as an effective stress intensity factor. It should therefore account for any combinations of local deformations normal to and tangential to the bondline. Furthermore, the crack profile

gradient could be thought of as a crack opening angle, which has been postulated as a fracture parameter for stable crack growth in ductile metals [8],[9].

As indicated earlier (Section 3.2.c), the crack profile could not be determined all the way to the crack front. The profile gradient was therefore obtained at 2.54 μm behind the crack front by differentiating equation (1) following a fit of the available data. In view of the tenuousness of this estimate, another measure of the gradient was taken to be the height of the maximum separation of the crack faces divided by its distance from the crack tip. The two measures differed by a factor of ten but gave otherwise very consistent results. In the following discussion only the first measure will be used.

The results for the crack profile measurements are now shown in figure 12 where the dependence of the velocity on the profile gradient is plotted for the two separate cases of displacements applied either normal or tangential to the bondline. The two curves are closely parallel on the logarithmic plot with the gradient, for a given velocity, being consistently greater in the normal loading case.

We have seen in section 3.3 (global criterion) that a time-shifting of the curves there could not be justified on the basis of a difference in cohesive zone sizes. Although we cannot relate the crack profile gradient to cohesive zone size at this time [2] we must suspect that such an analysis would also reveal an equivalence of cohesive zone sizes for the two loading cases.

The implication here is that the rheological response is independent of the loading direction and any curve shifting to provide a unifying criterion for all possible combinations of applied displacements must be done on the vertical axis. It is clear, at this point, that neither the global energy criterion nor our measure of profile gradient provide such a unifying criterion.

(b) Critical Normal Crack Opening Displacement (NCOD)

The NCOD is the mode I crack opening displacement commonly considered in the fracture of monolithic materials. In the present study, it was obtained at a distance of 2.54 μm from the crack front by fitting the crack profile data to equation (1). In figure 13, we plot the NCOD versus the crack propagation rate for displacements applied either normal to or tangential to the bondline. We see, once again, that the critical fracture parameter is different for the two loading cases; the critical NCOD being consistently higher under the normal loading.

(c) Critical Vectorial Crack Opening Displacement (VCOD)

For a crack at a bimaterial interface, we expect the local crack flank displacements to have components of displacements both normal to and tangential to the bondline, even in cases of purely normal or purely tangential applied displacements. We have just seen that the NCOD, which only accounts for crack flank displacements normal to the bondline, does not provide a unifying

criterion. It therefore seems reasonable to propose a vectorial crack opening displacement criterion (VCOD), which is obtained by a vectorial addition of the crack flank displacement components normal and tangential to the bondline. (figure 14).

We expect the (velocity dependent) critical VCOD to be the same regardless of loading direction. Under a normal applied displacement, the major contribution to the magnitude of the VCOD comes from crack flank displacements normal to the bondline (figure 14a), whereas a tangential applied displacement would provide mainly crack flank tangential displacements. (figure 13b). In addition, the fact that the critical VCOD should be the same in both cases explains why the NCOD considered earlier would be higher under a normal loading. With reference to figures 13a and 13b, we see that

$$|S_N| = |S_T| = S_C \quad \rightarrow V_N > V_T$$

where S_N is the VCOD due to a normal applied displacement
 S_T is the VCOD due to a tangential applied displacement
 S_C is the magnitude of the VCOD
and V_N and V_T are the NCOD for normal and tangential applied displacements, respectively.

Further support of the VCOD is provided by Achenbach et.al [7] who found it to be a natural and consistent criterion in the separation of a bimaterial interface regardless of the problem formulation in terms of normal or tangential cohesive stress

distributions. Finally, within the confines of linear elasticity, it can be shown [10] that the VCOD taken at a given distance from the crack front is equal to the square root of the sum of the local mode I and mode II stress intensity factors. The basis for the equivalence of the VCOD to the J integral was established by Smelser and Gurtin [11] and finalised in [12].

Experimental support of the VCOD criterion requires the measurement of both the crack flank normal and the crack flank tangential displacements. In the present study, the crack profile measurements only provide crack flank normal displacements. The measurement of crack flank tangential displacements was beyond the scope of this investigation, but could possibly be achieved using speckle holography.

An estimate of the crack flank tangential displacements was made in [2] for the separate loading cases of normal or tangential applied displacements. For normal applied displacements, it was assumed that the VCOD was equal to the NCOD already shown in figure 13; i.e., the crack flank tangential displacements are much smaller than the crack flank normal displacements. In the case of tangential applied displacements, the results of Rice and Shih [13] were used to estimate the crack flank tangential displacements. In particular, it was found [2] that the magnitude of the VCOD $|S_T|$ due to a tangential applied displacement, U_T , was

$$|S_T| = \sqrt{C U_T^2 + V^2} \quad (7)$$

where V = the crack flank normal displacements as obtained from crack profile measurements

and $c = 3.16 \times 10^{-2}$ for the particular choice of geometry, materials and VCOD location chosen for this study.

The VCOD due to the tangential applied displacements obtained from equation (7) is also shown in figure 13. We see that the VCOD for the two loading cases are very nearly the same. There is certainly an improvement over the NCOD criterion

3.6 Steady Crack Propagation Studies - Conclusion

The use of optical interferometry has provided some rather unique observations and measurements of the local fracture processes in a joint containing a steadily propagating interface crack. One global and three local fracture criteria were developed and compared on the basis of the interferometric measurements. It was noticed that there was less scatter in the data for the local criteria.

The global criterion, relating the applied displacements to the fracture energy, and two of the local criteria (critical crack profile gradient and normal crack opening displacement) were considerably greater when the direction of the applied displacements was normal to the bondline. A vectorial crack opening displacement in which the components of crack opening displacement both normal and tangential to the bondline are

added vectorially was then postulated. However, the tangential crack flank displacements could not be directly determined in the present set up and were therefore estimated based on the linearised theory. The results nonetheless indicate that the vectorial crack opening displacement criterion provided the most unified fracture parameter of the four criteria considered.

REFERENCES

1. Liechti, K.M. and Knauss, W.G., "Crack Propagation at Material Interfaces: I Experimental Techniques to Determine Crack Profiles", submitted to SESA for Publication 1980.
2. Liechti, K.M., "The Application of Optical Interferometry to Time Dependent Unbonding", PhD Thesis California Institute of Technology, May 1980.
3. Comninou, M. and Schmueser, D., "The Interface Crack in a Combined Tension-Compression and Shear Field", J. App. Mech., 46 (1979) pp. 345-348.
4. Knauss, W.G., "On the Steady Propagation of a Crack in a Viscoelastic Sheet: Experiments and Analysis", in Deformation and Fracture of High Polymers, ed. Kausch, Hassel and Jaffe, Plenum Press 1973.
5. Knowles, J.K. and Sternberg, E., "On the Singularity Induced by Certain Mixed Boundary Conditions in Linearized and Non-linear Elastostatics", Int. J. Solids and Structures, 11 (1975) p. 1173.
6. Stone, S.E., Westmann, R.A., and Fourney, M.E., "Analytical and Experimental Studies in Adhesive Mechanics", UCLA-ENG-7556 (1975), Univ. of Calif., Los Angeles.
7. Achenbach, J.D., Keer, L.M., Khetan, R.P. and Chen, S.H., "Loss of Adhesion at the Tip of an Interface Crack", J. of Elasticity, 9 (1979) pp.397-424.
8. Shih, C.F., deLorenzi, H.G., and Andrews, W.R., "Studies on Crack Initiation and Stable Crack Growth", Elastic-Plastic Fracture, ASTM STP 668, J.D. Landes, J.A. Begley, and G.A. Clarke, Eds., American Society for Testing and Materials, 1979, pp. 65-120.

9. Kanninen, M.F., et al., "Elastic-Plastic Fracture Mechanics for Two-Dimensional Stable Crack Growth and Instability Problems", Elastic-Plastic Fracture, ASTM STP 688, American Society for Testing and Materials, 1979, pp. 121-150.
10. Smelser, R.E., "Evaluation of Stress intensity factors for Bi-Material Bodies Using Numerical Crack Flank Displacement Data". Int. J. of Fracture, 15, (1979) pp. 135-143.
11. Smelser, R.E., and Curtin, M.E., "On the J-Integral for Bi-Material Bodies", Int. J. of Fracture, 13, (1977), pp. 382-384.
12. Quarterly Progress Report No. 4 (1 June to 31 August 1980) "Integrated Methodology for Adhesive Bonded Joint Life Predictions", General Dynamics, Fort Worth Division, Technical Report FZM-6931, September 1980.
13. Rice, J.R. and Shih, G.C.: Plane Problems of Cracks in Dissimilar Media, J. Appl. Mech., 32 (1965) pp. 418-423.

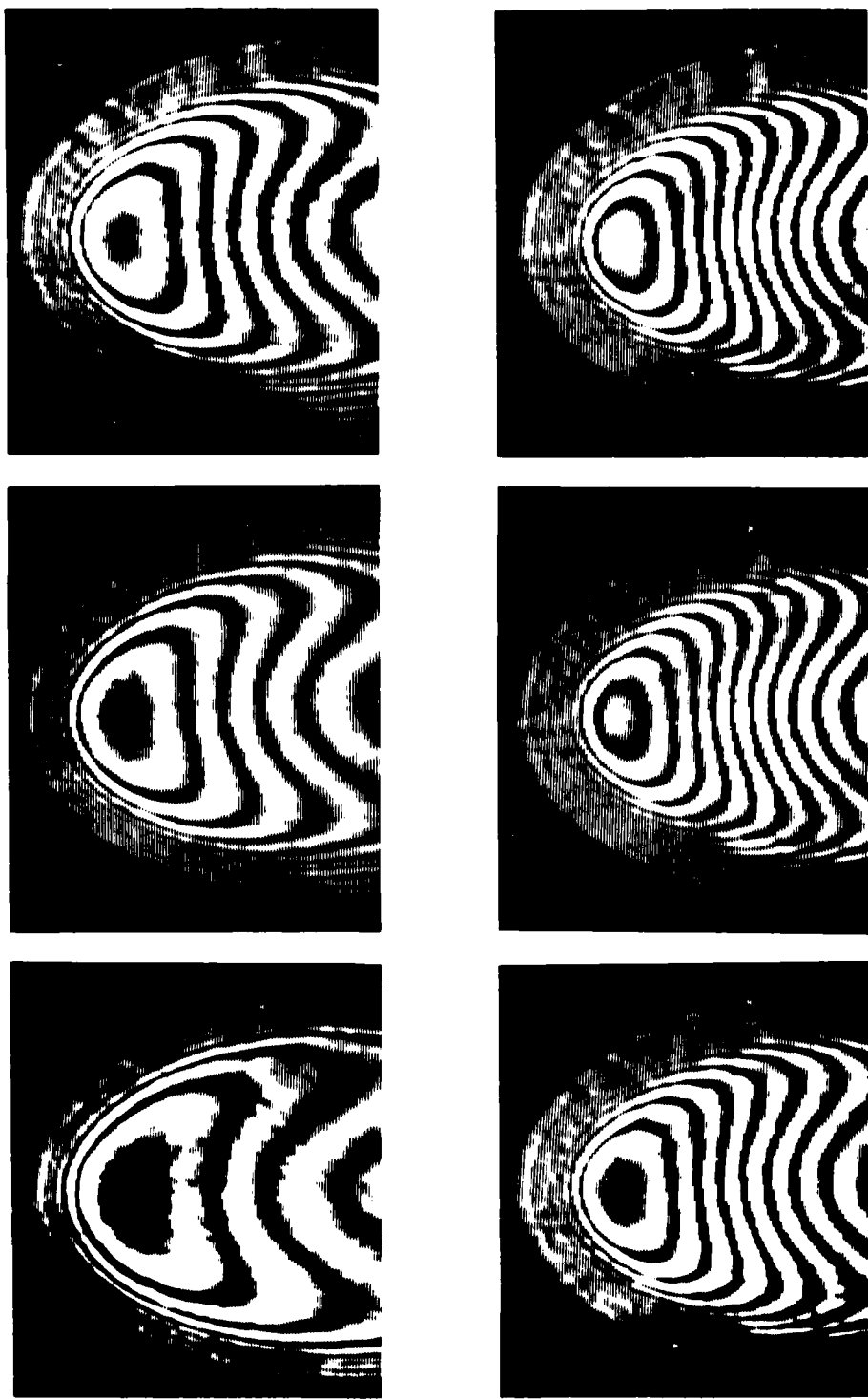


FIG. 1. INTERFERENCE FRINGE PATTERNS OF AN INTERFACE CRACK AT SUCCESSIVE NORMAL LOAD LEVELS.

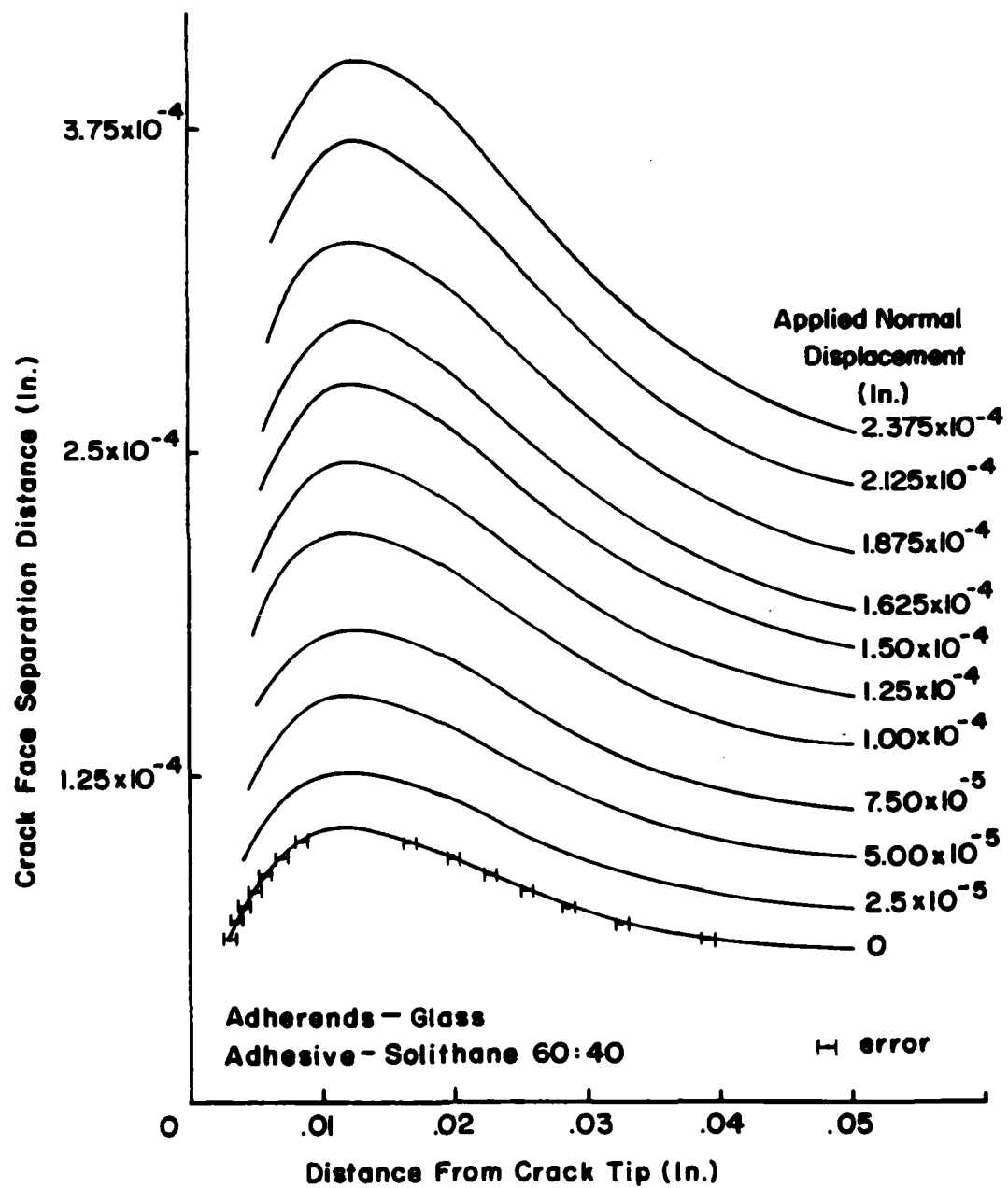


FIG. 2 CRACK PROFILES FOR DIFFERENT APPLIED NORMAL DISPLACEMENT

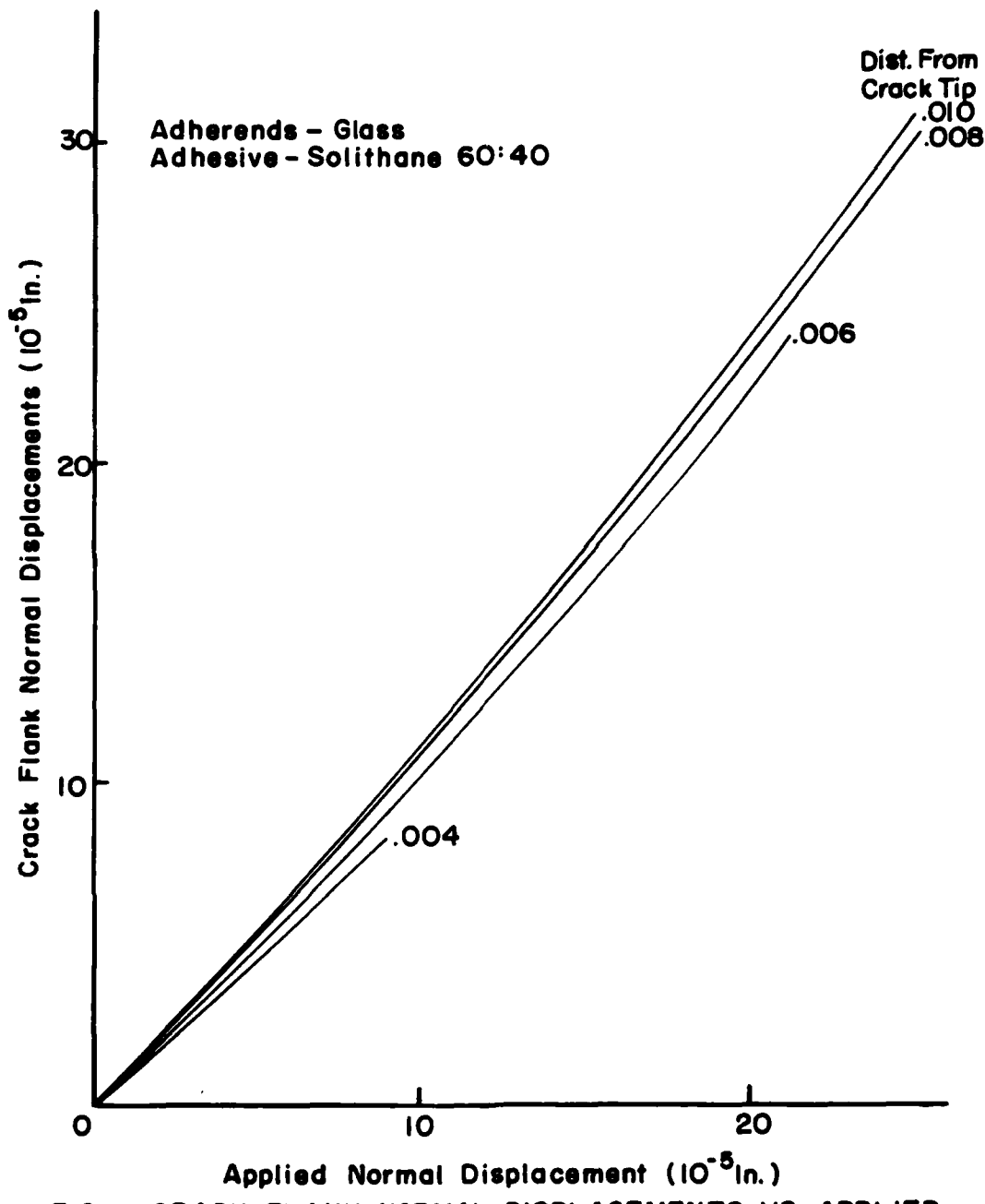


FIG. 3 CRACK FLANK NORMAL DISPLACEMENTS VS. APPLIED NORMAL DISPLACEMENTS

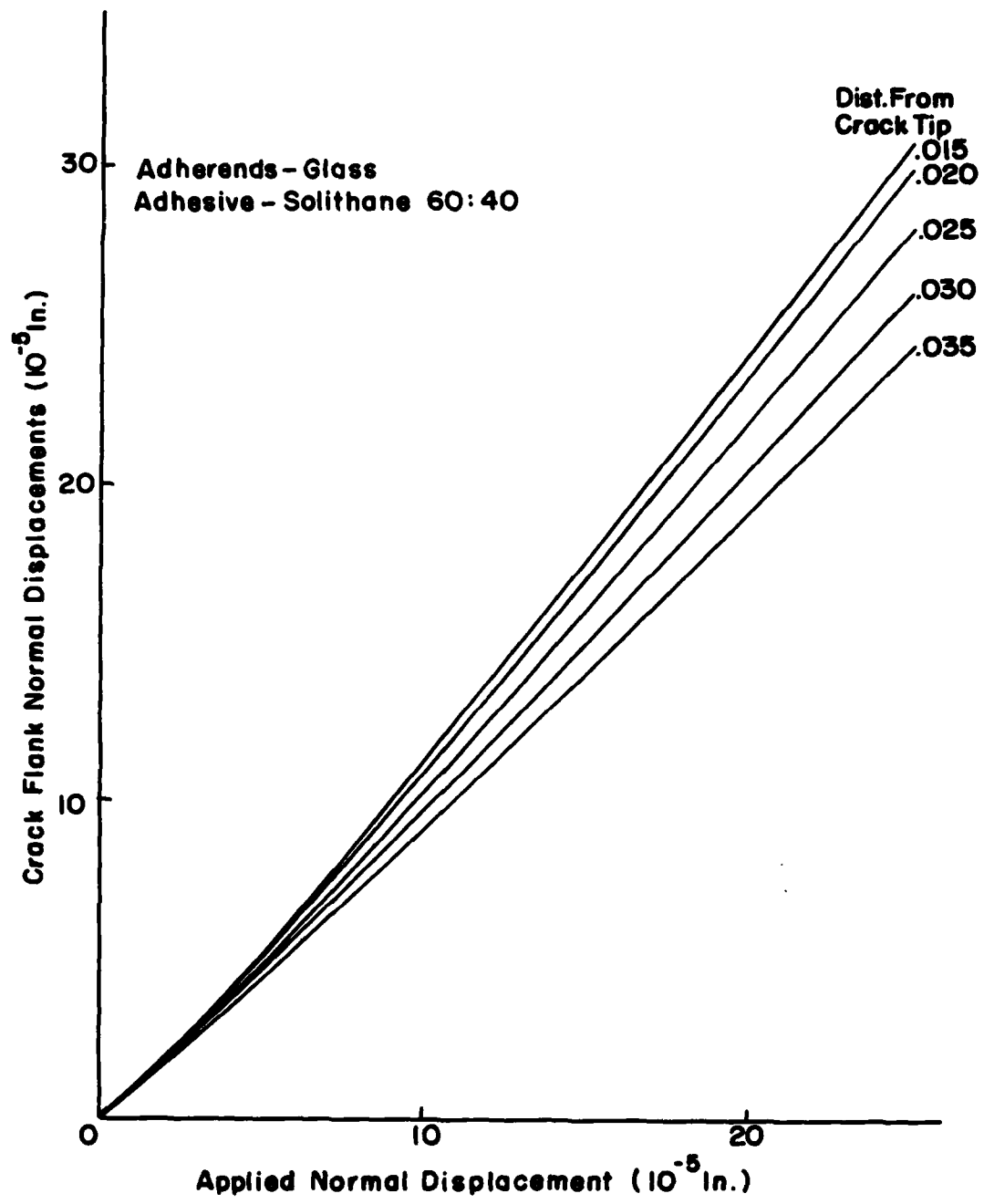


FIG. 4 CRACK FLANK NORMAL DISPLACEMENTS VS. APPLIED NORMAL DISPLACEMENT

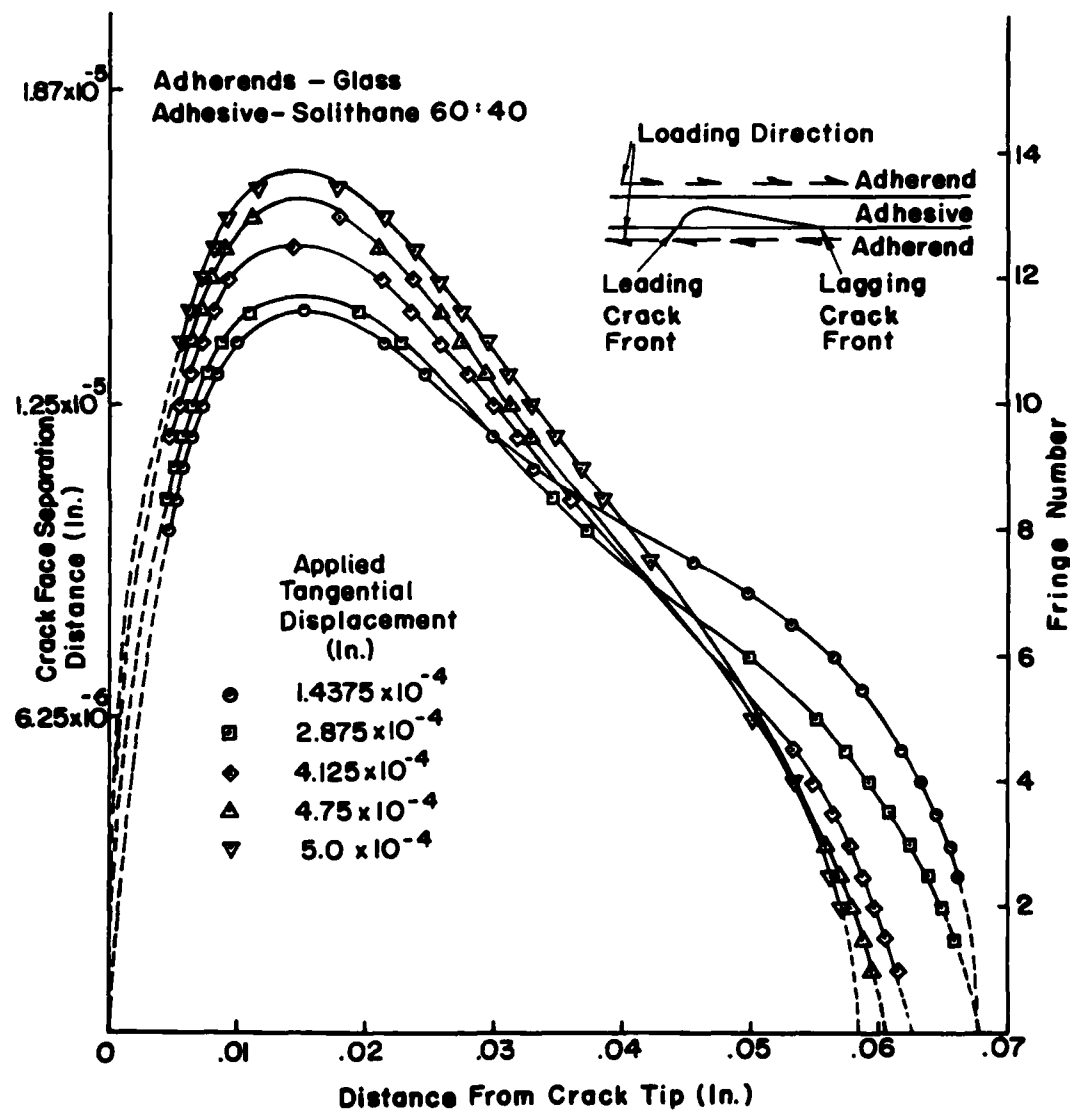


FIG. 5 CRACK PROFILE FOR DIFFERENT TANGENTIAL DISPLACEMENTS

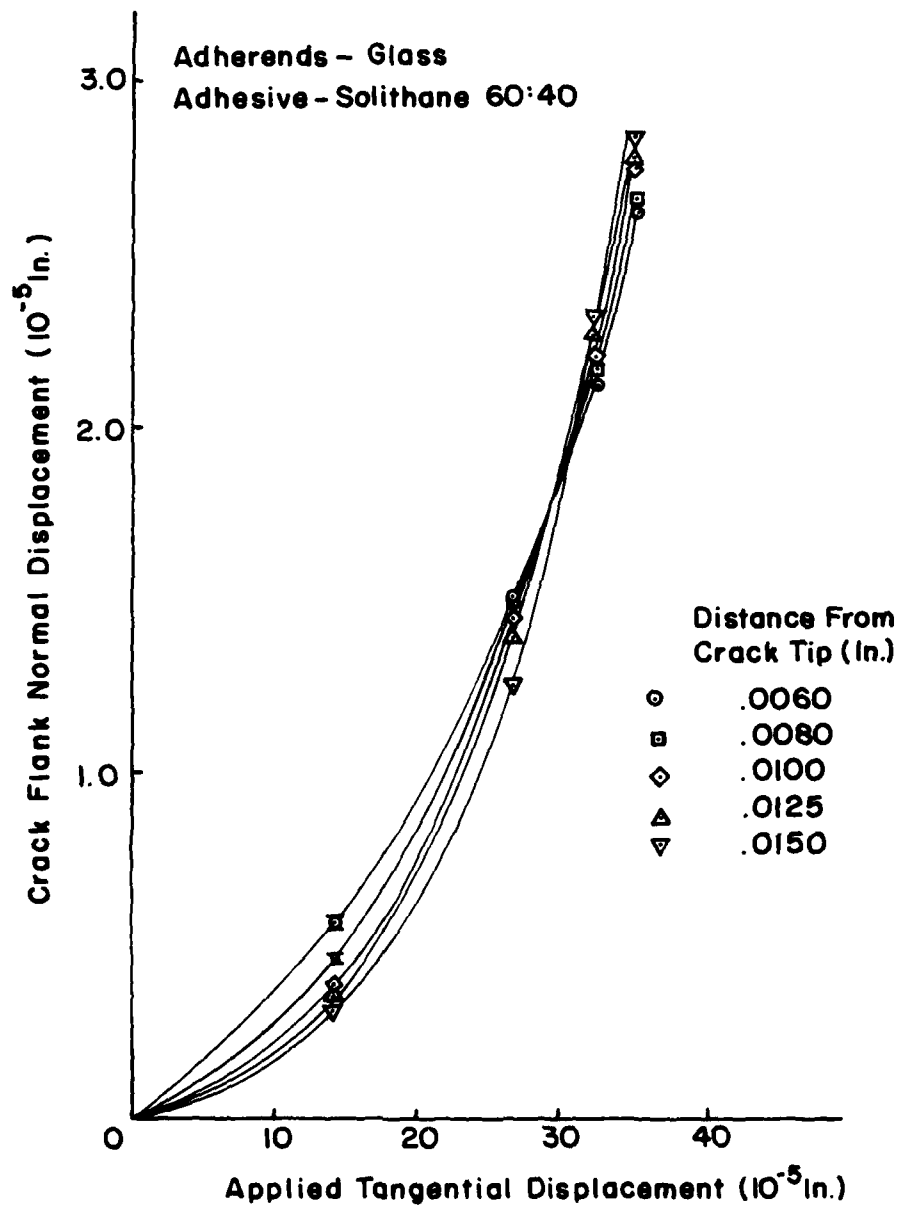


FIG. 6 CRACK FLANK NORMAL DISPLACEMENT VS.
APPLIED TANGENTIAL DISPLACEMENT

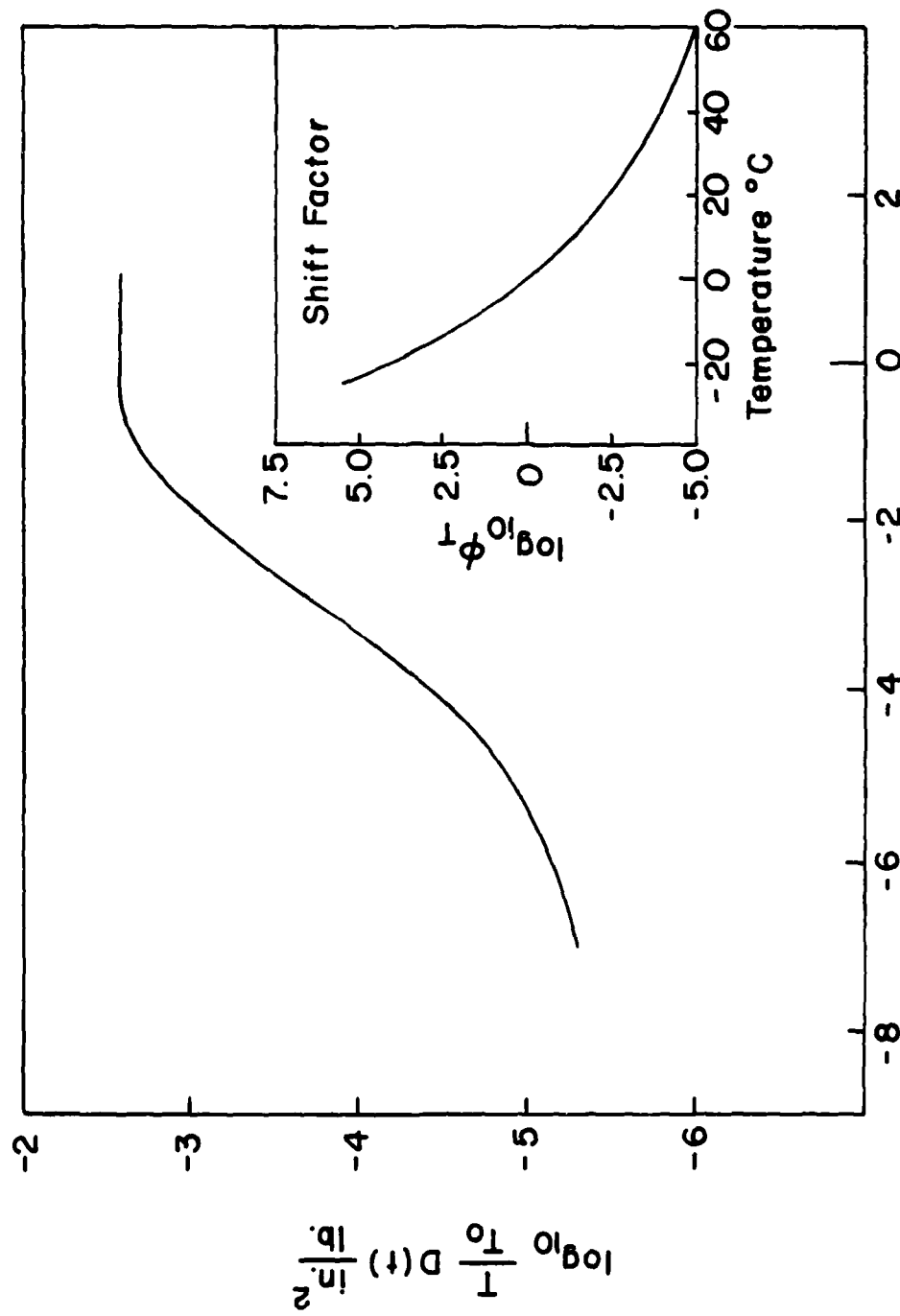


FIG. 7 MASTER CREEP COMPLIANCE AND SHIFT FACTOR CURVES FOR SOLITHANE

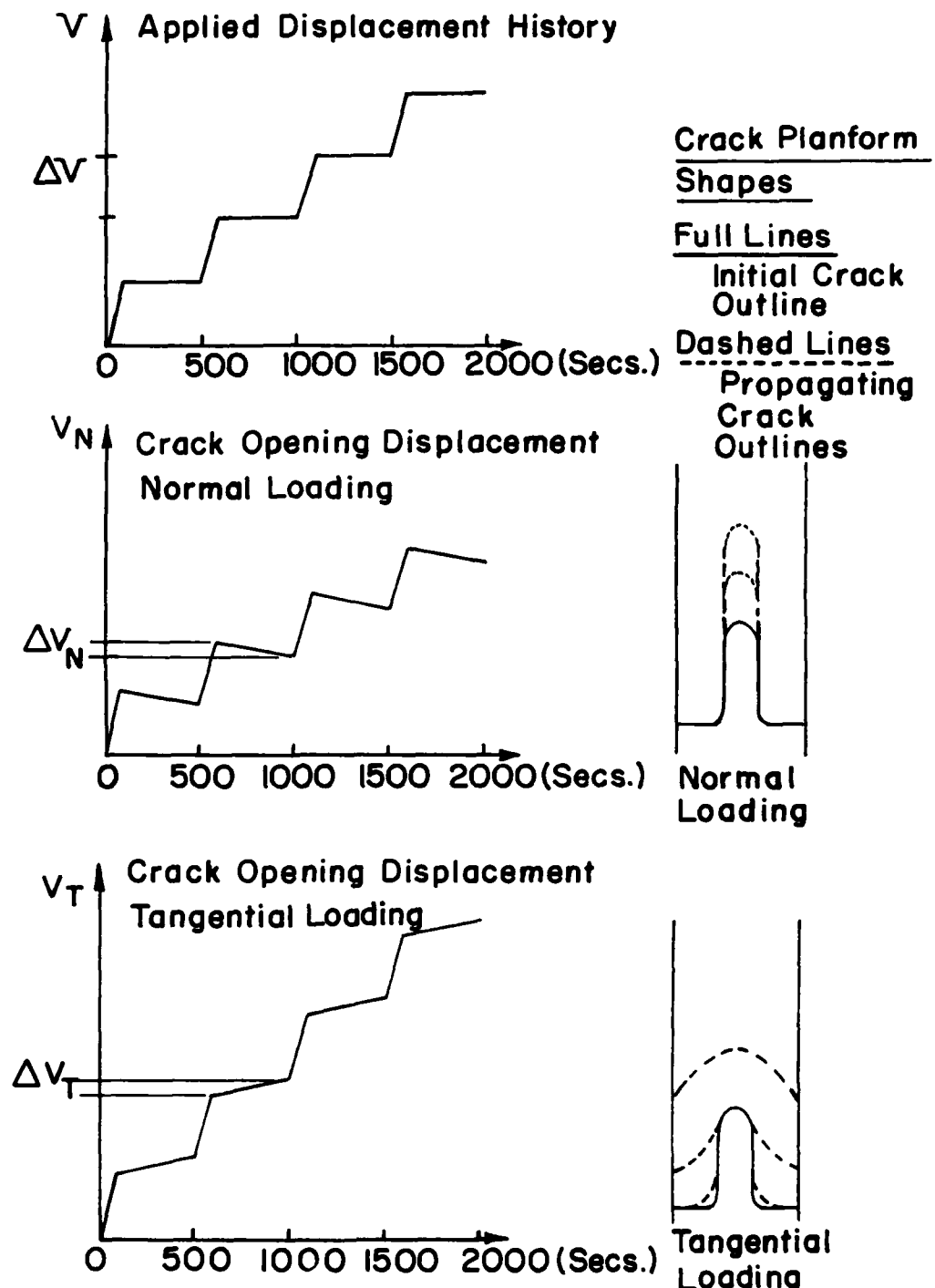


FIG. 8 CRACK PROPAGATION FEATURES FOR
NORMAL AND TANGENTIAL LOADING

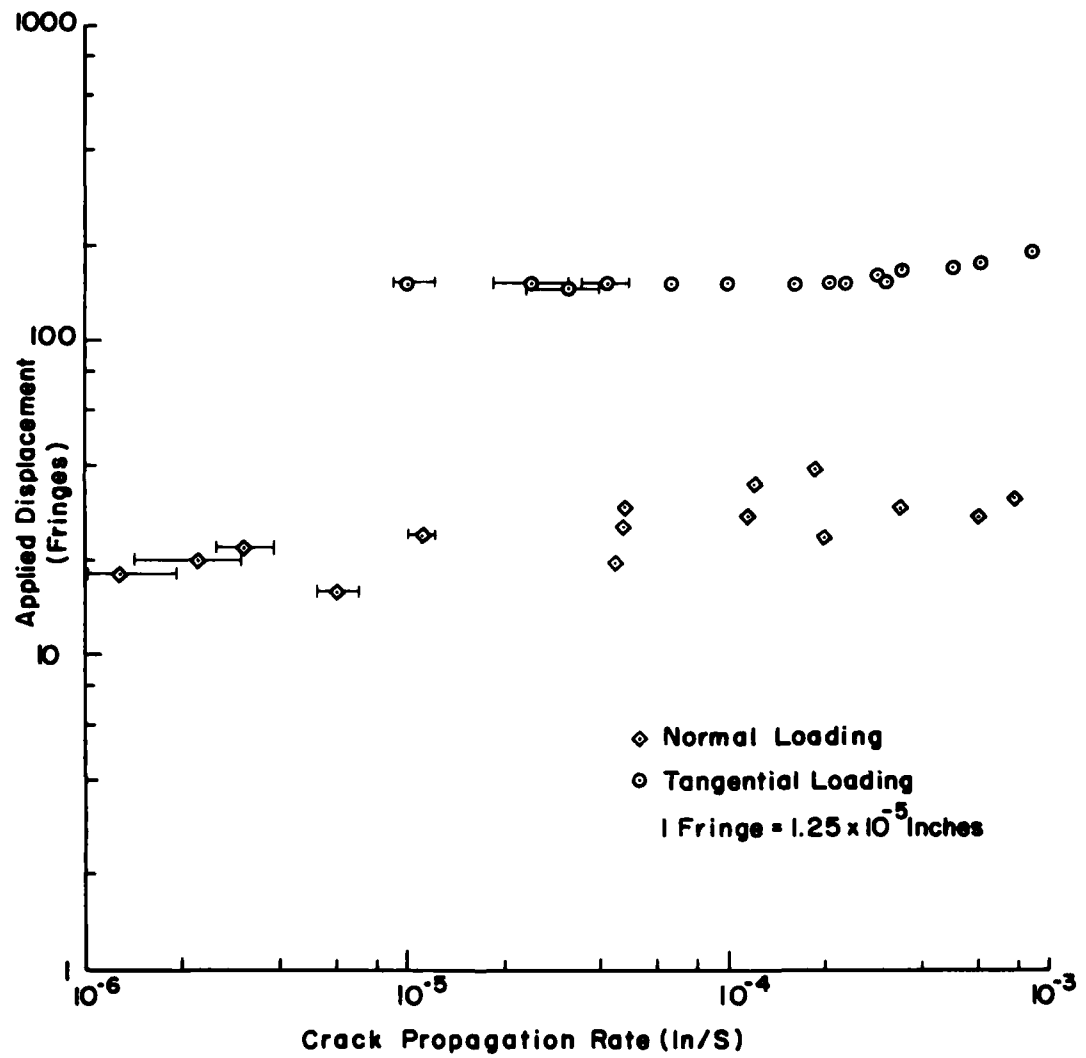


FIG. 9 APPLIED DISPLACEMENT VS. CRACK PROPAGATION RATE

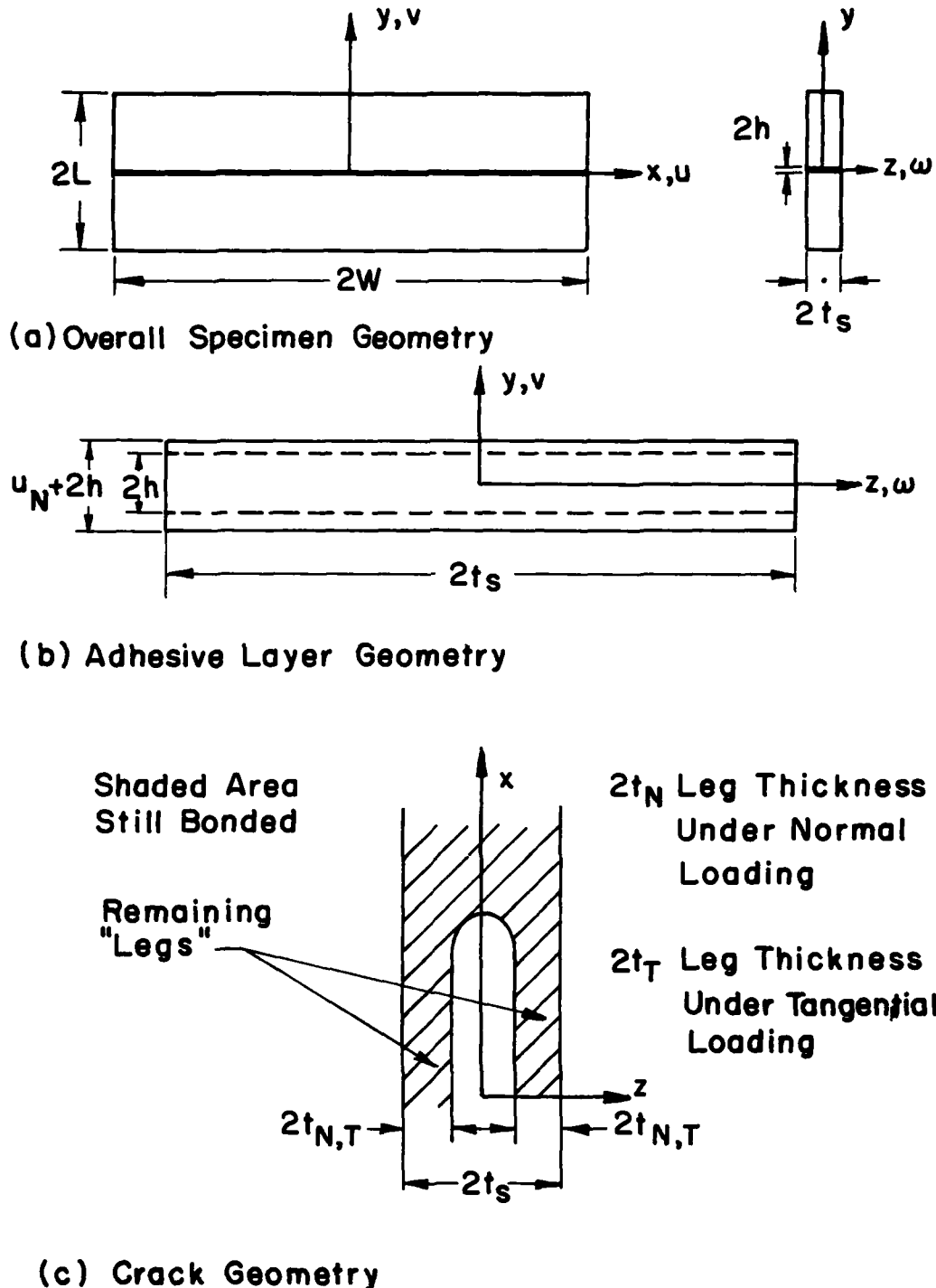


FIG. 10 SPECIMEN AND CRACK GEOMETRIES

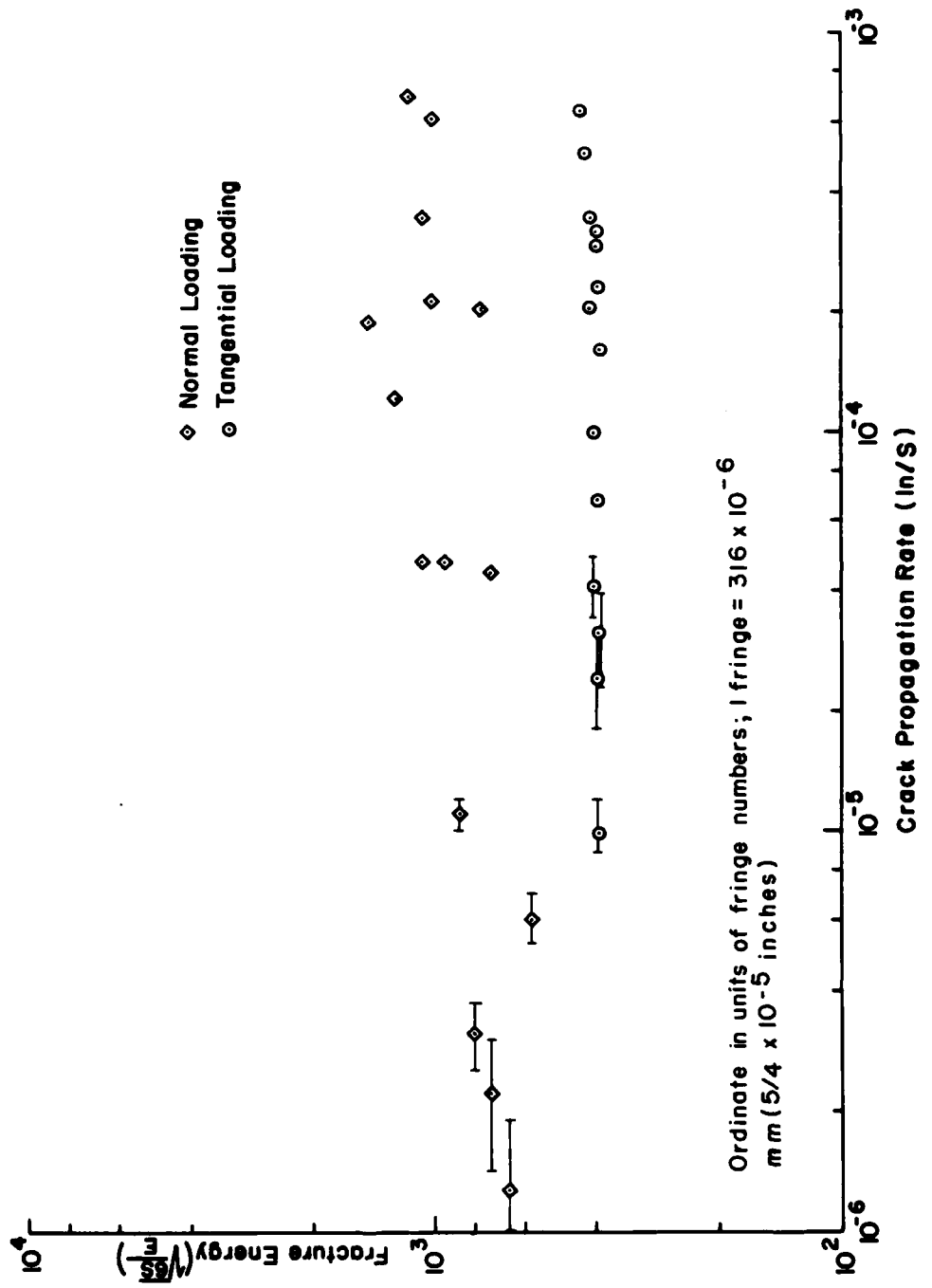


FIG. 11 FRACTURE ENERGY CRITERION

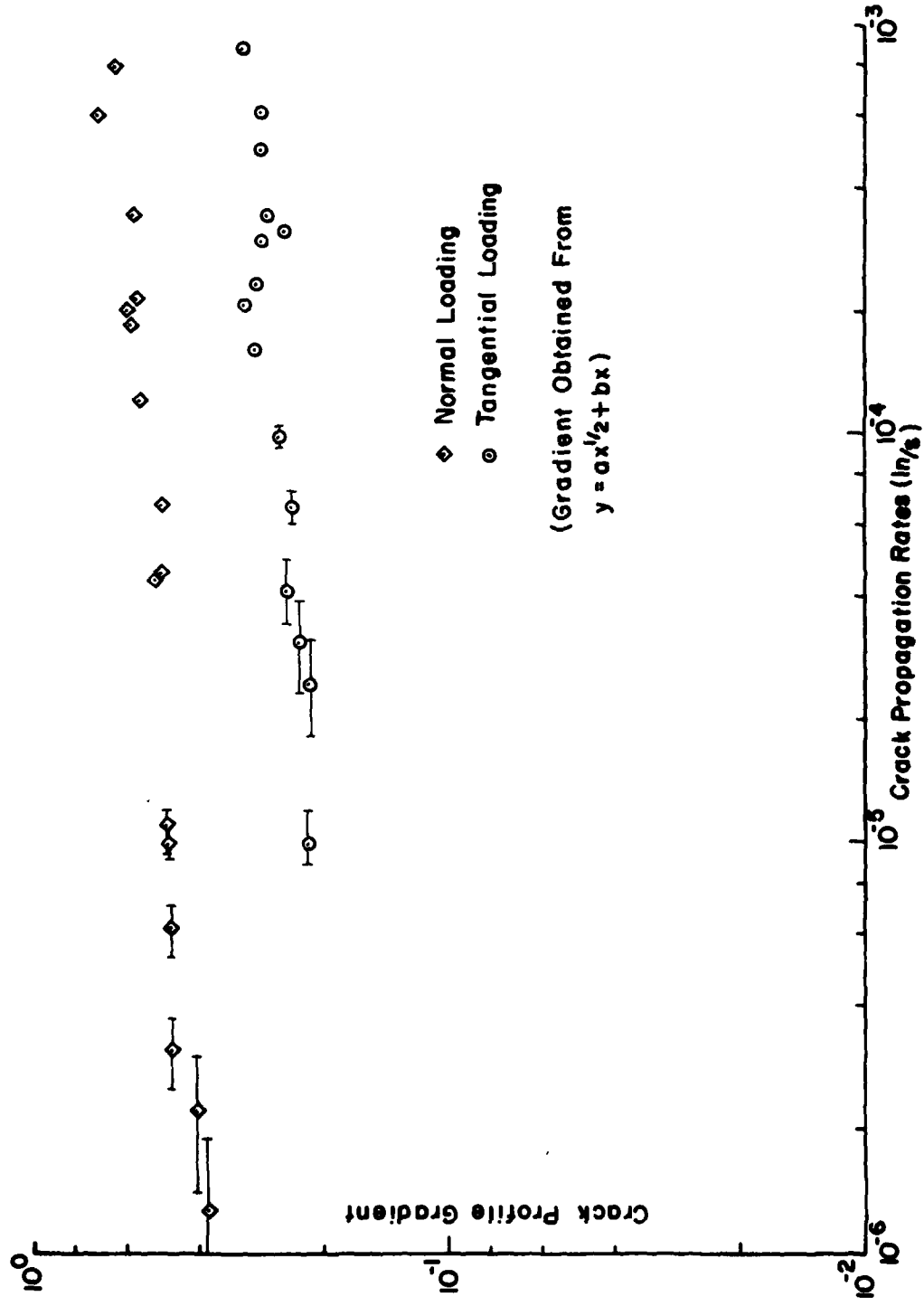


FIG.12 CRACK PROFILE GRADIENT CRITERION

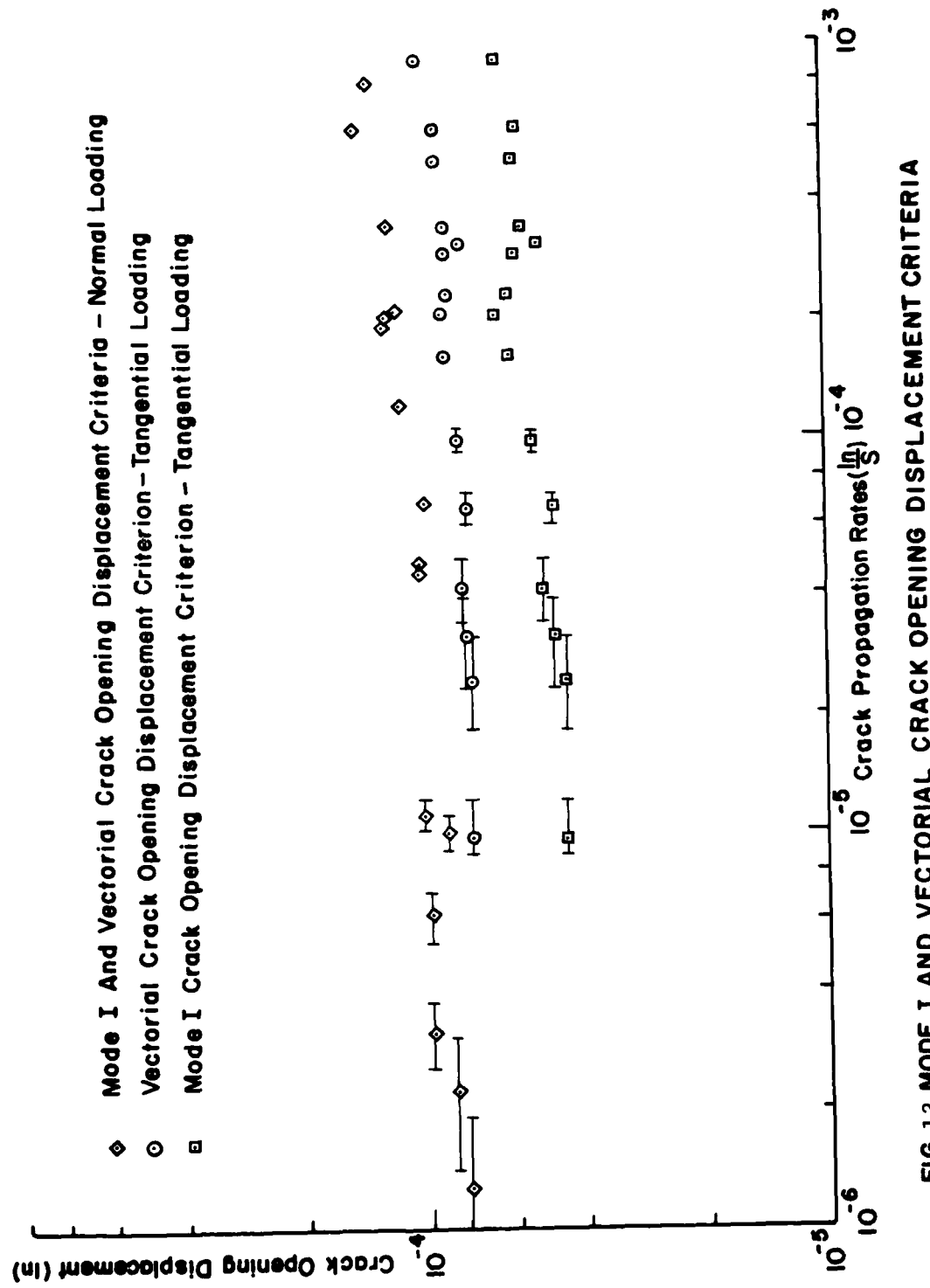
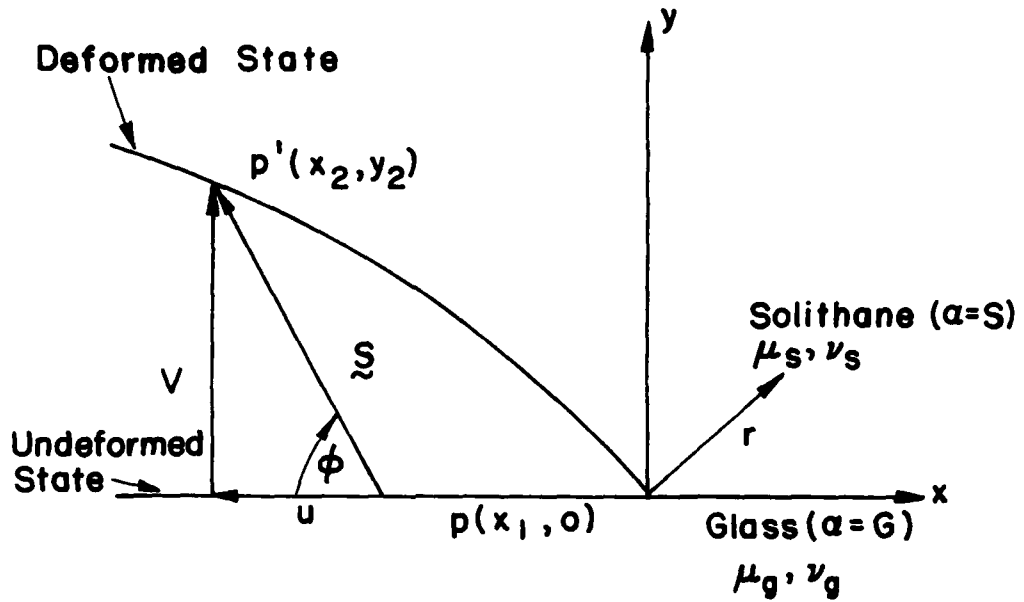


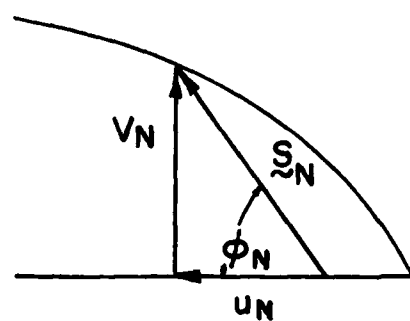
FIG. 13 MODE I AND VECTORIAL CRACK OPENING DISPLACEMENT CRITERIA



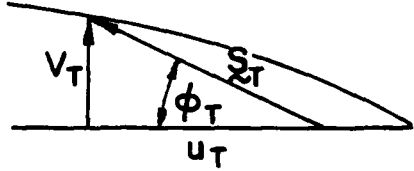
\tilde{S} Vectorial Crack Opening Displacement

V Mode I Crack Opening Displacement

u Mode II Crack Opening Displacement



(a) Normal Loading



(b) Tangential Loading

For Fracture $|S_N| = |S_T| = S_c \Rightarrow V_N > V_T$

FIG. 14 CRACK OPENING DISPLACEMENT CRITERION